Structural Integrity, Safety, and Durability of Critical Members and Connections of Old Railroad Bridges under Dynamic Service Loads and Conditions

Final Report
October 2024

Principal Investigator: Ramesh B. Malla, Ph.D., F. ASCE, F. EMI, Professor
UConn Institutional Lead for US DOT Region 1 UTC-TIDC Program
Department of Civil & Environmental Engineering, University of Connecticut, Storrs, CT

Authors
Celso de Oliveira (Graduate Assistant), Rahul Anand (Graduate Assistant), Sachin Tripathi (Graduate Assistant), and Ramesh B. Malla, Ph.D., F. ASCE, F. EMI, A.F. AIAA, M. CASE (Professor), Department of Civil & Environmental Engineering, University of Connecticut, Storrs, CT

Sponsored By
Transportation Infrastructure Durability Center
U.S. Department of Transportation, University Transportation Centers Program

TIDC
Transportation Infrastructure Durability Center
AT THE UNIVERSITY OF MAINE

A report from
University of Connecticut
Department of Civil & Environmental Engineering
261 Glenbrook Road, Unit - 3037
Storrs, CT 06269-3037, U.S.A.
Phone: +1 (860) 486-2992
Website: http://malla.engr.uconn.edu

THE UNIVERSITY OF MAINE · UMASS LOWELL · WESTERN NEW ENGLAND UNIVERSITY WNE · UCONN · THE UNIVERSITY OF RHODE ISLAND · The UNIVERSITY of VERMONT

About the Transportation Infrastructure Durability Center

The Transportation Infrastructure Durability Center (TIDC) is the 2018 US DOT Region 1 (New England) University Transportation Center (UTC) located at the University of Maine Advanced Structures and Composites Center. TIDC's research focuses on efforts to improve the durability and extend the life of transportation infrastructure in New England and beyond through an integrated collaboration of universities, state DOTs, and industry. The TIDC is comprised of six New England universities, the University of Maine (lead), the University of Connecticut, the University of Massachusetts Lowell, the University of Rhode Island, the University of Vermont, and Western New England University.

U.S. Department of Transportation (US DOT) Disclaimer

Acknowledgements

Funding for this research is in part provided by the Transportation Infrastructure Durability Center at the University of Maine under grant 69A3551847101 from the U.S. Department of Transportation's University Transportation Centers Program. The principal investigator of the project would like to acknowledge and thank the following individuals and organizations whose support (financial, material, and/or in-kind) assisted in this research and significantly contributed to the success of the project:

University of Connecticut Graduate Assistants involved in this project:
Celso de Oliveira, Ph.D. candidate, Department of Civil and Environmental Engineering
Rahul Anand, M.S. student, Department of Civil and Environmental Engineering
Sachin Tripathi, Ph.D. candidate, Department of Civil and Environmental Engineering
Santosh Dhakal, M.S. student, Department of Civil and Environmental Engineering

University of Connecticut Undergraduate Students involved in this project:
Max Raha, B.S. student, Department of Civil and Environmental Engineering

The following members of the project's Expert Panel for their time and attention by serving as technical champions and providing many valuable comments during the course of this project:

Mr. Haresh Dholakia, P.E., Transportation Engineering Supervisor, Rail Design (ConnDOT)
Mr. Manesh Dodia, P.E., Supervising Rail Officer, Rail Construction (ConnDOT)
Mr. Warren Best, P.E., Deputy Director- Structures (Metro-North Railroad Company), Retired
Mr. Randolph Pareja, P.E. Assistant Deputy Director- Structures (Metro-North Railroad Company)
Ms. Hong McConnell, P.E., Deputy Assistant Director – M.o.W – Structures/Capital (Metro-North Railroad Company)

Mr. Mario Pineda, Territory Manager (Polytec Inc.)
Mr. Paul DelSignore, P.E., Deputy Chief Engineer – Structures (Amtrak)
Mr. Rene Asuncion, P.E., Director Engineering-Structures Maintenance & Inspection (Amtrak)
Mr. Chad R. Boutet, P.E., Assistant Vice President – Engineering (Genesee & Wyoming Inc.)
Mr. Chuck Corliss, P.E., Railroad Operations Engineer (NHDOT)

The Connecticut Department of Transportation, Newington, CT for their support making the Devon railroad bridge and the Cos Cob railroad bridge available for testing and other in-kind contribution (Contact: Mr. Haresh Dholakia, P.E, Transportation Supervising Engineer, Rail Bridge Design and Mr. Manesh Dodia, P.E., Supervising Rail Officer, Rail Construction).

Metro-North Railroad Company, Bridgeport, CT for facilitating access to the Devon and the Cos Cob railroad bridge and other in-kind contribution (Contact: Mr. Warren Best, P.E., Assistant Deputy Director - Structures (Retired), Mr. Randolph Pareja, P.E., Assistant Deputy Director - Structures and Ms. McConnel Hong, P.E., Deputy Assistant Director – M.o.W – Structures/Capital).

Polytec, Inc., Hudson, MA for providing field test equipment (Single Point Laser Doppler Vibrometer), data processing software, software and equipment training and other in-kind contribution. (Contact: Mario Pineda, Territory Manager).

Amtrak, Philadelphia, PA for continued support and providing the train specifications. (Contact: Paul DelSignore, Deputy Chief Engineer – Structures, and René S. Asuncion, Sr. Principal Engineer - Structures Maintenance and Inspection).

Genesee & Wyoming Railroad, Northeast Region, Indianapolis, IN for continued support and providing technical feedback. (Contact: Chad R. Boutet, P.E, MBA, Director of Engineering – Grants).

New Hampshire Department of Transportation, Concordia, NH for continued support and providing technical feedback. (Contact: Chuck Corliss, P.E. Railroad Operations Engineer).

Special thanks to Sushrut Vaidya, Ph.D., Postdoctoral Research Associate (College of Engineering, University of Connecticut), for proofreading the report, providing valuable comments/edits on the report, and revising the report to prepare the final version.

Last, but not least, the University of Connecticut, its Department of Civil and Environmental Engineering, and Connecticut Transportation Institute (CTI) for cost share, in-kind support, laboratory facilities, and project administration help.

Technical Report Documentation Page

1. Report No.	2. Government Accession No.	3. Recipient Catalog No.
4 Title and Subtitle Structural Integrity, Safety, and Durability of Critical Members and Connections of Old Railroad Bridges under Dynamic Service Loads and Conditions		**5 Report Date** October 31, 2024 **6 Performing Organization Code**
7. Author(s) Celso de Oliveira: https://orcid.org/0000-0002-6074-8358 Rahul Anand: https://orcid.org/0009-0007-4459-3345 Sachin Tripathi: https://orcid.org/0000-0002-3629-9679 Ramesh B. Malla: https://orcid.org/0000-0002-8035-8402		**8 Performing Organization Report No.**
9 Performing Organization Name and Address University of Connecticut, Department of Civil & Environmental Engineering, 261 Glenbrook Road, Storrs, Connecticut 06269-3037, U.S.A.		**10 Work Unit No. (TRAIS)** **11 Contract or Grant No.**
12 Sponsoring Agency Name and Address U.S. DOT Region 1 University Transportation Center (UTC) -Transportation Infrastructure Durability Center (TIDC), ASCC, University of Maine, 35 Flagstaff Rd., Orono, Maine, U.S.A.		**13 Type of Report and Period Covered** Final Report; 10/01/2021 to 06/30/2024 **14 Sponsoring Agency Code**

15 Supplementary Notes

16 Abstract

Many railway bridges in New England were designed and constructed over a century ago, using now-outdated design codes and materials, making them susceptible to damage under modern service loads. These aging structures and their critical members such as eye-bars, pins, and gusset plates, are showing signs of deterioration, including corrosion, fatigue, and cross-sectional loss. This research aims to investigate the structural behavior of these critical components in old truss-type steel railroad bridges under dynamic loads and performance conditions, with a specific focus on the Devon Bridge and Cos Cob Bridge. The study also seeks to develop methodologies that can be applied to similar aging bridges throughout the region.

The research incorporates field testing, finite element (FE) modeling, and sensitivity analysis to evaluate the structural integrity of critical bridge components. Starting with a critical review of past issues and failures, the study authors worked closely with New England's Departments of Transportation (DOTs) and railroad companies to collect reliable data on bridge types and connection problems. Field tests were conducted on the Devon and Cos Cob bridges, using Laser Doppler Vibrometers (LDV) and accelerometers to measure vertical displacements and natural frequencies during train traversals. These data were then used to calibrate FE simulations, which replicate various operational scenarios such as cross-sectional loss and increased dynamic loads. Sensitivity analysis was employed to further refine the models, emphasizing dynamic behavior, impact, and material aging.

The results show a strong correlation between the field data and FE simulations, validating the models for structural health assessment. Critical members and connections were identified as being at high risk of failure due to significant deterioration. Recommendations are provided for targeted maintenance and rehabilitation strategies to extend the lifespan of these vital transportation assets. This research contributes to the ongoing preservation of aging infrastructure by providing a robust, scalable methodology for pinpointing, evaluating, and mitigating damage in steel truss bridges.

By combining analytical, computational, and experimental techniques, this research offers a comprehensive strategy for understanding and addressing the challenges faced in maintaining aging railroad bridges. The findings are particularly relevant for structures like the Devon and Cos Cob bridges, but the approach is adaptable for broader application across other aging bridges in the region.

17 Key Words	18 Distribution Statement
Aging Railroad Bridges, Finite Element Modeling, Dynamic Loading, Vertical Displacement, Natural Frequencies, Sensitivity Analysis, Laser Doppler Vibrometers (LDV), Accelerometers, Interaction Ratio	No restrictions.

19 Security Classification (of this report)	20 Security Classification (of this page)	21 No. of pages	22 Price
Unclassified	Unclassified	95	

Form DOT F 1700.7 (8-72)

Table of Contents

List of Figures

List of Tables

List of Key Terms

AREMA: American Railway Engineering and Maintenance-of-Way Association.

AMTK: Amtrak Company.

CONN DOT (CT DOT): Connecticut Department of Transportation.

FCM: Fracture-Critical Members.

FE: Finite Element.

FRA: Federal Railroad Administration.

LDV: Laser Doppler Vibrometer.

MTNR: Metro-North Railroad Company.

NEC: Northeast Corridor.

SHMS: Structural Health Monitoring System.

US DOT: United States Department of Transportation.

Abstract

Many railway bridges in New England were designed and constructed over a century ago, using now-outdated design codes and materials, making them susceptible to damage under modern service loads. These aging structures and their critical members such as eye-bars, pins, and gusset plates, are showing signs of deterioration, including corrosion, fatigue, and cross-sectional loss. This research aims to investigate the structural behavior of these critical components in old truss-type steel railroad bridges under dynamic loads and performance conditions, with a specific focus on the Devon Bridge and Cos Cob Bridge in Connecticut. The study also seeks to develop methodologies that can be applied to similar aging bridges throughout the region.

The research incorporates field testing, finite element (FE) modeling, and sensitivity analysis to evaluate the structural integrity of critical bridge components. Starting with a critical review of past issues and failures, the study authors worked closely with New England's Departments of Transportation (DOTs) and railroad companies to collect reliable data on bridge types and connection problems. Field tests were conducted on the Devon and Cos Cob bridges, using Laser Doppler Vibrometers (LDV) and accelerometers to measure vertical displacements and natural frequencies during train traversals. These data were then used to calibrate FE simulations, which replicate various operational scenarios such as cross-sectional loss and increased dynamic loads. Sensitivity analysis was employed to further refine the models, emphasizing dynamic behavior, impact, and material aging.

The results show a strong correlation between the field data and FE simulations, validating the models for structural health assessment. Critical members and connections were identified as being at high risk of failure due to significant deterioration. Recommendations are provided for targeted maintenance and rehabilitation strategies to extend the lifespan of these vital transportation assets. This research contributes to the ongoing preservation of aging infrastructure by providing a robust, scalable methodology for pinpointing, evaluating, and mitigating damage in steel truss bridges.

By combining analytical, computational, and experimental techniques, this research offers a comprehensive strategy for understanding and addressing the challenges faced in maintaining aging railroad bridges. The findings are particularly relevant for structures like the Devon and Cos Cob bridges, but the approach is adaptable for broader application across other aging bridges in the region.

Chapter 1: Introduction and Background

According to the ASCE 2021 Infrastructure Report Card, infrastructure-related issues are the largest source of delay on the Northeast Corridor (NEC) in 2019, causing 328,000 train delay minutes. The NEC plays an important role in passenger and freight mobility in the United States; for example, moving people and goods between Boston and Washington, DC. A single train can carry the freight of several hundred trucks, reducing highway gridlock, the cost of maintaining existing highways, and the need to build expensive new ones (Malla, Jacobs, et al. 2017, Malla, de Oliveira and Dhakal, Condition/Health Monitoring of Railroad Bridges for Structural Safety, Integrity, and Durability 2022). The NEC is the busiest rail corridor in the United States. Sustaining a viable railroad system requires that infrastructure be maintained through capital investments to upgrade, improve, or replace facilities.

A large percentage of the country's railroad bridges were built in the 20th century using discontinued design codes and steel material, for example Devon and Cos Cob Bridges. Although those bridges still operate under a well-supervised maintenance plan, they often exhibit unusual characteristics due to wear and tear over the years. Sufficient research should be conducted to identify and develop cost-effective methods of extending the lifespan of older structures, especially along passenger routes, where they need to be evaluated and rated for higher speed trains (Malla, Jacobs, et al. 2017, Malla, de Oliveira and Dhakal, Condition/Health Monitoring of Railroad Bridges for Structural Safety, Integrity, and Durability 2022). Although time-dependent factors such as fatigue, dynamic behavior, and material weakening, are conservatively considered during the design phase, they may vary or change during the life span of the structure due to traffic pattern change, global warming, and maintenance techniques.

Figure 1 -Devon Bridge Span 7 (left), and Eye-bars Pin Connection (right)

Figure 2 - Cos Cob Bridge Span 3 (left), and Gusset Plate Connection (right)

1.1 Project Motivation

. Not many studies have been conducted to understand the time-dependent factors that may affect the durability of structural members and connections of railroad bridges, especially for the components that may be categorized as Fracture-Critical Members (FCMs), underscoring the need for studies similar to those undertaken in this project. The American Railway Engineering and Maintenance-of-Way Association (AREMA) define the FCMs as tension components whose failure would collapse or not enable the bridge to perform its design function (AREMA 2022).

Research is needed to fully understand the behavior of such critical members and connections under dynamic service loads and bridge performance conditions, especially for connections such as gusset plates and pins from eye-bars (Jacobs, Dhakal and Ramesh 2021, Mazurek 2016). Historically, the usually unannounced failure of those connections has proven to be catastrophic.

Figure 3 - I-95S bridge collapse (Photograph by Bob Child)

Figure 4 - Tempe Lake railroad bridge collapse (The Arizona Republic)

Figure 5 - I-35W bridge collapse (National Transportation Safety Board)

For example, the highway bridge collapse, due to gusset plate failure, of the I-35W Mississippi River bridge in Minneapolis, Minnesota on August 1, 2007 (**Figure 5**), and the highway bridge collapse, due to pin failure, of the I-95 Mianus River bridge in Cos Cob, Connecticut on June 28, 1983 (**Figure 3**). The need for research to understand bridge behavior and innovative methods which apply twenty-first-century technology to preserve and improve the current infrastructure is obvious. This research provides an additional tool to New England's DOTs and railroad companies to identify, evaluate, and mitigate issues that threaten the structural integrity of critical members and connections on old railroad bridges. **Figure 4** shows the Tempe Lake railroad bridge collapse in 2017, where the investigation is still ongoing to determine if the bridge collapsed due to train derailment or due to structural failure of the bridge.

1.2 Research Objectives and Tasks

The project objectives are directly aligned with the Thrust Area 1, with a primary objective of this proposed research being the development of an efficient and cost-effective methodology to identify, mitigate, and validate repair techniques of critical members and connections, such as gusset plates and pins from eye-bars, of old steel railroad bridges, due to wear and tear caused by dynamic service loads and conditions. Different service scenarios will be investigated using analytical, computational, and experimental techniques including field tests. Specific objectives include:

1. Compilation of reliable data records and the evaluation of bridge types versus connection problems, current repair techniques, and existing mitigation methods.
2. Development of a global FE model to identify critical members and connections under different operational and environmental simulations, such as different train types and conditions.
3. Accurate measurement and validation of the global structural response of the old bridge under service conditions using limited field test data.
4. Field test and validation of the FE model result with analytical methods and experimental techniques, such as design codes.
5. Development of study methodology to better evaluate and understand the critical connections and members using performance-based methodologies.

The proposed research will be built upon the PI's previous UTC-TIDC research project #1.2 "Condition/Health Monitoring of Railroad Bridges for Structural Safety, Integrity, and Durability"

(Malla, de Oliveira and Dhakal, Condition/Health Monitoring of Railroad Bridges for Structural Safety, Integrity, and Durability 2022). The information collected during the previous project, and the findings of that project, were used to complete the current research. In this study, the information collected, method developed and findings from the PI's previous research are used, but the present study goes beyond the previous project, to explore more areas of practical importance related to the safety and durability of railroad bridges (Malla, de Oliveira and Dhakal, Condition/Health Monitoring of Railroad Bridges for Structural Safety, Integrity, and Durability 2022). To achieve the overall goal of the research, analytical, computational, and experimental techniques are used to locate and evaluate critical members and connections of old steel railroad bridges, such as pins of eye-bars and gusset plates, and to develop appropriate failure mitigation techniques. The present research was carried out in close collaboration with several New England DOTs and railroad companies to better understand the typical issues encountered in truss-type bridges and their members and connections, as well as existing mitigation methods used in the industry and region. Using an updated FE model, the critical members and connections were identified and analyzed under different dynamic operational scenarios, such as varying speeds and train types, using available bridge performance information.

The main objective of this research is to create and apply a reliable methodology for detecting and monitoring the conditions of critical components of railroad bridges in the medium-- to long-term. This objective is achieved by utilizing computational modeling and analysis (Finite Element Analysis) and conducting limited field tests on bridges under typical service loads to ensure efficiency and effectiveness.

1.3 Report Overview

This report is aligned with TIDC Project # 1.13: "Structural Integrity, Safety, and Durability of Critical Members and Connections of Old Railroad Bridges under Dynamic Service Loads and Conditions," where technical reports, limited field testing, and computational modeling were employed to characterize and identify critical connections and members of old railroad bridges at performance level.

The report provides a comprehensive analysis of the condition assessment and structural evaluation of three railroad bridges in the New England area. It encompasses the methodology, results, and discussions related to the field testing, finite element modeling, and identification of critical members and connections for each bridge. The summary, conclusions, and recommendations derived from the findings are also presented to guide future actions and decision-making processes in maintaining the safety and integrity of the bridge structures.

Chapter 2: Methodology

The following section provides an overview of the current state of New England's bridges and the methods currently employed to identify critical members and connections. It also presents information on the performance conditions of the selected bridges examined in this report. Additionally, it outlines the typical service train, the equipment utilized for field tests, and the methodology employed for collecting, processing, and interpreting the recorded data. Finally, it discusses the Finite Element (FE) model developed for this research and the computational analysis of the model.

2.1 Literature Review

The aging infrastructure of New England's railroad bridges presents a significant challenge, as these structures were not originally designed to handle the heavier loads and faster speeds of modern trains. Over time, issues such as corrosion and fatigue cracking have compromised the structural integrity of critical components, raising concerns about the long-term safety and reliability of these bridges. To address these challenges, current industry practices emphasize the identification of critical members and connections through a combination of non-destructive testing techniques, load testing, and structural health monitoring systems. By understanding these current practices, we can work towards ensuring the continued safety and functionality of New England's vital rail infrastructure.

2.1.1 Existing Condition of the New England Railroad Bridges

Most of the railroad bridges in the New England region are over a century old, having been constructed between the late 19th and early 20th century with old standards, materials, and technologies. These bridges were designed for lighter train loads and slower speeds, but now they face heavier train loads with higher speeds. Modern design requirements and materials have outpaced those old standards and technologies. Today, these bridges are critical components of the region's infrastructure, supporting freight operations and vital passenger rail services, including the busy Northeast Corridor (NEC).

One of the biggest concerns about these bridges is the cumulative impact of time and service loads on their structural integrity. These bridges were originally designed for lighter train loads and slower speeds, but now these bridges regularly handle much heavier and faster trains than they were originally designed for. This change in loading conditions has accelerated wear and deterioration, particularly in critical connection components such as gusset plates, pins, and eye-bars. Due to the increased level of stress and fatigue conditions, the initial design strength of these components is often inadequate, leading to significant deterioration over time.

Corrosion is one of the most common issues affecting the steel components of New England's railroad bridges. Moisture, deicing salts, and exposure to the elements have caused considerable section loss in many critical members. Eye-bars and gusset plates, key components in older truss bridges, are particularly susceptible to corrosion, especially at joints and connections where moisture accumulates. This loss of cross-sectional area not only compromises the load-carrying capacity of individual members but also affects the overall stability of the structure, raising concerns about long-term serviceability and safety.

Fatigue cracking is another serious issue in these aging bridges. Many of the bridges in New England were designed without the benefit of modern fatigue design criteria. The repeated load cycles over the decades have introduced fatigue-related cracks in critical members and connections. This is particularly problematic in fracture-critical bridges, where the failure of a single member could lead to the collapse of the entire structure. Older bridges, especially those that utilize pin connections and riveted joints, are at a higher risk of fatigue cracking due to stress concentrations at these connections. While these structures have served well beyond their original design life, the demand for their continued use under modern rail traffic conditions poses a significant challenge. The need for ongoing assessment, rehabilitation, and in some cases, replacement, is essential to maintaining the safety and reliability of the region's rail infrastructure.

2.1.2 Current Practices to Identify Critical Members and Connections

To ensure the structural integrity and safety of aging railroad bridges, it is necessary to identify the critical members and connections of the bridges. To prevent failure, the current industry practices prioritize identifying the critical members and connections involving a combination of field testing, non-destructive evaluation (NDE), and data-driven approaches.

Non-Destructive Testing (NDT) techniques such as visual inspection, ultrasonic testing, magnetic particle testing, and acoustic emission monitoring are commonly used to identify critical members and connections. These techniques allow engineers to assess the internal integrity of steel members and pinpoint locations where fatigue cracking or corrosion has compromised structural performance. Ultrasonic testing, for instance, is highly effective in detecting internal defects within critical components such as eye bars and gusset plates, which are prevalent in older truss bridges like those investigated in this study.

Load testing, both static and dynamic, is another widely adopted practice. Static load tests apply known forces to the bridge and monitor its response, often using sensors such as strain gauges to capture data on deflections and stress distributions. Dynamic load testing, on the other hand, focuses on the bridge’s behavior under moving loads, such as passing trains, and utilizes sensors such as accelerometers to measure the dynamic response of the bridge. By comparing the response of the structure under controlled loading conditions to the predictions of theoretical models, engineers can identify areas of concern—such as members or connections that exhibit unexpected deformations or vibrational anomalies.

Additionally, Structural Health Monitoring (SHM) systems are increasingly being integrated into critical bridges, providing real-time data on the structural performance of members and connections. SHM systems use a network of sensors—commonly accelerometers, displacement transducers, and strain gauges—that continuously monitor the bridge's response to service loads. Over time, this data helps identify trends in performance, highlighting members or connections that show signs of deterioration. These systems are particularly valuable for assessing fatigue-prone components, allowing for preventative maintenance before significant damage occurs.

Field test data, such as that collected for this project, also plays a vital role in identifying critical members and connections. In this research, the use of a Laser Doppler Vibrometer (LDV) provided precise measurements of bridge deck velocity and displacement under train loading, offering insight into how the structure behaves under dynamic service conditions. This data is essential for calibrating computational models, which are then used to predict the performance of critical members and connections over time.

Additionally, condition assessment reports based on routine visual inspections, combined with data from NDT and load tests, remain a key part of the industry's approach to identifying critical members. In the case of century-old railroad bridges, condition ratings from agencies such as AASHTO and AREMA guide engineers in determining the most at-risk members and connections. These reports, along with real-time data from SHM systems, allow engineers to prioritize maintenance and rehabilitation efforts.

2.1.3 Moving Load Analysis and Interpretation

The train's velocity and axle configuration heavily affect the railroad bridge response under a moving train. As a result, many studies were conducted in the early 1900s (Yang, Yau and Wu, Vehicle-bridge interaction dynamics - with appilcation to high-speed railways 2004, Yoon, et al. 2013). The studied span of the Cos Cob and Devon bridge is idealized as a simply supported beam. Therefore, the theory described below can be applied.

Biggs (1964) developed a method to determine the effect of a single moving axle over a simply supported beam (Biggs 1964, Yang, Zhang, et al. 2019, de Oliveira, Dhakal and Malla 2024). He found that the loading/excitation period (T_a) is the critical factor in analyzing the bridge forced vibration in the *nth* mode. For example, the vertical deflection of a simply supported beam, under the action of a load moving over the beam, can be represented as the summation of an infinite number of sine waves. The first mode (n = 1), the primary mode of vibration, is a half-sine wave and is related to the force/vehicle traveling speed over the span length, as shown in **Figure 6**. The summation of the displacement response of other modes of vibration (n = 2, 3, 4…), i.e., secondary modes, will, in theory, overlap and cancel each other (Tedesco, McDougal and Ross 1999, Polytec Inc. 2015).

The frequency of the excitation force/load required for resonance is determined by the relationship between the constant vehicle travelling speed and the effective length of the bridge span in the *n*th mode, as shown in **Equation 1** (Biggs 1964, Yang, Zhang, et al. 2019, de Oliveira, Dhakal and Malla 2024).

$$nf_a = \frac{n}{T_a} = n\frac{v}{2L} \qquad \textbf{Equation 1}$$

Where f_a is the loading/excitation frequency, T_a is the single moving force excitation period, v is the constant speed of the moving force/vehicle, L is the span length, and n is the integer multiplier of the frequency in the *n*th mode.

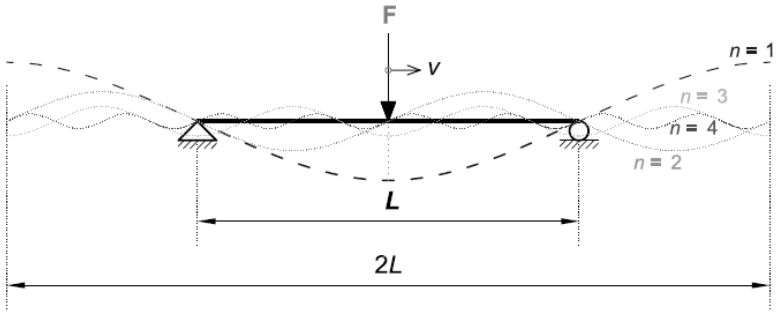

Figure 6 - Relationship between loading/excitation period and bridge span length for a simply supported beam under a single moving load

Frýba (2000) concluded that the forced steady-state vibration response would reach its maximum when the time intervals between two successive moving loads are equal to some natural

period of the beam under free vibration or an integer multiple thereof, designated as the *n*th respective mode of vibration (Frýba 2000, Yang, Yau and Wu, Vehicle-bridge interaction dynamics - with appilcation to high-speed railways 2004, Yang, Zhang, et al. 2019). Yang et al. (2004) concluded that the structural dynamic interaction between a bridge and the train's moving axles is predominantly governed by the primary axle period (T_d), when n = 1 (Frýba 2000, Yang, Yau and Wu, Vehicle-bridge interaction dynamics - with appilcation to high-speed railways 2004, Yang, Zhang, et al. 2019). **Figure 7** shows the vertical displacement of the beam under a series of moving axles at a specific time.

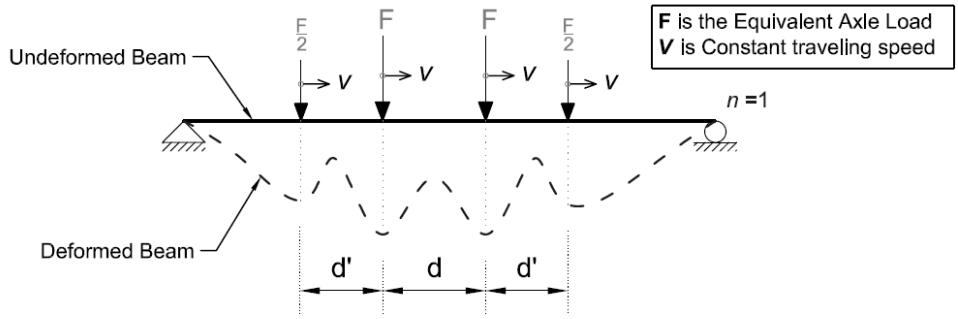

Figure 7 - Axle loading period and the vehicle axle distance in a simply supported beam under a set of equally-spaced moving loads

The axle load periods T_d and $T_{d\prime}$ are calculated by dividing the equivalent axle distance d and d' by the average constant velocity (v), as given by **Equations 2** and **3** below. The axle spacing is related to the vehicle's characteristics. The axle loading frequencies can be determined by inverting the axle loading periods (Frýba 2000, Yang, Yau and Wu, Vehicle-bridge interaction dynamics - with appilcation to high-speed railways 2004, Yang, Zhang, et al. 2019). f_{dn} and $f_{d\prime n}$ represent the nth axle loading frequency corresponding to d and d', respectively.

$$f_{dn} = \frac{n}{T_d} = \frac{nv}{d} \qquad \textbf{Equation 2}$$

$$f_{d\prime n} = \frac{n}{T_{d\prime}} = \frac{nv}{d\prime} \qquad \textbf{Equation 3}$$

Where f_d is the axle loading frequency, T_d is the axle load period, d is the typical axle spacing, d' is the edge axle spacing, and n is the integer multiplier of the frequency in the *nth* mode. The period T_d can be measured directly from the interval between the consecutive crests or valleys in the vertical displacement response curve. **Equations 2** and **3** differ in the spacing used to estimate the forcing period, the double bridge span, and the typical vehicle axle spacing, respectively.

2.2 Bridge Structures Investigated

Two bridges located in southern Connecticut (CT) and one bridge from New Hampshire (NH) were chosen for this study. The bridges in southern CT are located along the New Haven Line, an NEC section built in the early 19th century, and both experience daily traffic of more than 200 trains, where the majority are passenger trains, based on the Operation Schedule Order No. 104 of April 12, 2021. Cos Cob Bridge is located at a mile point of 29.90, and the Devon Bridge is at a mile point of 60.42. The mile point on the New Haven line is the distance from the bridge to the Grand Central Terminal in New York. Therefore, the Devon Bridge is approximately 48 km (30 miles) north of the Cos Cob Bridge. In addition, a preliminary result from a third bridge, Tilton-Belmont Bridge located in New Hampshire (NH) has been presented.

2.2.1 Devon Bridge

The Devon Bridge is located over the Housatonic River between Milford and Stratford in Connecticut. The bridge was built in 1906. Under this one name are two parallel and physically identical long-span through-truss steel bridges (North and South bridges). Each bridge has seven spans: four trusses, two deck girders, and one Scherzer rolling lift bascule (**Figure 8**). The bridge has an approximate overall length of 325.22 meters (1,067 feet). Span 1 is a through truss with a length of 44.12 m (144'-9"). Spans 2 and 3 are plate girders with a span length of 33.53 m (110'-0") and 10.56 m (34'-8"), respectively. Span 4 is a bascule section with a length of 33.53 m (110'-0"), and spans 5-7 are identical trusses with a length of 66.32 m (217'-7") (de Oliveira, Dhakal and Malla 2024, Jacobs, Dhakal and Ramesh 2021, Malla, Jacobs, et al. 2017, Malla, de Oliveira and Dhakal, Condition/Health Monitoring of Railroad Bridges for Structural Safety, Integrity, and Durability 2022). The bridge structure has four train tracks; tracks 1 and 3 are located on the North bridge and tracks 2 and 4 are on the South bridge (de Oliveira, Dhakal and Malla 2024, Jacobs, Dhakal and Ramesh 2021, Malla, Jacobs, et al. 2017, Malla, de Oliveira and Dhakal, Condition/Health Monitoring of Railroad Bridges for Structural Safety, Integrity, and Durability 2022). The field test data were collected from span 7, a long-span truss, on the South bridge.

Figure 8 - Devon Bridge: Google Earth image (left), span 7 South bridge elevation (right)
(41°12'20"N; 73°06'28"W)

2.2.1.1 Devon Bridge: Current Condition

This study used existing inspection and load rating reports to assess bridge members' current conditions and ratings. As described in subsequent sections, the bridges' performance reports were also used to validate finite element (FE) modeling assumptions, such as boundary conditions, element behavior, and cross-section properties.

The inspections and load rating report summarized the average cross-section loss due to corrosion as well as wear and tear, and the current members governing the live load carrying capacity.

Based on the most recent inspection report (Lochner & TranSystem 2021), **Figure 9** illustrates the average cross-section loss of the South Bridge span 7 of the Devon Bridge. It is important to note that the extent of the section loss varies significantly across different bridge components, adding a layer of complexity to the maintenance and repair process. Specifically, regarding the truss members, the cross-section loss is notably more pronounced in the eye bars than in the built-up members. The maximum cross-section loss observed in the eye bars is 36%, while for the built-up members, the maximum cross-section loss is 11%. Therefore, the eye bars were considered the

primary members at risk of losing their load-carrying capacity over the medium- to long-term range, with the loss of load-carrying capacity and mechanical properties being quantified, in this case, by the cross-section loss.

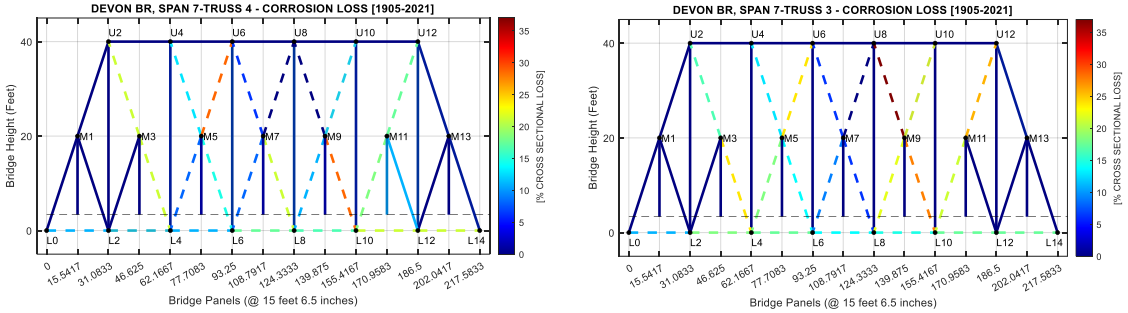

Figure 9 - Devon Bridge: Average cross-section loss for the truss members of Span 7

The load rating report (Lochner & TranSystem 2021) for the Devon Bridge southbridge, span 7, indicates that the diagonal eye bars determine the bridge rating. The ratio of the existing capacity to the live load under the Cooper load rating system indicates that the governing members are M5-L4 & M9-L10, M5-U6 & M9-U8, M5-U4 & M9-U10, M5-L6 & M9-L8, M3-U2 & M11-U12, and M3-L4 & M11-L10.

Figure 10 illustrates the typical live load carrying capacity according to the most recent load rating report (Lochner & TranSystem 2021). Members M3-L4 and M11-L10 have a rating equivalent to E49 on the Cooper load scale per AREMA. The selected member for this study has a rating factor lower than E60 in the Cooper load scale.

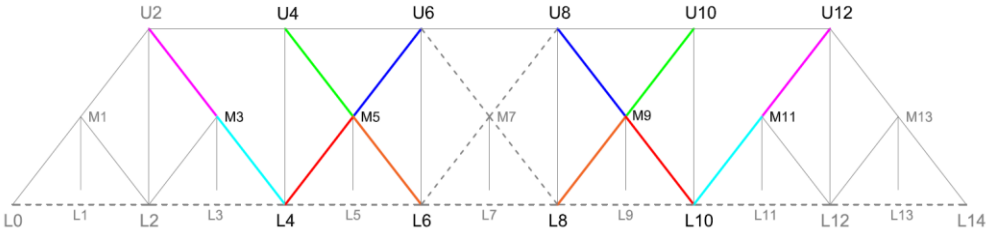

Figure 10 - Devon Bridge: Load rating governing member diagram

2.2.2 Cos Cob Bridge

The Cos Cob bridge is located over the Mianus River in Greenwich, Connecticut. The bridge was built in 1904. Under this one name are two parallel and physically identical long-span, deck-trussed steel bridges (North and South bridges). Each bridge has eleven spans, three deck girders, seven trusses, and one rolling lift bascule (**Figure 11**). The bridge has an approximate length of 322.78 meters (1059 feet). Spans 1, 2, and 8 are plate girders with a length of 11.36 m (37'-3"), 16.15 m (53'-0"), and 16.61 m (54'-6"), respectively. Spans 3 to 6 are identical deck trusses with a length of 37.08 m (121'-8"). Span 7 is a bascule section with a length of 35.76 m (117'-4"). Spans 9 to 11 are identical deck trusses with a length of 32.18 m (105'-7") (Malla, de Oliveira and Dhakal, Condition/Health Monitoring of Railroad Bridges for Structural Safety, Integrity, and Durability 2022, de Oliveira, Dhakal and Malla 2024). The bridge structure has four train tracks; tracks 1 and 3 are located on the North bridge and tracks 2 and 4 are on the South bridge (Malla, de Oliveira and Dhakal, Condition/Health Monitoring of Railroad Bridges for Structural Safety,

Integrity, and Durability 2022, de Oliveira, Dhakal and Malla 2024). The field test data were collected from span 3, a long-span truss, on the South bridge.

Figure 11 - Cos Cob Bridge: Google Earth image (left), span 3 South bridge elevation (right) (41°01'50"N; 73°35'45"W)

2.2.3 Tilton-Belmont Railroad Bridge

The Tilton-Belmont Railroad Bridge is located in New Hampshire (NH), spanning the Winnipesaukee River between the towns of Tilton and Belmont. This bridge was built in 1881 as part of the Boston, Concord & Montreal Railroad to facilitate transportation and commerce in NH. It is a single-span deck truss bridge with a span of 37.8 meters (124 feet), a width of 3.7 meters (12 feet), and a height of 4.3 meters (14 feet). The snapshot view of the bridge along with its original drawing are presented in Figure 12**.**

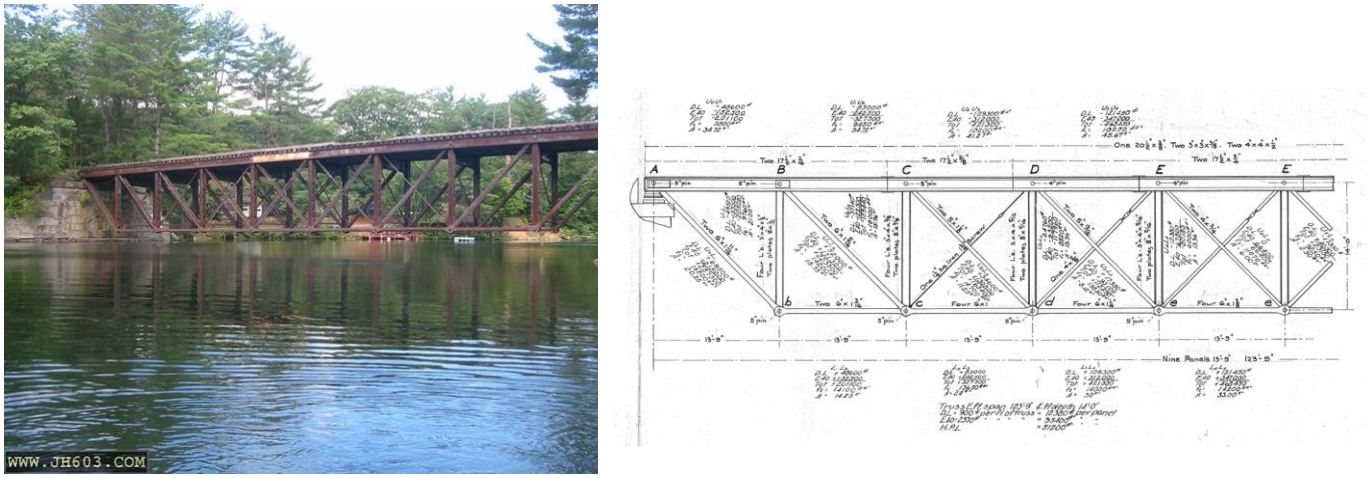

(a) (b)

Figure 12: Tilton-Belmont Bridge: (a) Snapshot view, and (b) original drawing from 1893

Furthermore, the original drawing of the half cross-sections of the floor and side view of stringers are presented in Figure12-1.

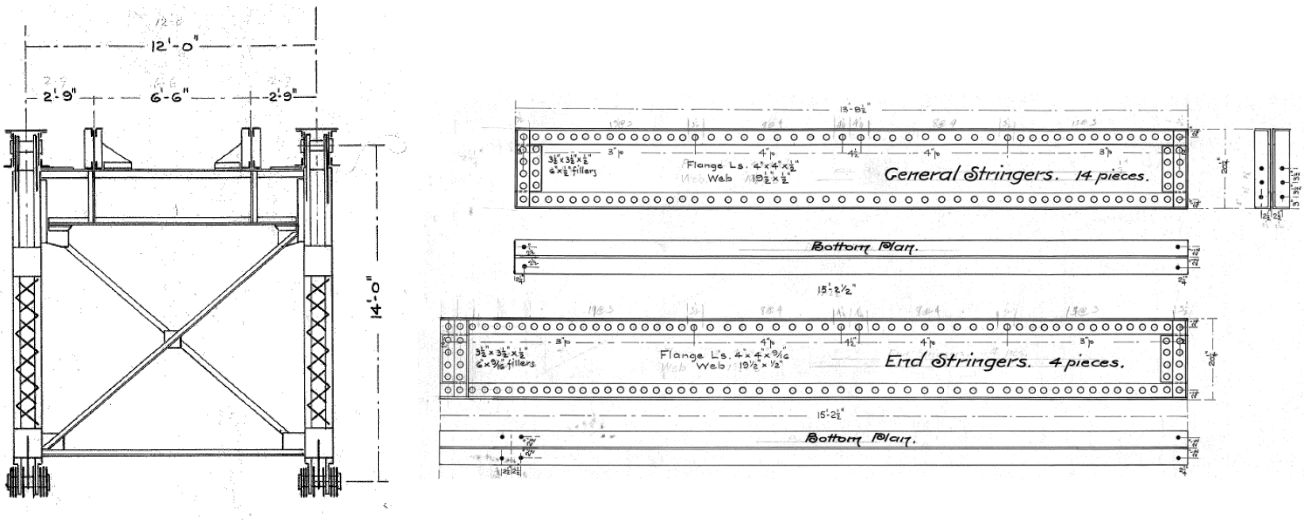

(a) (b)

Figure 12-1: Original Drawing of Tilton-Belmont Bridge: (a) Half Cross-section of Floor, and (b) Stringers from 1893

The Finite Element (FE) model of the Tilton-Belmont Railroad Bridge in New Hampshire was constructed using ABAQUS 6.19-1 software based on the original design drawings from 1893 . The static analysis was performed to evaluate the bridge's structural response under various loading conditions, while modal analysis was conducted to determine its natural frequencies and mode shapes. These analyses provided insights into the dynamic behavior and structural integrity of the bridge, helping to assess its performance under real-world operational scenarios.

2.2.4 Typical Vehicle (Train) Loading on the Bridges

This study analyzes the bridge response based on the axle characteristics of specific trains. **Table 1** provides the relevant axle characteristics for each train considered in this study (AREMA 2017, Siemens 2019, Lochner 2011, de Oliveira, Dhakal and Malla 2024).

Table 1 - Service train axle characteristics for typical train compositions

Composition	Vehicle	Total Weight	Wheelbase	Truck Centers	Cal Length (Pulling faces)
MTNR M8	M8	641.43 kN (144,200 lbs)	2.59 m (8'-6")	18.14 m (59'-6")	25.91 m (85'-0")
AMTK Regional	ACS-64 locomotive	965.26 kN (217,000 lbs)	3.00 m (9'-10.1")	9.68 m (31'-9.1")	20.32 m (66'-8")
	Amfleet Coach	489.30 kN (110,000 lbs)	2.59 m (8'-6")	18.14 m (59'-6")	25.91 m (85'-0")
AMTK Acela	Alstom locomotive	889.64 kN (200,000 lbs)	2.85 m (9'-4")	10.74 m (35'-3")	21.22 m (69'-7 3/8")
	Alstom Coach	587.16 kN (132,000 lbs)	2.99 m (9'-10")	18.14 m (59'-6")	26.64 m (87'-5")

The MTNR M8 is an electric multiple-unit railroad car built by Kawasaki Rail Car, Inc. for exclusive use on the Metro-North Railroad's New Haven Line and the CT*rail* shoreline east. The

train can reach a maximum speed of 161 km/h (100 mph) (de Oliveira, Dhakal and Malla 2024, Malla, Baniya and Jaccobs, Study of Dynamic and Static Response of an Old Truss Railroad Bridge 2016, Lochner 2011, Malla, de Oliveira and Dhakal, Condition/Health Monitoring of Railroad Bridges for Structural Safety, Integrity, and Durability 2022). The MTNR M8 consists of married (double) coaches and/or one single car with approximately the same axle weight.

The AMTK Regional is an intercity rail service that connects major cities along the NEC between Washington, D.C., and Boston, MA. The trains' composition consists of 7-9 passenger coaches hauled by a locomotive. For the New Haven line, the passenger cars are Amfleet, and the locomotive is an electric power engine designed by Siemens Mobility, the ACS-64. The Siemens ACS-64 can reach a maximum speed of 217 km/h (135 mph) (AREMA 2017, Siemens 2019, de Oliveira, Dhakal and Malla 2024, Malla, de Oliveira and Dhakal, Condition/Health Monitoring of Railroad Bridges for Structural Safety, Integrity, and Durability 2022).

The AMTK Acela was built to specification by the consortium of Bombardier Transportation and Alstom. It is currently the fastest and busiest passenger train in North America, reaching a maximum speed of 240 km/h (150 mph). The fixed composition comprises two end power engines with heavier axle loads and six coaches with lighter axle loads (AREMA 2017, de Oliveira, Dhakal and Malla 2024, Lochner 2011, Malla, de Oliveira and Dhakal, Condition/Health Monitoring of Railroad Bridges for Structural Safety, Integrity, and Durability 2022).

Figure 13 shows the train composition of MTNR M8, AMTK Regional, and AMTK Acela compiled using the train axle characteristics.

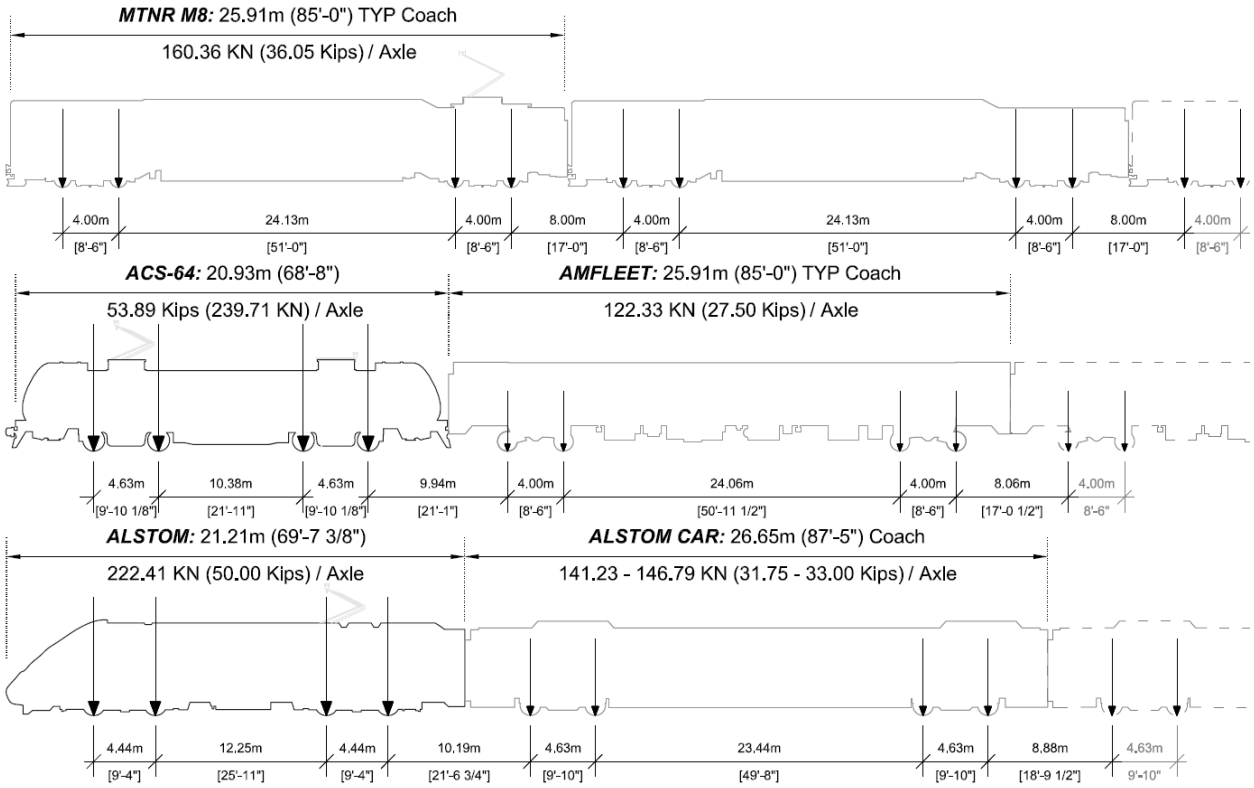

Figure 13: Typical train axle characteristics and equivalent axle distance: MTNR M8 (top), AMTK Regional (middle), and AMTK Acela (bottom)

The Tilton-Belmont Bridge is occasionally traversed by a freight train weighing approximately 263,000 lbs, utilizing a standard 4-axle car (**Figure 14**) as the worst-case scenario. This train

configuration, used by the New Hampshire Department of Transportation (NH-DoT) for their analyses, was also adopted for this study.

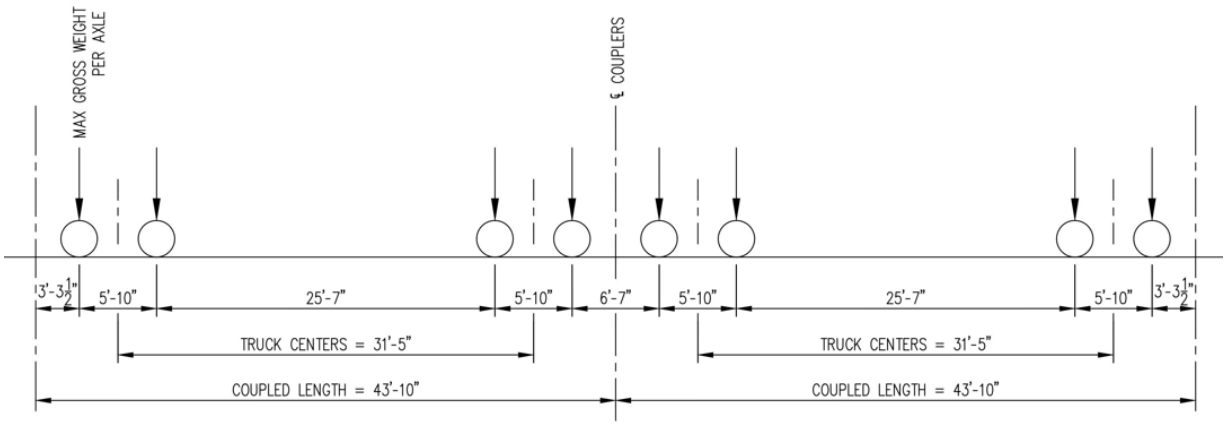

Figure 14: Standard 4-axle Car for Bridge Rating for NH bridge

2.3 Field Testing

Two sets of field tests were conducted on span seven of Devon and Cos Cob Bridges to measure the dynamic responses of their bridge decks under service loads. All the field tests utilized single-point Laser Doppler Vibrometers (LDVs) and uniaxial accelerometers. The sensors were placed at strategic locations to allow the personnel easy access to the equipment. **Table 2** presents a summary of the field tests conducted on Devon and Cos Cob Bridges during the Summer 2021 and Fall 2023, respectively. Detailed train logs are presented in the appendix section of this document.

Table 2 - Field Tests conducted on span seven of Devon Bridge and Cos Cob Bridge

Test #	Date	Data Collected	Number of Trains Recorded	Location
1	June 7 and 8, 2021	Laser Doppler Vibrometer (10 Locations) Accelerometers (3 references)	38	Cos Cob Bridge
2	June 9, 2021	Laser Doppler Vibrometer (5 Locations) Accelerometers (2 references)	11	Devon Bridge
3	November 2 and 3, 2023	Laser Doppler Vibrometer (4 Locations) Accelerometers (2 references)	24	Devon Bridge
4	November 13 and 14, 2023	Laser Doppler Vibrometer (3 Locations) Accelerometers (2 references)	25	Cos Cob Bridge

2.3.1 Field Testing Equipment

The field tests employed a range of instruments to estimate the response of a bridge deck when a train passes over it. These instruments included a Polytec VibroFlex QTec® single-point LDV (Polytec Inc. 2015, Rossi, Gussella and Gioffré 2002) and uniaxial quartz sensing element

accelerometers from PCB Piezotronics® 393B04 (Rossi, Gussella and Gioffré 2002, Schiefer and Dosch 2012). The LDV measured vertical velocity at different nodes, while the accelerometers provided a fixed reference for measuring acceleration.

LDV is a non-contact measurement tool that utilizes a laser beam to detect the frequency shift from reflected laser beams during surface vibration (i.e., the Doppler shift). The output of an LDV is typically a continuous analog voltage directly proportional to the target velocity component along the direction of the laser beam. The Doppler effect refers to a wave's frequency change that occurs when either the source or detector moves relative to the medium through which the wave is transmitted, such as air (Halliday, Resnick and Walker 2014).

Accelerometers, particularly uniaxial quartz sensing element accelerometers, have been widely used for field tests. The accelerometers used in this study are rated for low frequencies and are utilized as a fixed reference. When the measurement system experiences vibrations, the accelerometer's internal inertial mass compresses and stretches the piezoelectric crystals. According to Newton's second law of motion, the compression and stretch forces are proportional to the acceleration and generate a small electrical charge. This charge is demodulated and amplified via a servo circuit, resulting in an output in Volts proportional to the acceleration signal (Schiefer and Dosch 2012).

Figure 15 - LDV setup during field tests: (left) Cos Cob Bridge and (right) Devon Bridge shows the LDV setup during the field test. The picture on the left shows the LDV installed to record the vertical bridge response from the Cos Cob Bridge, and the image on the right shows the LDV installed to record the vertical response of the Devon Bridge.

Figure 15 - LDV setup during field tests: (left) Cos Cob Bridge and (right) Devon Bridge

2.3.2 Devon Bridge Field Test

The South Devon bridge's easternmost span, adjacent to the abutment, was selected for data collection for both field tests. A single-point LDV was installed beneath the bridge to collect the vertical velocity response of the bridge deck system while a service train passed over it. The plan view locations of the LDV and accelerometers installed on span 7 of Devon Bridge during the Summer 2021 field test are shown in **Figure 16**. Two accelerometers were used as references at fixed points, denominated ACC 1 and ACC 2, to record the bridge acceleration response. The two accelerometers were mounted to record the vertical and horizontal accelerations, respectively, of the bridge node during the Summer 2021 field test. Both accelerometers were installed to record vertical acceleration during the Fall 2023 field test.

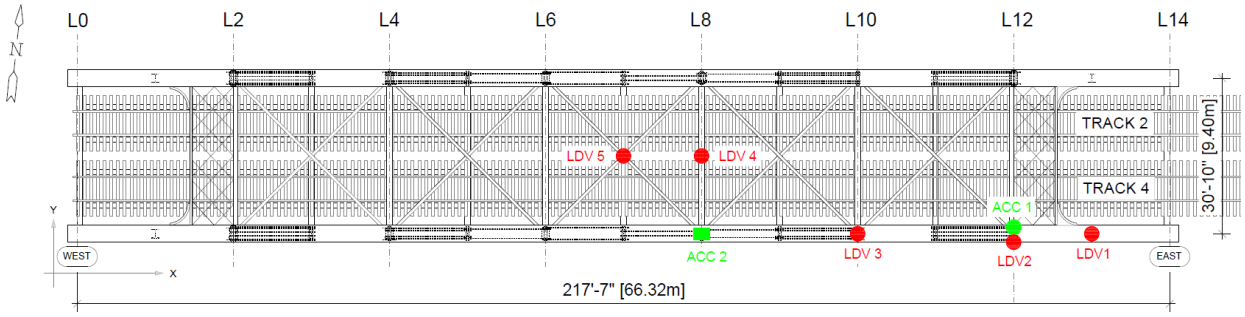

Figure 16 - Span7 of South Devon Bridge: Summer 2021 Field Test Setup (LDV and ACC locations)

Below is a clear representation of the log of trains that crossed the bridge during the Summer 2021 field test. **Table 3** displays relevant information such as travel, equipment, and LDV data. Please note that only the trains pertinent to the test are included in the table. The Fall 2023 field test data log and schematics are shown in **Appendix A**.

Table 3 - Recorded data from field tests conducted on Devon Bridge (June 9, 2021)

Train #	Speed	Direction	Track #	Cars	Train Type	LDV Loc
1	42.38 mph	West-East	4	8	MTNR M8	1
3	43.13 mph	West-East	4	8	AMTK Regional	2
4	41.90 mph	West-East	4	10	MTNR M8	2
5	42.57 mph	West-East	2	8	AMTK Acela	3
7	41.93 mph	West-East	2	8	AMTK Regional	3
10	17.89 mph	East-West	2	8	MTNR M8	4
11	41.28 mph	West-East	4	8	AMTK Regional	5

2.3.3 Cos Cob Bridge Field Test

An interior span (Span 3) next to the western abutment on the south Cos Cob bridge was selected for the field test bridge response recording (**Figure 17**). The single-point LDV was installed at four different locations beneath the bridge. The LDV pointed vertically upward to the bottom chord recorded the bridge deck's vertical velocity response when a service train passed over the bridge. In addition, two accelerometers were placed at fixed points to serve as a reference by recording the bridge acceleration response. In **Figure 17**, the labels REF 1 and REF 2 denote the accelerometer locations. Accelerometer REF 1 was installed to record vertical response and REF 2 was mounted to record horizontal bridge response. The uniaxial accelerometers were placed and fixed using the epoxy-glued base and connected to the LDV manufacturer's Data Acquisition (DAQ) system using low-noise coaxial cables. **Table 4** presents the information about the trains recorded during the field tests on Nov 13 and 14, 2023.

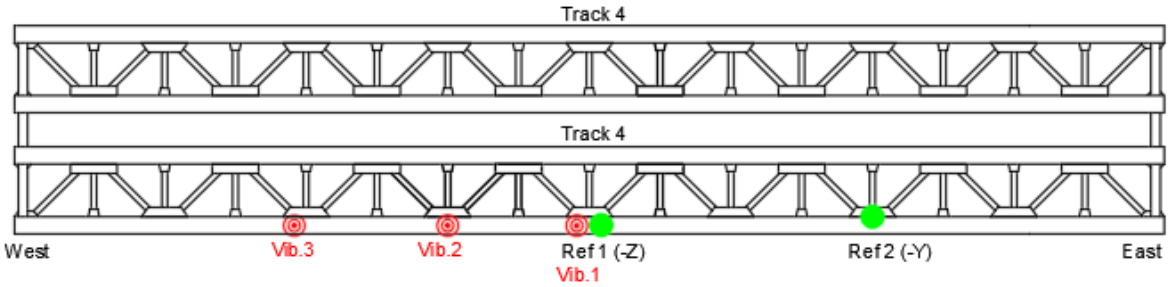

Figure 17 - Span 3 of South Cos Cob Bridge: Plan view with LDV and accelerometer locations

Table 4 - Recorded data from field tests conducted on Cos Cob Bridge (November 13 & 14, 2023)

Train#	Speed (mph)	Direction	Track #	# of Cars	Train Type	LDV Location
1		West-East	4	8	Metro north M8	Vib 1
2		West-East	4	6	Metro north M8	Vib 1
3		West-East	4	9	Metro north M8	Vib 1
4		West-East	4	8	Metro north M8	Vib 1
5		West-East	4	5	Metro north M8	Vib 1
6		West-East	4	8	Acela	Vib 1
7		West-East	4	8	Metro north M8	Vib 1
8		West-East	4	8	Metro north M8	Vib 1
9		N/A	N/A	N/A	N/A	N/A
10		West-East	4	6	Metro north M8	Vib 1
11	40	West-East	4	6	Metro north M8	Vib 2
12	35	West-East	4	7	Metro north M8	Vib 2
13	40	West-East	4	8	Metro north M8	Vib 2
14	35	West-East	4	7	Metro north M8	Vib 2
15	25	West-East	4	8	Metro north M8	Vib 2
16	37	West-East	4	8	Amtrak Regional	Vib 2
17	40	West-East	4	6	Metro north M8	Vib 2
18	40	West-East	4	7	Metro north M8	Vib 2
19	38	West-East	4	8	Acela	Vib 2
20	40	West-East	4	8	Metro north M8	Vib 3
21	40	West-East	4	6	Metro north M8	Vib 3
22	25	West-East	4	9	Metro north M8	Vib 3
23	43	West-East	4	8	Metro north M8	Vib 3
24	36	West-East	4	5	Metro north M8	Vib 3
25	41	West-East	4	8	Metro north M8	Vib 3

2.3.4 Data Processing Procedure

The LDV and accelerometers record the bridge deck velocity and acceleration response in the time domain when the train crosses the bridge span. The velocity response was converted to displacement and acceleration response using integration and differentiation, respectively. Then, the time domain data was converted to the frequency domain using the Fast Fourier Transform algorithm (FFT) to understand the bridge's vibration frequency range. The data was recorded using the Polytec PSV® software (Polytec Inc. 2015) and processed using the MATLAB® software (The MathWorks, Inc. 2022), in which a code was written using the data processing and moving load theory principles presented here. The LDV system provides automatic built-in alias suppression of the frequencies above the chosen bandwidth (Polytec Inc. 2015).

The raw data from LDV and accelerometers was recorded at 512 samples per second (f_S). Thus, the Nyquist frequency is 256 Hz, calculated as half of the sample rate (Tedesco, McDougal and Ross 1999). The LDV raw data presents an offset from the horizontal axis (time) due to the frequency shift, the Direct Current bias, or DC offset (Bro and Age 2003, The MathWorks, Inc. 2022, Polytec Inc. 2015). The DC offset was removed by subtracting the average of the total y-axis data from the point on the same axis (Bro and Age 2003, The MathWorks, Inc. 2022, Polytec Inc. 2015).

In the time domain, the LDV output in velocity time variation was integrated or differentiated, as may be the case, to convert it to displacement or acceleration, respectively (Polytec Inc. 2015). Integration in the time domain is usually only satisfactory if the time signal does not have a DC offset because it can cause a ramp in the integrated signal (Bro and Age 2003, The MathWorks, Inc. 2022, Polytec Inc. 2015). The equation below shows the relation for obtaining displacement, x_i at a time instant using the integration of the velocity in the time domain (Chopra 2017, Polytec Inc. 2015, The MathWorks, Inc. 2022, Tedesco, McDougal and Ross 1999)

$$\boldsymbol{x_i = x_{i-1} + \dot{x}_i \Delta t} \qquad \textbf{Equation 4}$$

Where $\Delta t = 1/f_S$, x_{i-1} is the displacement at the preceding time instant, $\dot{x}_i$ is the velocity at the time instant under consideration, and f_S is the sampling frequency.

The time differentiation is performed to convert the LDV measured velocity data into acceleration ($\ddot{x}_i$) at a time instant as shown below (Chopra 2017, Polytec Inc. 2015, The MathWorks, Inc. 2022, Tedesco, McDougal and Ross 1999):

$$\boldsymbol{\ddot{x}_i = \frac{\dot{x}_i - \dot{x}_{i-1}}{\Delta t}} \qquad \textbf{Equation 5}$$

Where $\dot{x}_i$ is the velocity at a given time instant, and $\dot{x}_{i-1}$ is the velocity at the preceding time instant.

Any recorded signals in the time domain can be transformed to corresponding functions in the frequency domain using the Fourier transform principle. In this principle, the original signal (a function of time) is split into a sum of terms with different frequencies containing the information of the original signal (Chopra 2017, Polytec Inc. 2015, Tedesco, McDougal and Ross 1999). Theoretically, convergence of a Fourier series requires an infinite number of terms. Still, relatively few terms will sufficiently accurately approximate harmonic vibration signals (Chopra 2017, Polytec Inc. 2015, Tedesco, McDougal and Ross 1999). An FFT is a computer algorithm that computes the discrete Fourier transform of a signal from the original domain (time domain) to convert the signal into its corresponding representation in the frequency domain and vice versa (The MathWorks, Inc. 2022, Polytec Inc. 2015). The frequency response from FFT can be

calculated using either the entire bandwidth or a selected signal section of the velocity response of the LDV and the acceleration response given by the accelerometers.

The MATLAB (The MathWorks, Inc. 2022) FFT algorithm was used to generate the corresponding linear frequency spectrum from the time domain velocity and acceleration data. **Figure 18** shows the data processing methodology used in this study, where the raw data is imported in the time domain and centralized by removing the DC on steps 1 and 2, respectively. Then, the data was integrated or differentiated in step 3, and the frequency domain was analyzed using the FFT algorithm in step 4.

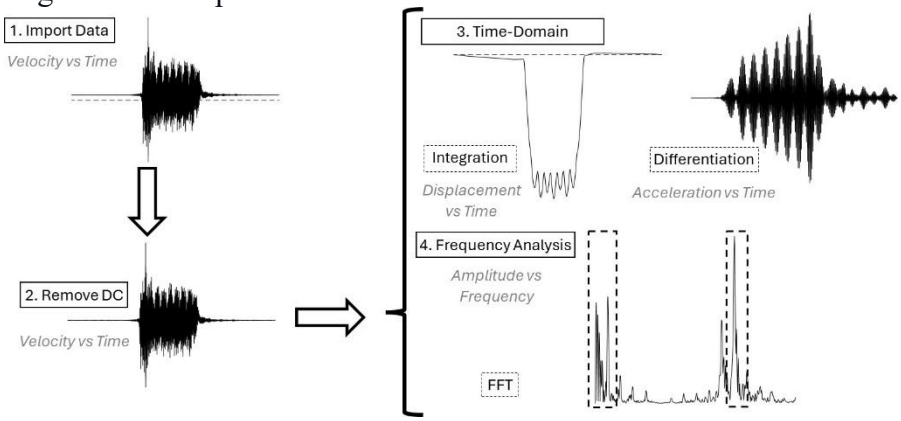

Figure 18 - Data processing methodology

2.4 Computational Model

In this research project, a detailed Finite Element (FE) model was developed to simulate the behavior of the selected span of a specific bridge. The FE models consider various performance-based conditions, including the degradation of structural capacity over time.

Each FE model was subjected to a comprehensive parametric study, using sensitivity-based methods, to better understand the structural response and vulnerabilities of the bridge span under consideration. The research, which implemented sensitivity analysis, uncovered valuable insights into how changes in material and mechanical properties and geometric parameters influence the bridge's structural responses. The findings from this analysis will serve as a foundation for making well-informed decisions regarding potential design modifications and optimizations.

Ultimately, this approach aims to significantly enhance the bridge's overall performance and safety, thereby ensuring stakeholders' confidence in its long-term structural integrity and functionality.

2.4.1 Finite Element Model

The Finite Element (FE) model was developed to replicate the current bridge conditions under dynamic loads, to a sufficient degree of accuracy. This comprehensive study employed technical references, including detailed inspection reports and as-built drawings, to meticulously model the existing bridges.

Moreover, the bridge's dynamic response data, carefully collected during the field test, was exhaustively analyzed to estimate the vehicle traveling speed and the bridge's dynamic

characteristics and response. Several assumptions, based on engineering judgment, were integrated into the development of the overall FE analysis methodology:

1. The FE model deliberately excluded track irregularities to focus on the primary dynamics of the bridge structure.
2. The vehicle-bridge interaction for the transient analysis was not considered, and the axle loads were approximated as triangular pulse loads to account for the time variation of the loads.
3. It was assumed that the train crossed the bridge span at a constant speed, with the model accounting for this specific condition.
4. The bridge structural members were assumed to have uniform cross-sections, with the laced sub-members being idealized as continuous thin plates, ensuring a reasonably accurate, yet computationally efficient, representation of the bridge's structural elements.

Figure 19 provides an in-depth visual representation of the process employed to generate the built-up cross-sections. The as-built drawings, inspection report, and detailed pictures were utilized to develop a simplified cross-section that broadly accounts for the existing condition of the bridge span, ensuring a fairly detailed representation of the bridge's structural integrity.

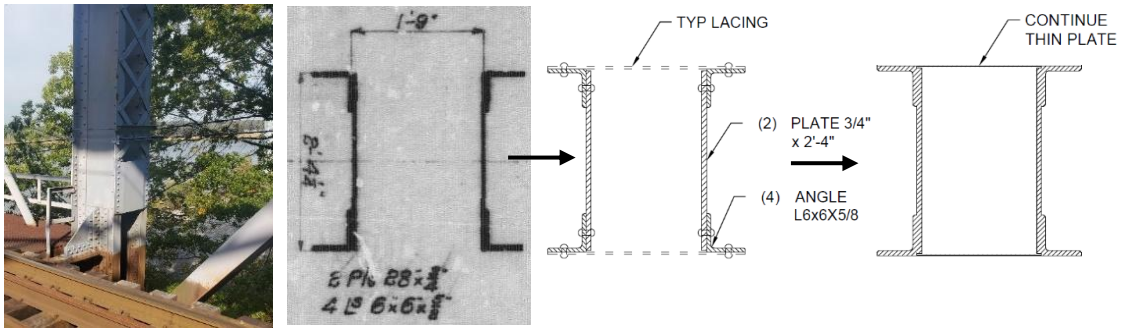

Figure 19 - Devon Bridge: Vertical post picture, original drawings, gross cross-section, and equivalent cross-section (left to right)

The bridge three-dimensional (3D) model has been created using ANSYS® modeling software SpaceClaim® (ANSYS Inc. 2009, Hatch 2000). The model was mainly developed using line elements and the boundary conditions were manually defined to represent the bridge behavior. The original drawings and field inspection reports (dating from the 1900s) were used to generate the gross cross-section and equivalent cross-section, respectively.

Two types of computational analysis were performed on the selected bridge spans: modal analysis and transient analysis (ANSYS Inc. 2009, Hatch 2000). The modal analysis results were initially used to calibrate and verify the global FE model in the frequency domain, through comparison with the field test data. Subsequently, the transient analysis results were used to calibrate and verify the FE model in the time domain, again through comparison with the field test data. To represent the moving axles of vehicles, a series of triangular pulse loads were used in this study. The load time was defined by dividing the axle load spacing by the appropriate vehicle traveling speed. The integration time was defined in the software using sub-steps of the pulse load. This involves specification of a triangular pulse load, where the load begins at zero, increases to a maximum value, and then decreases back to zero within a specified duration. Additionally, the software has the capability to divide this triangular pulse load into equal parts, which facilitates better convergence of results.

Modal Analysis: The modal analysis, used to determine natural frequencies and mode shapes, is restricted to a free vibration, without prestressing and damping acting on the structure, using a constant mass and stiffness matrix. The structure has no time-varying forces or displacements (ANSYS Inc. 2009, Hatch 2000).

Transient Analysis: For the transient analysis solution, assuming that the initial conditions are known, the software uses the second-order system. The software employs the Newmark time integration method for solving the implicit transient analysis problem (ANSYS Inc. 2009, Hatch 2000).

2.4.1.1 Devon Bridge Finite Element Model

The global FE model in this study was generated using line elements and surface elements, where 33 different cross-sections were assigned to the 483 members, including eye bars, stringers, floor beams, and diagonals. The top chord members, vertical posts, floor beams, stringers, hangars, and bracing members were modeled as beam elements (BEAM188). The built-up diagonals from nodes L2 and L12 were modeled as link/truss elements with tension and compression behavior (LINK8). The bottom chord members and diagonal eye bars were modeled as link/truss elements with tension-only behavior (LINK10). The support bearings and portal frame corner plates were modeled using a shell element (SHELL41). All the cross-sections and thicknesses were assigned in accordance with existing conditions. **Figure 20** shows the FE elements used for the global model (ANSYS Inc. 2009). This figure illustrates that using line elements reduces the total number of degrees of freedom associated with the model, which reduces the computational effort needed to solve the model. The cross sections assigned to truss members in the FE model are shown in **Appendices B and C**. The following material properties, representative of steel, were used for FE modeling of the Devon Bridge: Density (ρ): 7860 kg/m^3; Young's modulus (i.e., modulus of elasticity) (E): 200 GPa; Poisson's ratio (ν): 0.3.

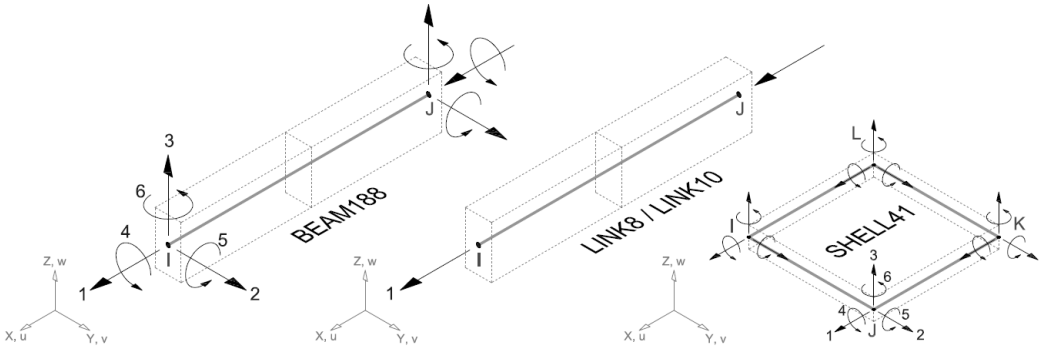

Figure 20 - Global FE model elements: BEAM188 (left), LINK8/LINK10 (middle), SHELL41 (right)

Figure 21 shows the 3D model of the Devon bridge. While the line model and proper boundary conditions are shown on the left, the rendered view (displaying the assigned cross-sections) is shown on the figure's right. The mesh was generated with 19527 nodes and 10740 elements and an average mesh element size of 4.64 inches (117.86 mm).

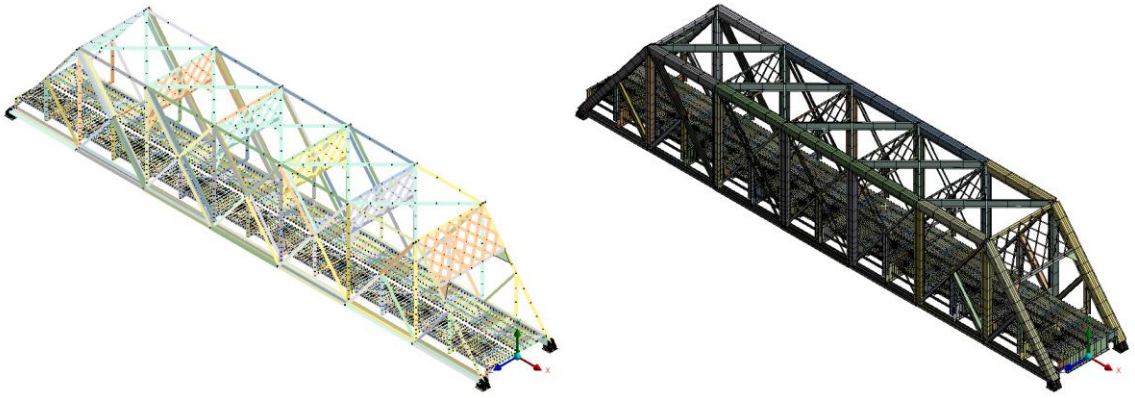

Figure 21 - Devon Bridge: (left) FE model meshed with line elements, (right) rendered view of the model

2.4.1.2 Cos Cob Bridge Finite Element Model

The global FE model of span 3 (track 4) of the Cos Cob Bridge was developed using commercial FEA software package ANSYS and is based on an 'as-built' drawing (Under Water Construction, 1990), repair plan drawing (A.G. Lichtenstein & Associates, 1998), and load rating report (Clough, Harbour, and Associates, 2010). The model was developed using wire elements and the boundary conditions were manually defined to represent the bridge supports and connections. The support conditions of the bridge include a longitudinal spring on the west side that allows movement along the x-axis (i.e., the longitudinal axis in the horizontal plane) while restraining movement along the y and z axes (i.e., the vertical axis, and the lateral axis in the horizontal plane, respectively), whereas the east side of the bridge is fully restrained in all three directions (i.e., along the x, y, and z axes). (**Figure 22**). The cross sections were assigned to the wire elements of the bridge according to the as-built drawing. The bottom chords, top chords, side diagonals and vertical members connected to them, and two vertical members on the end of the bridge are considered beam elements while other members are assumed to be truss elements. For the ties, oak wood properties were assigned and for all other members, structural steel properties were specified. The following material properties were specified for the structural steel members during the FE analysis of the Cos Cob Bridge: Density (ρ): 7850 kg/m^3; Young's modulus (i.e., modulus of elasticity) (E): 200 GPa; Poisson's ratio (ν): 0.3; Yield strength (σ_y): 250 MPa; Ultimate strength (σ_u): 460 MPa. For the oak wood ties, the following material properties were specified: Density (ρ): 935.7 kg/m^3; Young's modulus (i.e., modulus of elasticity) (E): 22.78 GPa; Poisson's ratio (ν): 0.3742; Yield strength (σ_y): 47.76 MPa; Ultimate strength (σ_u): 146.7 MPa. The picture on the left in **Figure 22** depicts the 3D FE wire model of Span 3 of the Cos Cob Bridge, and the picture on the right shows the rendered view of the model.

.

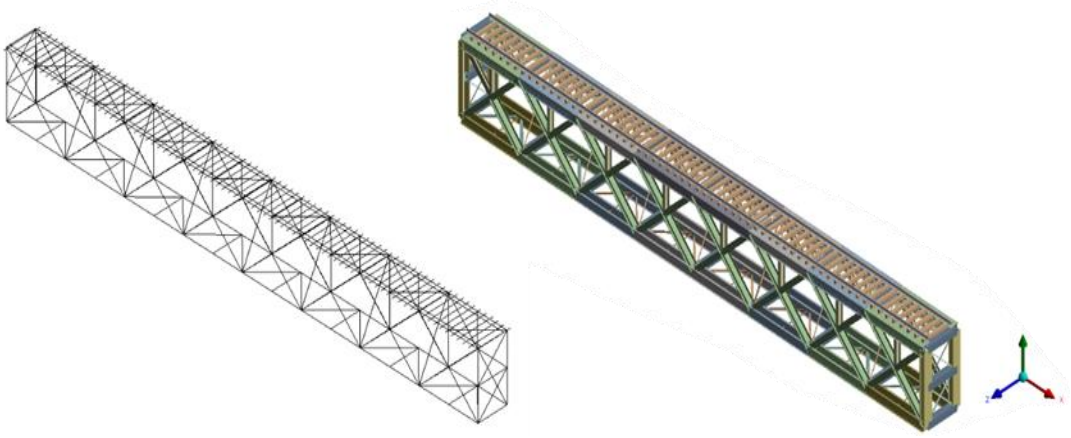

Figure 22 - Cos Cob Bridge FE model (a) 3D wire model; (b) Rendered view.

2.4.1.3 Tilton-Belmont Bridge Finite Element Model

The global FE model of the Tilton-Belmont bridge was constructed using commercial Finite Element (FE) software, ABAQUS 6.19-1. The 3D bridge span model of the Tilton-Belmont bridge (length: 123.75'; width:12'; height:14') was created using 483 members in wire elements, with 33 different cross-sections, such as eye bars, stringers, floor beams, and diagonals. **Figure 23** presents the 3D rendered view of the bridge modeled in ABAQUS.

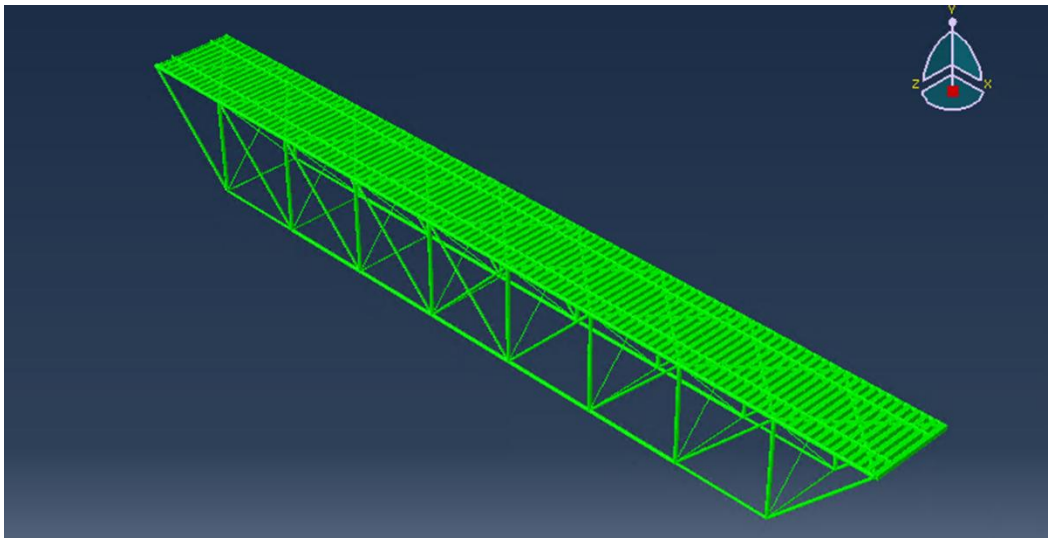

Figure 23 - Rendered View of 3D FE Wire Model of Tilton-Belmont Bridge

The finite element (FE) model of the Tilton-Belmont Railroad Bridge was developed using 1893 as-built design drawings. A total of 736 elements were used, with 644 being B31 beam elements (3D, 2-node linear beam element based upon the Timoshenko beam theory with six d.o.f per node), for components such as the top chord, rails, ties, stringers, and floor beams, capturing their bending and axial behavior. The remaining 92 elements were T3D2 truss elements (3D, 2-node linear truss element with three d.o.f per node), representing the bottom chord, diagonals, sway bracing, and lateral bracing, which primarily experience axial forces. Connections were modeled based on the original drawings as well, with either pinned or fixed connections used between the members, depending on the specific requirements of the design. The following material properties,

representative of steel, were used for the FE analysis of the Tilton-Belmont Bridge: Density (ρ): 7800 kg/m^3; Young's modulus (i.e., modulus of elasticity) (E): 200 GPa; Poisson's ratio (ν): 0.2; Yield strength (σ_y): 250 MPa. The boundary conditions were modeled as simply supported, with hinge and roller supports to replicate the bridge's real-world response. This model enabled detailed static and modal analyses, assessing the bridge's structural integrity and performance.

Chapter 3: Results and Discussion

The following chapter presents the findings of the sensitivity/calibration study, the parametric/optimization study, and the methodology employed to identify critical members using performance-based analysis. The initial step involves using limited field test data to assess the finite element model in both time and frequency domains. Subsequently, a parametric study was conducted to gain a deeper understanding of the capabilities and constraints of the computational model. Finally, various finite element analyses of the optimized model were carried out to replicate the service conditions at a performance-based level for the selected bridges to identify critical members and connections.

3.1 Devon Bridge

The LDV field test has shown consistent bridge displacement responses (which were measured at several different nodes) across various service trains for a given measurement location, as well as reasonably consistent estimates of natural frequencies during free vibration. The performance reports for the Devon bridge indicate that the loss of cross-section due to corrosion as well as wear-and-tear governs the medium- to long-term changes in stiffness. The FE analysis results were compared with field test data, and sensitivity factors for selected nodes were calculated using the maximum and minimum displacements due to MTNR M8 loading. Bridge natural frequencies were compared using a normal distribution to account for variations in the identified natural frequencies in the field test data and the cross-section loss from the FE model. Finally, critical members were identified using a combination of a score-based method and performance rating reports.

3.1.1 Field Test Results and Comparison with FE Model Predictions

The field test results were used as a baseline for the sensitivity analysis study of the computational model. In this study, the MTNR M8 train was utilized for model validation and necessary calibration to represent the current conditions of the South Bridge of Devon Bridge span 7. The LDV data recorded from four nodes, L10, L11, L12 and L13 from south span of the section of the bridge selected for this study, was converted to displacement response and frequency response to be evaluated in the time and frequency domains, respectively.

Figure 24 - Devon Bridge: Velocity response recorded using the LDV for two MTNR M8 trains: Train 1 (left) and Train 6 (right)

shows the velocity response recorded using the LDV. The LDV response was divided into two parts, the forced and free vibrations. The forced vibration part contains information relating to the effect of the vehicle's traversal of the bridge, whereas the free vibration part contains information relating to the bridge behavior after the vehicle crosses the bridge span.

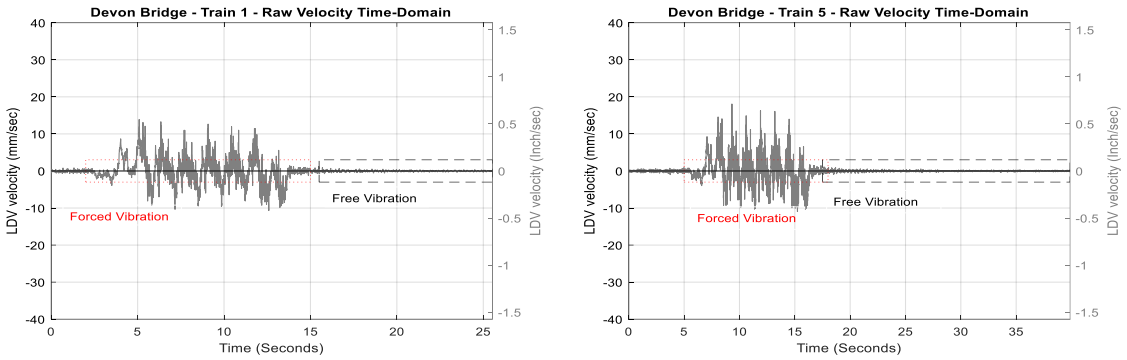

Figure 24 - Devon Bridge: Velocity response recorded using the LDV for two MTNR M8 trains: Train 1 (left) and Train 6 (right)

In this study, the forced vibration part of the data was used to estimate the displacement response when the train is crossing the bridge span, and the free vibration part was used to estimate the bridge span natural frequency. The data was processed using the theory described previously, in the Data Processing section. The displacement response when the train is crossing the bridge, and the bridge span natural frequencies, were estimated using the LDV data and verified with accelerometers.

Figure 25 and **Figure 26** show the displacement response obtained from the LDV readings. The plot depicts three different recordings of the MTNR M8 traveling in the same direction, at approximately the same speed, with different numbers of cars.

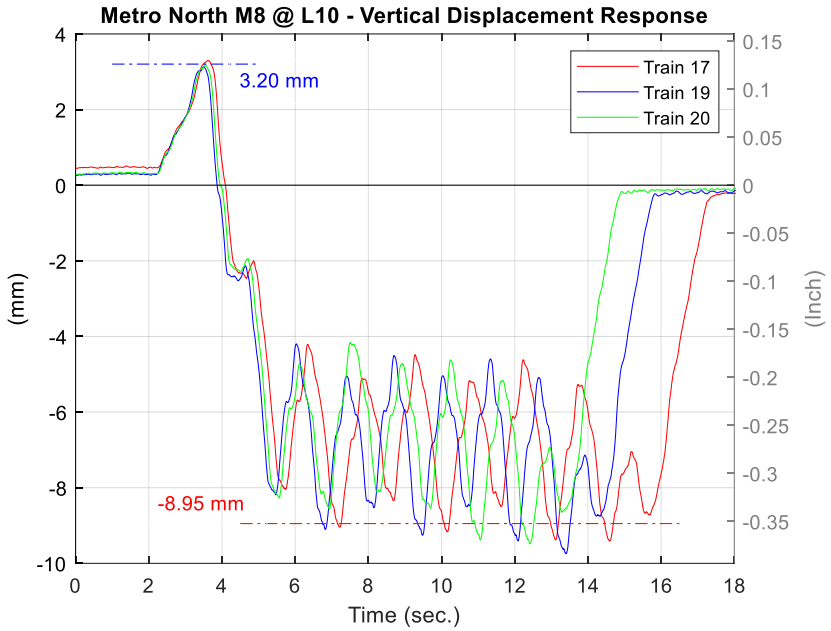

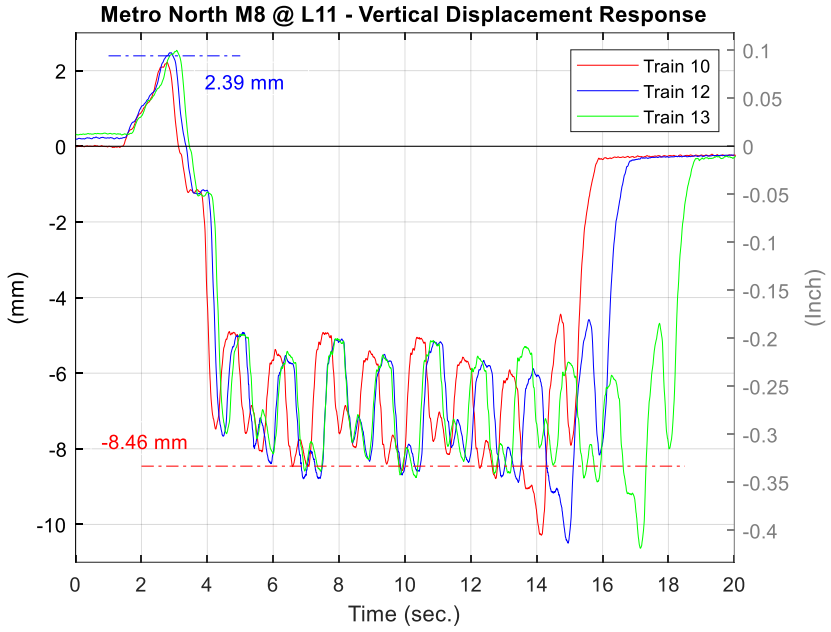

Figure 25 - Devon Bridge: LDV-based vertical displacement response of MTNR M8, Node L10 (upper), Node L11 (lower)

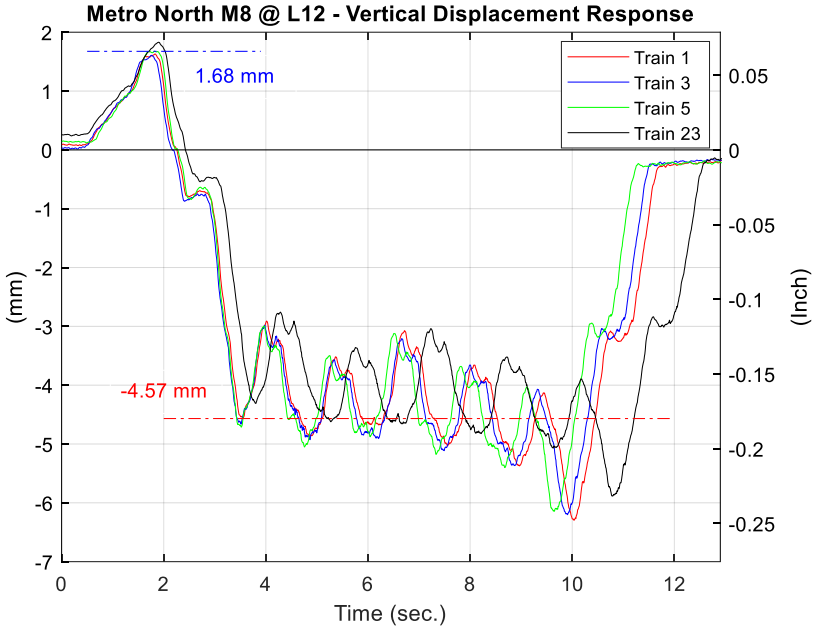

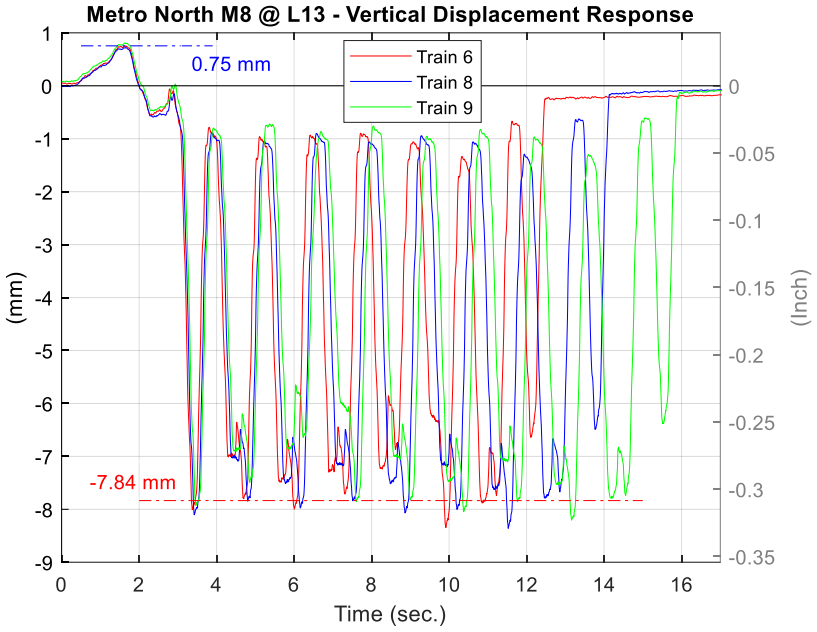

Figure 26 - Devon Bridge: LDV-based vertical displacement response of MTNR M8, Node L12 (upper), Node L13 (lower)

The LDV displacement response data shows consistent trends across different MTNR M8 trains. The results recorded for other trains, such as AMTK Regional and Acela, show the same consistency, although due to the limited number of recordings these results are shown only to demonstrate the consistency of the recorded data. **Figure 27** shows the vertical displacement response, obtained from LDV recordings for Amtrak trains, at nodes L11 and L12.

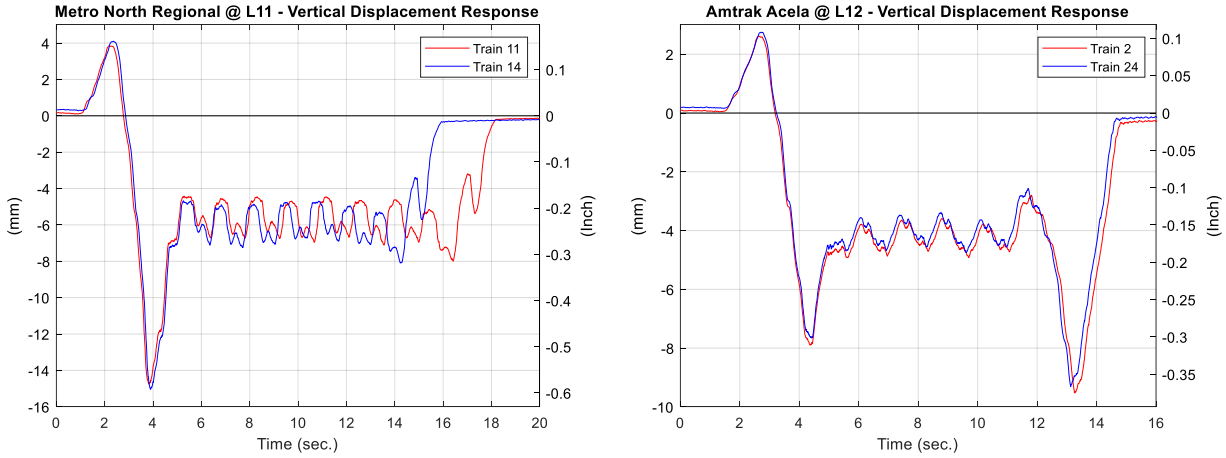

Figure 27 - Devon Bridge: LDV vertical displacement response of Amtrak trains at Node N11, Regional (left), Acela (right)

The displacement response from LDV and the field test were compared with the result from the FE model under similar operational conditions, such as train type, traveling speed and approximately the same point of response. **Figure 28** shows the displacement response from node N12 under Train 23 recorded in the Fall 2023 test. Train 23 is an MTNR M8 with six car composition traveling at approximately 41 mph. Similar operational conditions were replicated in the FE model under a transient analysis, and the displacement results were used as a basis of comparison to evaluate the model behavior.

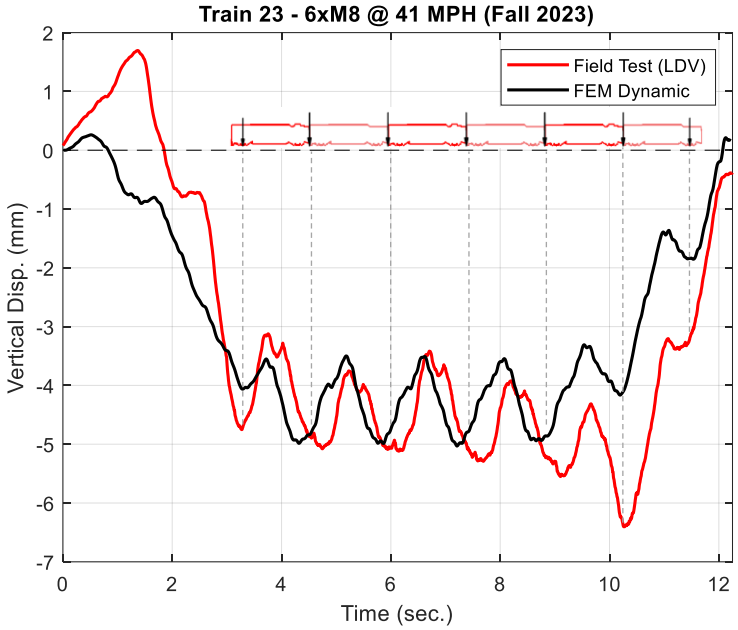

Figure 28 - Devon Bridge: Displacement response comparison of the LDV and FE model under Train 23

Similar analysis has been performed for other train types that operated on the Devon Bridge. **Figure 29** shows the displacement comparison of the field test and the FE model for the AMTK Regional and Acela at nodes L12 and L11 respectively.

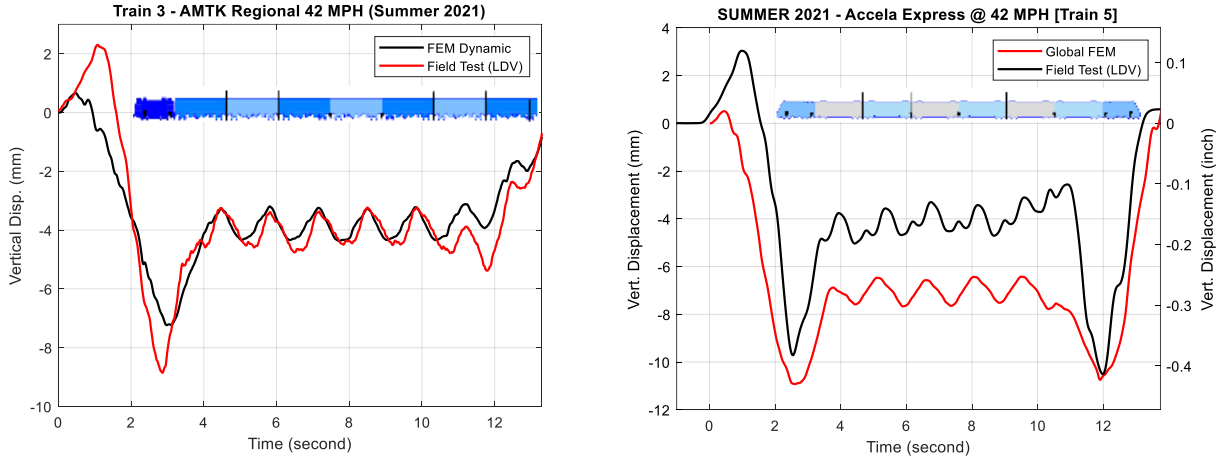

Figure 29 - Devon Bridge: Displacement response comparison of the LDV and FE model under Train 3 (left) and Train 5 (right)

Since the LDV and accelerometers were synchronized and recorded from different locations from node N12, the velocity response of the LDV was converted to acceleration and qualitatively and quantitatively compared with the acceleration response from the accelerometers. **Figure 30** - Devon Bridge: Acceleration comparison of LDV and accelerometers at node L12: Train 3 (left), Train 5 (right) shows acceleration response plots from the Train 3 and Train 5 reading at node N12 using the LDV (top graph) and accelerometers (bottom graph).

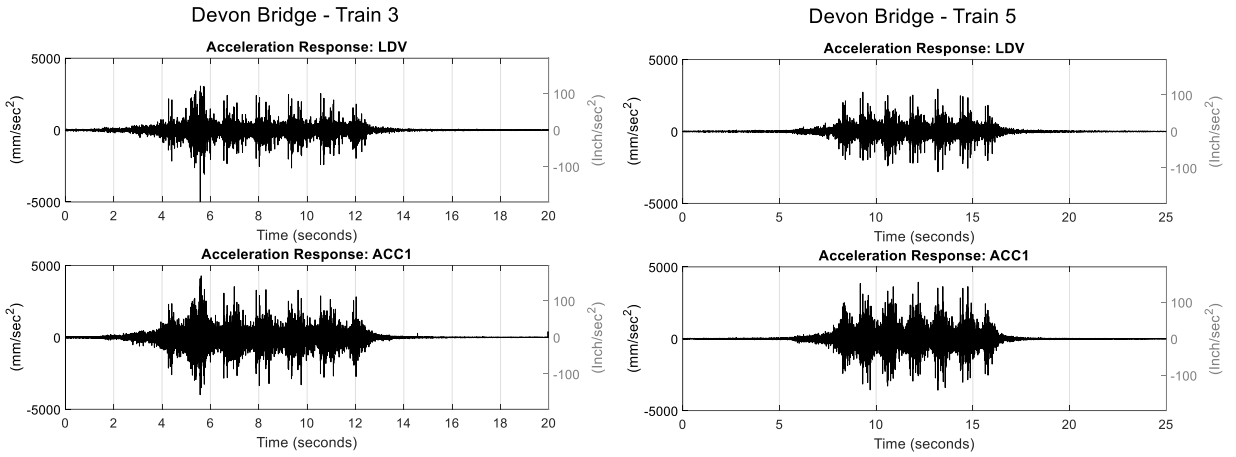

Figure 30 - Devon Bridge: Acceleration comparison of LDV and accelerometers at node L12: Train 3 (left), Train 5 (right)

The bridge span natural frequencies were estimated using the FFT plots from frequency domain analysis. The frequency peaks were identified from the frequency range of 0 to 10 Hz based on past research experience. The frequencies (**Figure 31** - Devon Bridge: FFT of the free vibration of LDV for MTNR M8: Train 1 (left), Train 5 (right)) were identified in most of the data depending on the node and the bridge natural frequencies.

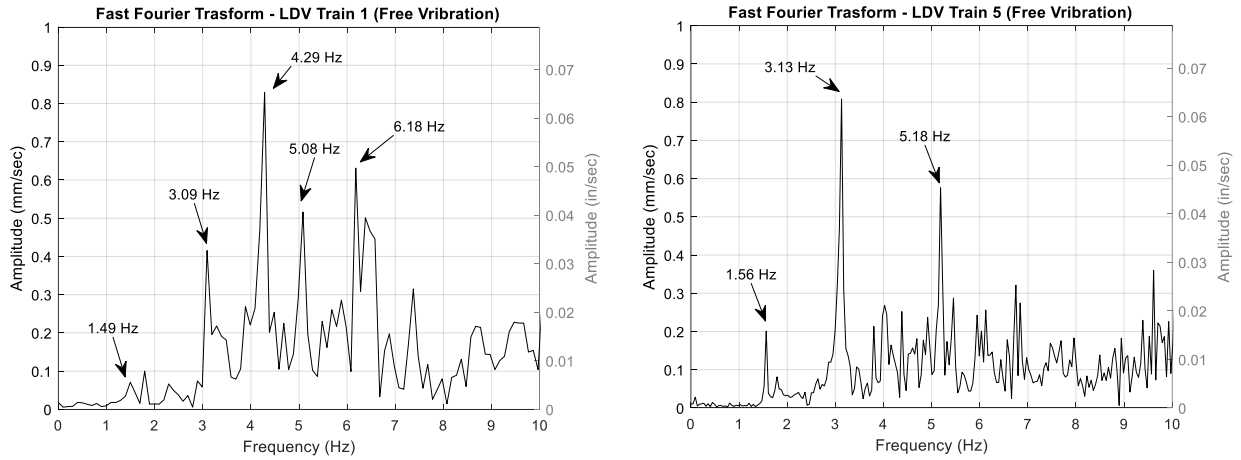

Figure 31 - Devon Bridge: FFT of the free vibration of LDV for MTNR M8: Train 1 (left), Train 5 (right)

The natural frequencies from the bridge span were estimated using a pick-and-choose method and limited to the bandwidth of the free vibration data. The identified natural frequencies from all the recording data were averaged. **Table 5** shows the average and the standard deviation of the identified bridge span natural frequencies.

Table 5 - Devon Bridge: Natural frequencies identified using LDV during field tests

Bridge Frequency / Mode	1st Lateral	1st Torsional	2nd Torsional	1st Vertical	2nd Lateral	3rd Torsional
Average Nat. Frequency (Hz)	1.620	2.492	3.121	4.241	5.135	5.980
Standard Deviation (Hz)	0.131	0.101	0.032	0.097	0.057	0.252

The design points (DP), which represent the variation of the average cross-section loss of the eye bars, have been established using technical reports on the bridge's performance. The cross-section loss is the primary factor for the parametric study. The cross-section loss ranges from the original conditions (DP0) to double the average of the current cross-section loss (DP8).

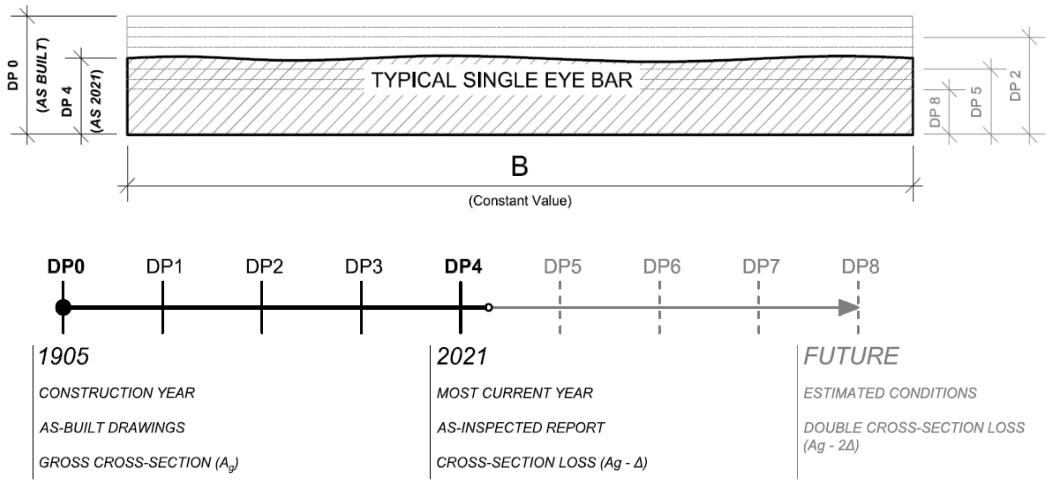

Figure 32 - Devon bridge: Typical single Eye bar with thickness variation (upper), time variation of the parameterized cross-section loss of the Eye bars (lower)

In **Figure 32**, the upper section displays a typical single-eye bar, and the assumed cross-section loss used in a performance-based parametric study. The eye bars are categorized into ten types, with a constant width (8 or 10 inches) and a parameterized thickness. The lower part of the figure illustrates the cross-section loss over time, ranging from DP0, representing the original condition in 1905, to DP8, a future scenario. According to the technical report, the current condition of the bridge span is estimated to be between DP4 and DP5.

The FE model was developed under the same conditions, incorporating a parametric eye bar thickness variation to simulate theoretical cross-section loss. This parameterized study assessed the bridge's characteristics and response under decreasing cross-sectional areas of members, which were then compared with the field test data under current conditions.

3.1.2 Finite Element Analysis: Displacements and Natural Vibration Modes

The FE model was verified using the field test data from LDV as a baseline for the comparison. The comparison was made in time and frequency domains using the vertical displacement time histories from the forced vibration part of the response and bridge natural frequencies from the free vibration part of the response, respectively. The verification process was carried out using the MTNR M8 train, which was chosen because of its uniform axle load, and also because it is a frequent user of the bridge.

The node displacement response derived from the LDV was averaged and used to compare the typical downward displacement under the wheel loads (denominated here as "axle displacement") as well as the initial upward displacement (denominated here as "uplift") observed in the LDV-based vertical displacement response plots (see Figures 25 and 26). The average field test axle displacement and uplift are as shown in Figure 33 and Figure 34, in red and blue, respectively. The ratio of the field test displacement response and the computational (FE) model response at different Design Points (DP) was used to better assess the accuracy of the FE model.

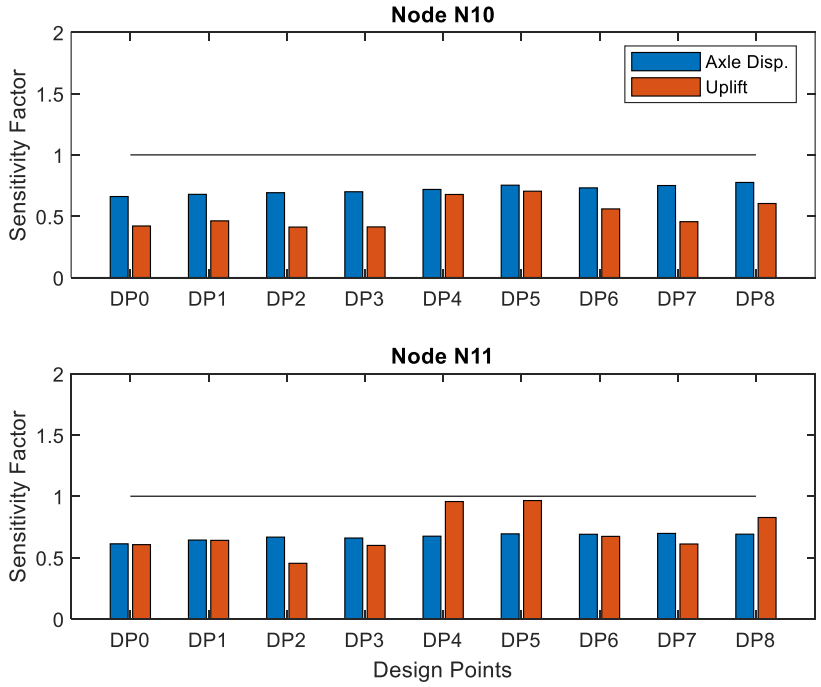

Figure 33 - Devon Bridge: LDV Sensitivity Factor vs Design Points of MTNR M8, Node L10 (upper), Node L11 (lower)

Figure 33 and **Figure 34** show the comparison of the axle displacement and uplift sensitivity ratio for nodes L10, L11, L12 and L13. The values closest to one indicate a better compatibility between the FE model at different conditions (DP) and the real-life response (field test).

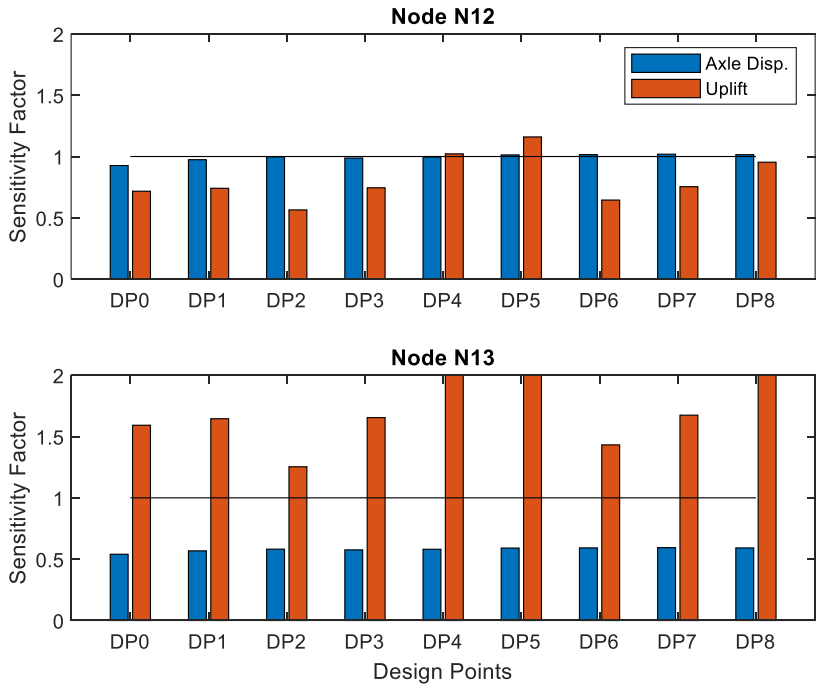

Figure 34 - Devon Bridge: LDV Sensitivity Factor vs Design Points of MTNR M8, Node L12 (upper), Node L13 (lower)

Modal analysis of the FE model identified six global modes of vibration. The first mode is lateral, the second and third are torsional modes, the fourth is the vertical mode, the fifth is a second lateral mode, and the sixth is the third torsional mode. **Figure 35** shows the frequency variation of the identified modes of vibration obtained using the FE model, for different Design Points.

The natural frequencies identified from the field test using the LDV were represented in the form of a normal distribution using the average and the standard deviation of the observed values. Additionally, modal analyses conducted on FE models representing the condition of the Devon Bridge at different Design Points predicted changes in natural frequencies with deterioration of the bridge's condition, as expected. These variations are shown in **Figure 35.**

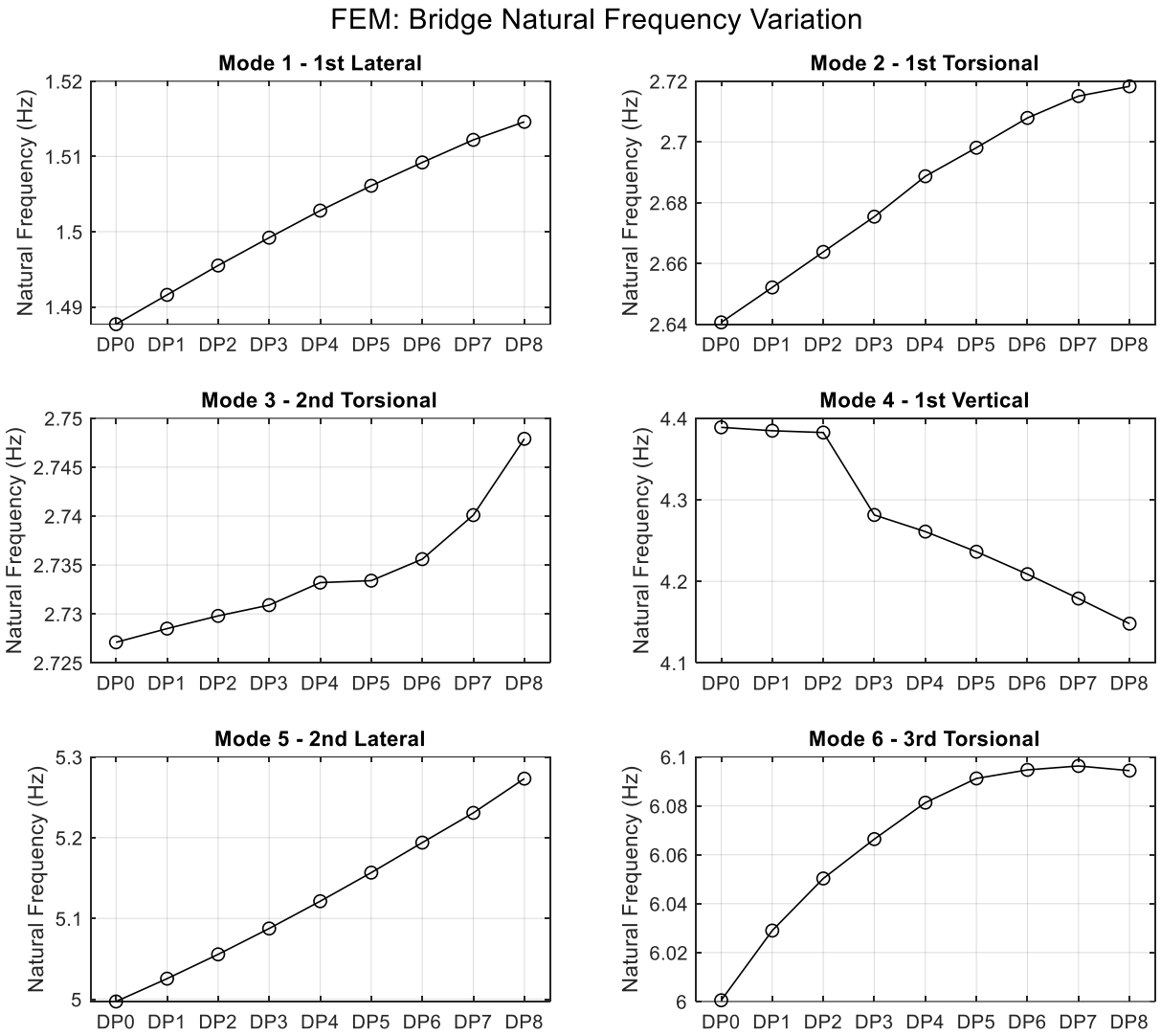

Figure 35 - Devon Bridge: Natural frequencies variation of bridge modes of vibration identified using the FE model at different design points

As corrosion- and fatigue-related effects reduce the cross-sectional area of a structural member, its stiffness decreases, which typically leads to a reduction in natural frequencies. However, it should be noted that the mass of the member is also likely to decrease due to the loss of cross-sectional area. Thus, it is plausible that this reduction in mass may be more than sufficient to counterbalance the loss of stiffness, especially in the lateral and torsional vibration modes, in which the reduced stiffnesses of individual structural members may not significantly affect the overall global structural response. This may explain the overall increase in natural frequencies, with loss of cross-sectional area, seen in Figure 35 for the lateral and torsional modes of vibration of the structure.

On the other hand, for the vertical modes of vibration, the overall expectation is that the natural frequency would actually decrease as the structure experiences corrosion- and fatigue-related effects, including reduction in stiffnesses of individual structural members due to reduction in cross-sectional areas of the members. This expected decrease in natural frequency is indeed noted for Mode 4 (which is a vertical vibration mode) in Figure 35.

Figure 36 shows the normal distribution of the identified bridge span natural frequencies from field tests and the FE model. The figure graphically shows the correlation of the bridge natural frequencies, where most of the modes except mode 3 are within acceptable overlapping range.

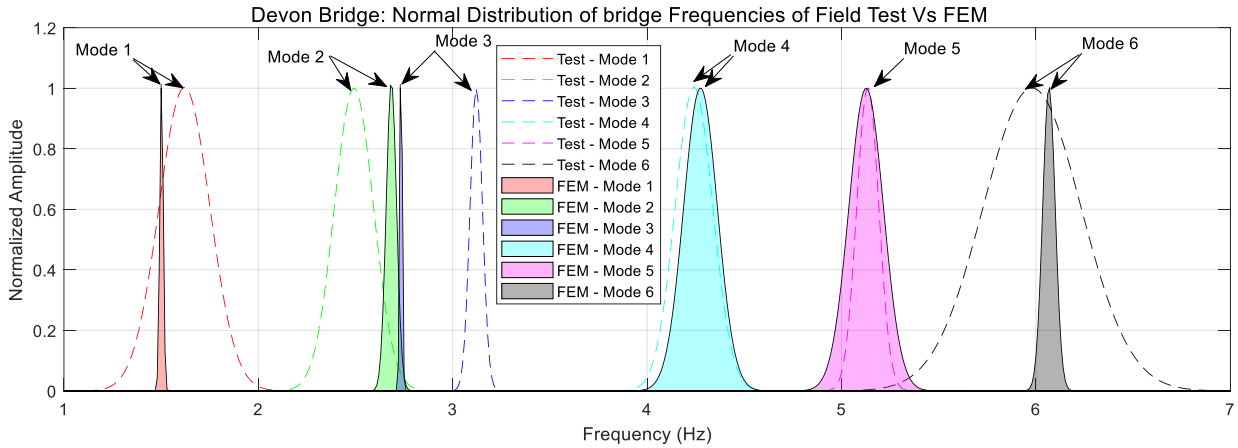

Figure 36 - Devon Bridge: Normal Distribution of bridge Frequencies of Field Test Vs FEM

Comparisons of the field test data and the FE model in time and frequency domains show good agreement, and it can be concluded that DP4 and DP5 closely represent the current conditions of the bridge span.

3.1.3 Identification of Critical Members and Connections

The critical members were identified using the following parameters: the reported member ratings and cross-section loss data obtained from the load rating report, the Cooper equivalent for the train specific, obtained from static analysis of the FE model, and the dynamic effects of the train specific on the bridge span, obtained from transient analysis of the FE model. The train specific is defined as the typical equipment primarily used on the Devon Bridge, in this case the MTNR M8, AMTK Regional, and AMTK Acela.

The Load Rating (LR) reports (Lochner & TranSystem 2021) provided valuable insights regarding current bridge conditions, including current data on cross-section loss. The six (6) selected critical members were identified using the LR reports.

Since the AREMA Cooper load does not represent the current loading conditions of the bridge, it was decided to convert the equipment specific into the Cooper equivalent to correlate both trains and identify the critical member within the selected list of members. The Cooper equivalent load (AREMA 2022) for the equipment specific (E_{XX}), for a particular member, was calculated by dividing the maximum axial force response due to the equipment specific (S_{sp}) by the maximum axial force due to one-half of the AREMA Cooper load (S_{E40}) as shown in **Equation 6**.

$$E_{XX} = \frac{S_{sp}}{S_{E40}} \times 40$$

Equation 6

Figure 37, **Figure 38** and **Figure 39** show the equipment-specific axial response converted to AREMA Cooper equivalent load using **Equation 6**.

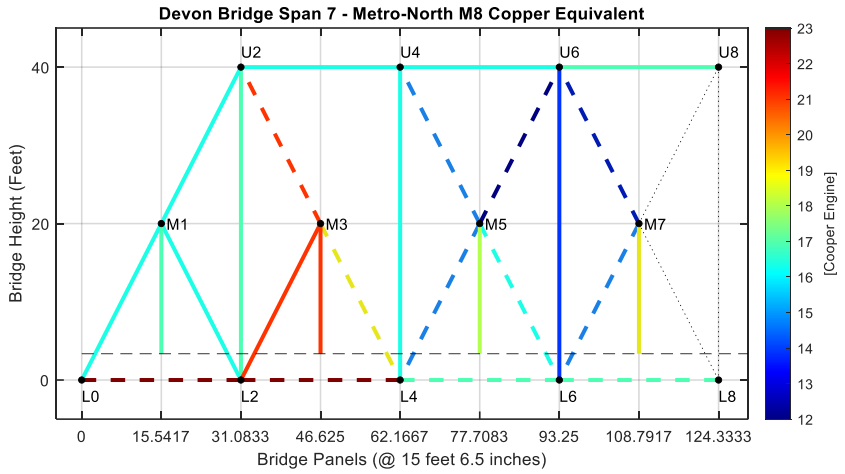

Figure 37 - Devon Bridge: MTNR M8 AREMA Cooper Engine Load Equivalent

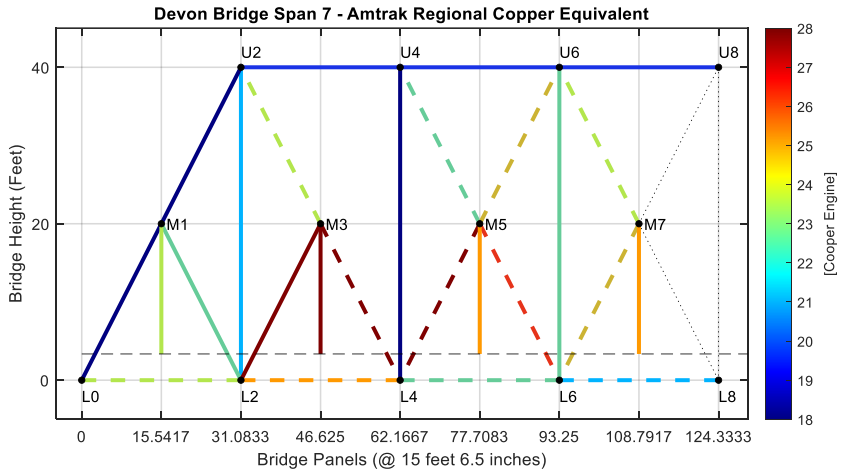

Figure 38 - Devon Bridge: AMTK Regional AREMA Cooper Engine Load Equivalent

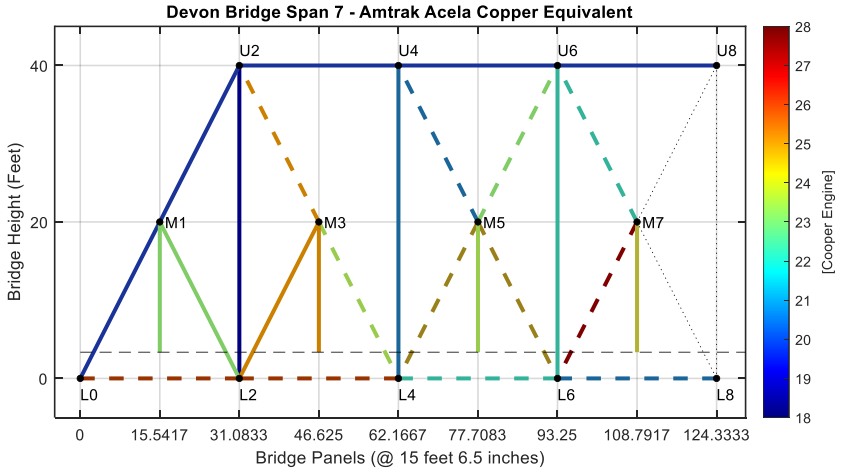

Figure 39 - Devon Bridge: AMTK Acela AREMA Cooper Engine Load Equivalent

The other important factor in identifying critical members is the interaction of the train equipment specific with the bridge span. This was achieved by utilizing the results of the transient FE analyses at different vehicle traveling speeds. The AREMA Chapter 15 (AREMA 2022) is only

applicable to a maximum vehicle traveling speed of 90 mph, and since the chances of operating at higher speed on the New Haven line are very low, the analysis was limited to 90 mph. This study used the FE model with conditions of the DP 4 and with a constant damping ratio of 5% for the transient analysis.

Figure 40 shows the Dynamic Magnification Factors (DMFs) of critical members, calculated as the ratio of the maximum axial force in a given member due to transient loading effects, to the axial force in the same member due to static loading.

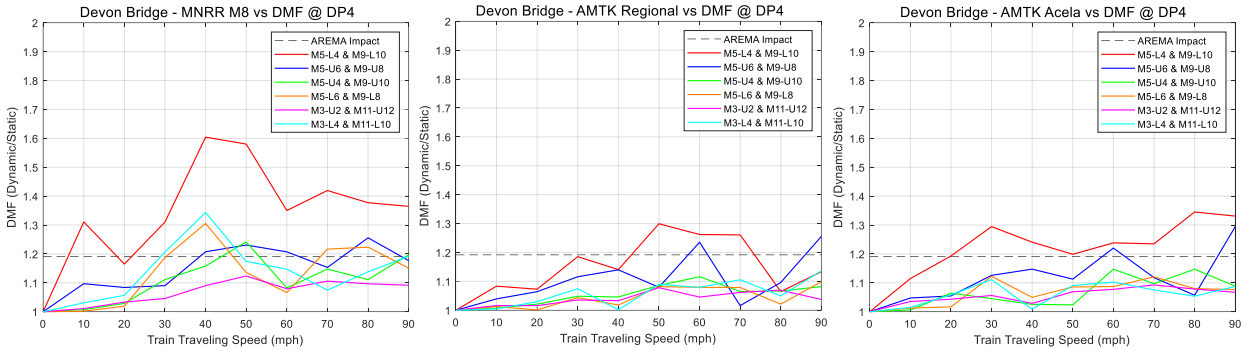

Figure 40 - Devon Bridge: Dynamic Magnification Factor (DMF) of critical members, MTNR M8 (left), AMTK Regional (center), and AMTK Acela (right)

Finally, the different factors determining a member's criticality, such as rating, cross-section loss, and the results of static and dynamic analyses, were used to allocate point-based scores, ranging from 0 to 5 points, to critical members. In this scoring method, a higher score corresponds to a worse condition or response. **Table 6** show the points allocated for different factors and the analysis used to identify critical members of Devon Bridge.

Table 6 - Table with score points used to identify critical members of Devon Bridge

Selected Member	LR Report		FEM - Cooper Equivalent			FEM - Dynamic Effect		
	Rating Report	Cross-Section Loss	MTNR M8	AMTK Regional	AMTK Acela	MTNR M8	AMTK Regional	AMTK Acela
M5-L4 & M9-L10	0	4	1	5	4	5	5	5
M5-U6 & M9-U8	1	5	0	2	1	4	4	2
M5-U4 & M9-U10	2	3	2	0	0	3	3	1
M5-L6 & M9-L8	4	1	3	3	3	2	1	3
M3-U2 & M11-U12	3	2	5	4	5	1	0	0
M3-L4 & M11-L10	5	0	4	1	2	0	2	4

The total points for each selected member were calculated and divided by the possible maximum achieved (40 points) to calculate the member criticality factor. **Figure 41** shows a bar graph of the selected members with member criticality factor calculated using **Table 6**.

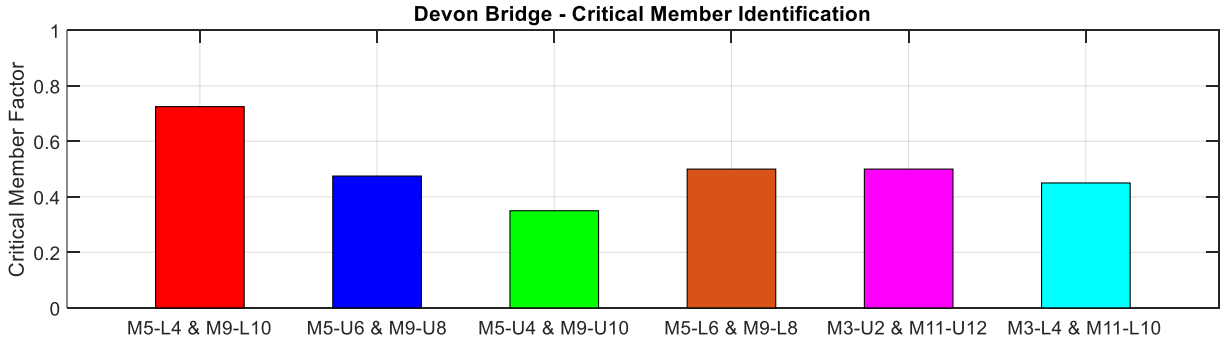

Figure 41 - Devon Bridge: Critical Member Factor for the selected members

The results show that the member M5-L4 & M9-L10 presents the highest member criticality factor based on the dynamic and bridge performance conditions.

3.2 Cos Cob Bridge

3.2.1 Field Test Results

The data from LDV and accelerometers collected from the field test were processed using MATLAB to obtain the vertical displacement time histories and the natural frequencies of the bridge. Both the LDV and accelerometer data were analyzed using the Fast Fourier Transform (FFT) algorithm to identify the natural frequencies of the bridge. **Table 7** presents the vertical peak displacement results of the different trains. **Figure 43**, **Figure 44** and **Figure 47** - Vertical Deflection of the Cos Cob Bridge @ Vib 3 represents the typical vertical displacement results of the Cos Cob bridge during the passage of Metro-North M8 trains at Vib 1, Vib 2, and Vib 3 respectively. **Figure 42** and **Figure 46** represent the typical vertical displacement of the the Cos Cob bridge at Vib 1 and Vib 2 during Amtrak Acela passage. **Figure 45** represents the vertical displacement of the Cos Cob bridge at Vib 2 during Amtrak Regional passage. **Table 8** and **Figure 48** present the natural frequencies of the bridge during the free vibration.

Table 7 - Vertical Displacement Results of Cos Cob Bridge

Train#	Train Type	LDV Location	Vertical Peak Deflection (mm)	Remarks
1	Metro North M8	Vib 1	-3.03711	Figure E1
2	Metro North M8	Vib 1	-3.29352	Figure E2
3	Metro North M8	Vib 1	-3.11985	Figure E3
4	Metro North M8	Vib 1	-3.28847	Figure E4
5	Metro North M8	Vib 1	-2.97532	Figure E5
6	Amtrak Acela	Vib 1	-4.31324	Figure 42
7	Metro North M8	Vib 1	-3.13323	Figure 43
8	Metro North M8	Vib 1	-3.07991	Figure E6
9	N/A	N/A	N/A	N//A
10	Metro North M8	Vib 1	-3.17142	Figure E7
11	Metro North M8	Vib 2	-3.23253	Figure E8

12	Metro North M8	Vib 2	-3.11557	Figure E9
13	Metro North M8	Vib 2	-3.0356	Figure E10
14	Metro North M8	Vib 2	-3.15103	Figure E11
15	Metro North M8	Vib 2	-3.05442	Figure 44
16	Amtrak Regional	Vib 2	-4.42897	Figure 45
17	Metro North M8	Vib 2	-3.08546	Figure E12
18	Metro North M8	Vib 2	-3.10057	Figure E13
19	Amtrak Acela	Vib 2	-4.35585	Figure 46
20	Metro North M8	Vib 3	-2.50185	Figure E14
21	Metro North M8	Vib 3	-2.63495	Figure E15
22	Metro North M8	Vib 3	-2.46849	Figure E16
23	Metro North M8	Vib 3	-2.6641	Figure 47
24	Metro North M8	Vib 3	-2.44095	Figure E17
25	Metro North M8	Vib 3	-2.64689	Figure E18

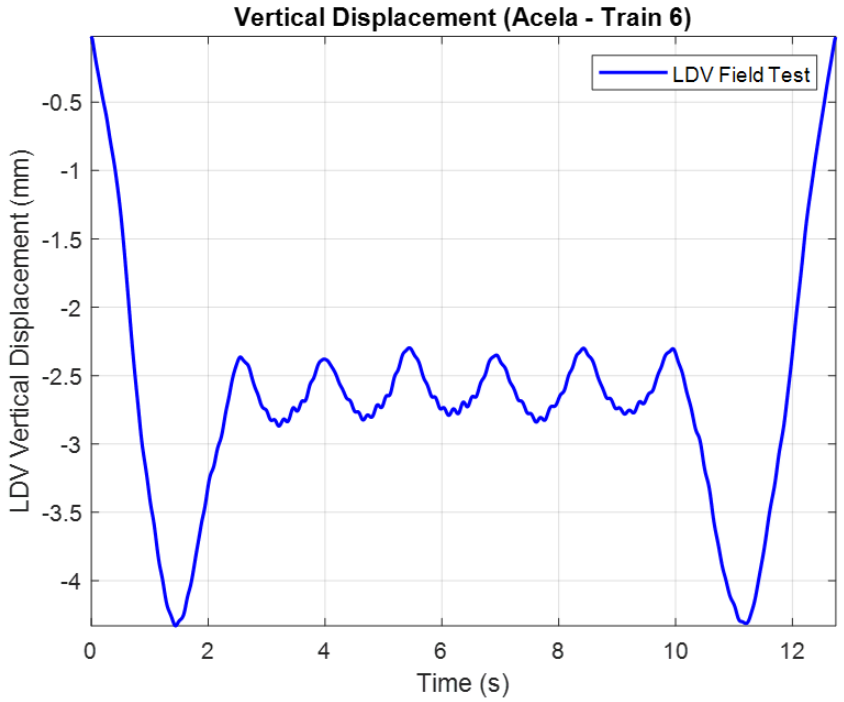

Figure 42 - Vertical Displacement of Cos Cob Bridge @ Vib 1 during Amtrak Acela Traversal (Train 6)

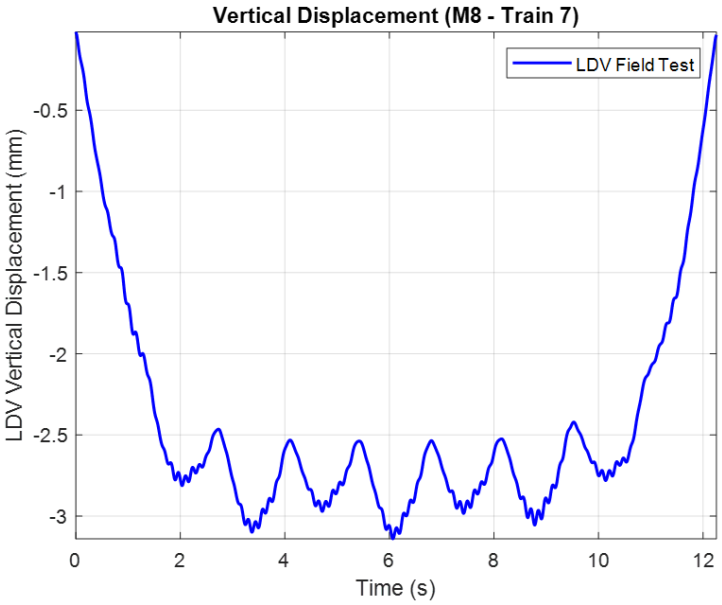

Figure 43 - Vertical Deflection of Cos Cob Bridge @ Vib 1 during Metro-North M8 Traversal (Train 7)

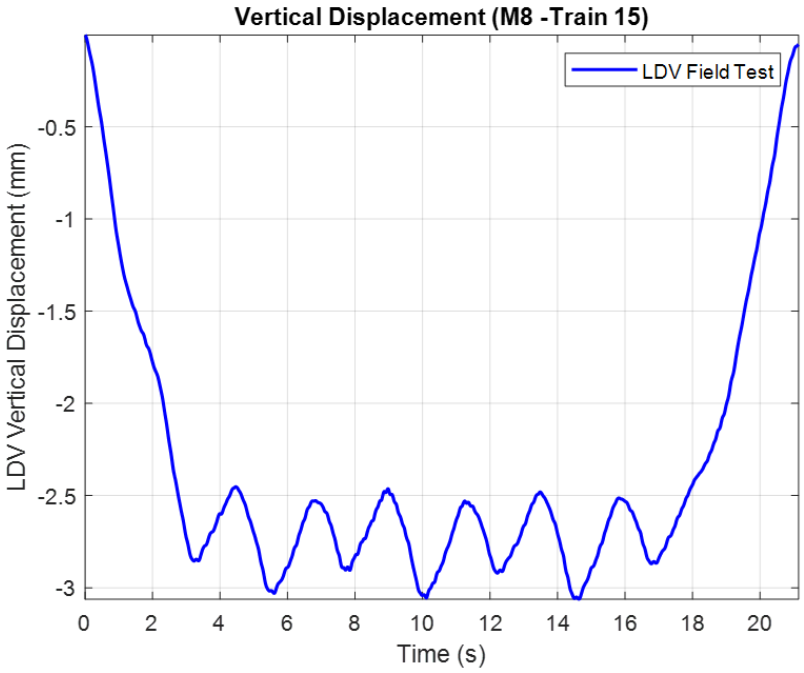

Figure 44 - Vertical Deflection of the Cos Cob Bridge @ Vib 2 during Metro-North M8 Traversal (Train 15)

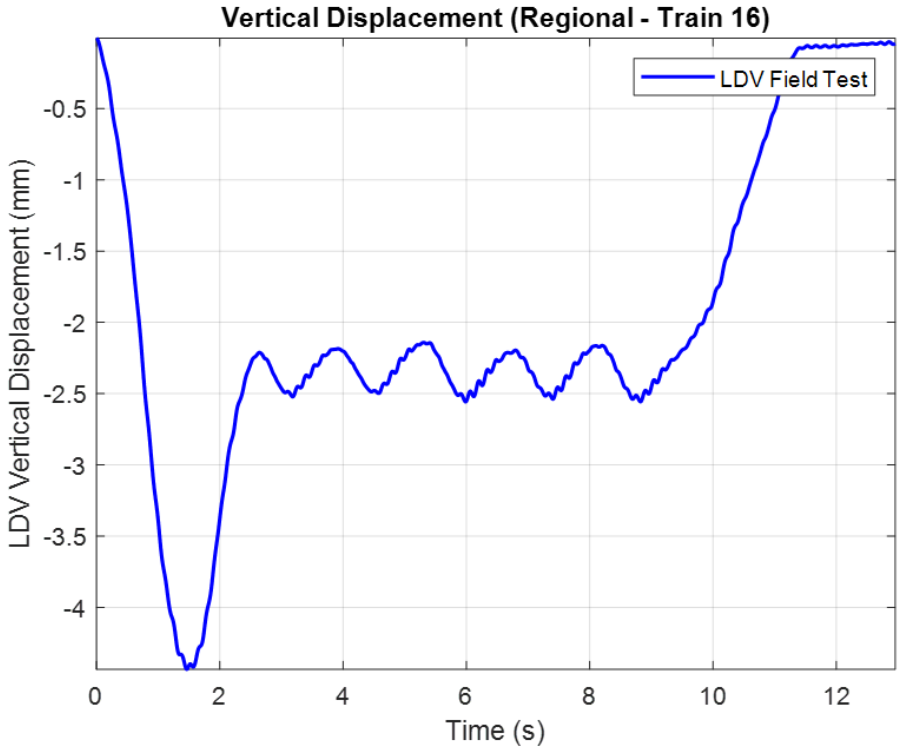

Figure 45 - Vertical Deflection of the Cos Cob Bridge @ Vib 2 during Amtrak Regional Traversal (Train 16)

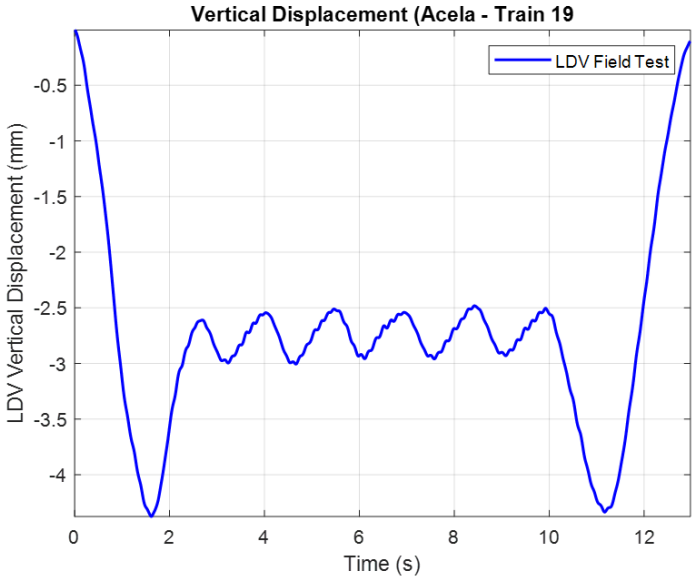

Figure 46 - Vertical Deflection of the Cos Cob Bridge @ Vib 2 during Amtrak Acela Traversal (Train 19)

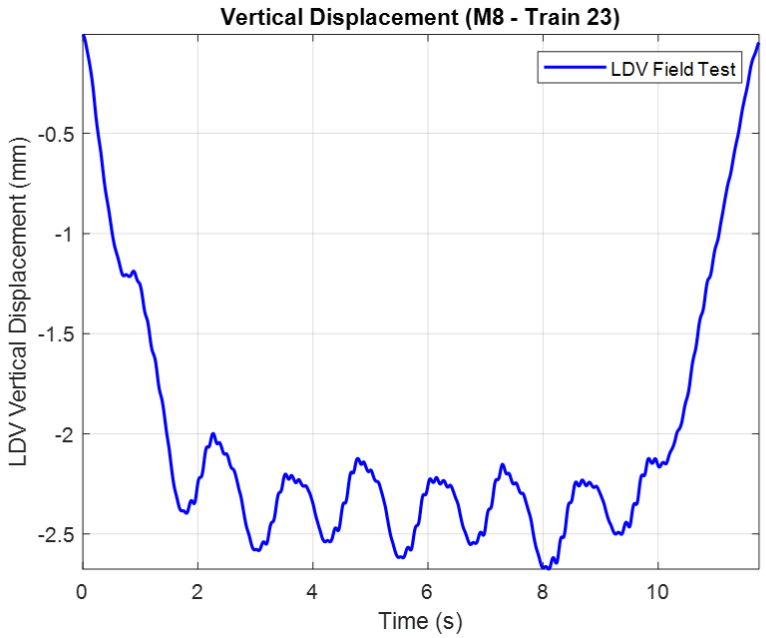

Figure 47 - Vertical Deflection of the Cos Cob Bridge @ Vib 3 during Metro-North M8 Traversal (Train 23)

Table 8 - Natural Frequencies of the Cos Cob Bridge during Free Vibration after Metro-North M8 Passage

Mode	Natural Frequency (Hz)
1st Lateral	3.22
2nd Lateral	8.51
1st Vertical	7.56

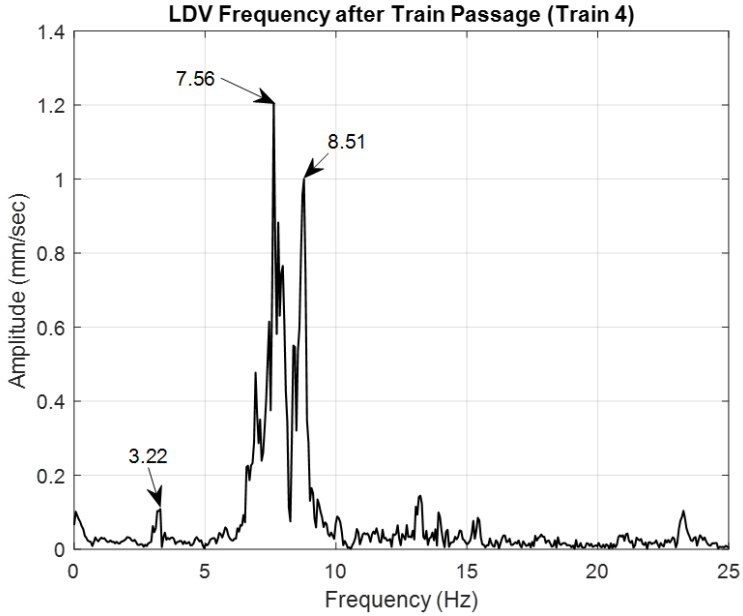

Figure 48 - Natural Frequency of the Cos Cob Bridge during Free Vibration after Metro-North M8 Traversal (Train 4)

The displacement responses from the field test were compared with the FE model results of the Cos Cob Bridge under similar operational conditions, such as train type, traveling speed, and approximately the same point of response. **Fig.** 49, **Figure 50** and **Figure 51** show the displacement results of the Cos Cob Bridge under Metro-North M8 train load at Vib 1, Vib 2, and Vib 3 respectively. **Figure 52** and **Figure 53** show the vertical displacement result of the Cos Cob Bridge under Amtrak Acela and Amtrak Regional train at Vib 2 respectively.

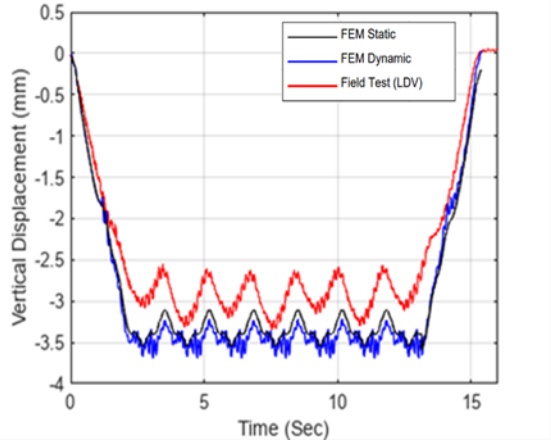

Fig. 49 Cos Cob Bridge Vertical Displacement @ Vib 1, Metro-North M8 Train Load, Train speed: 37 mph

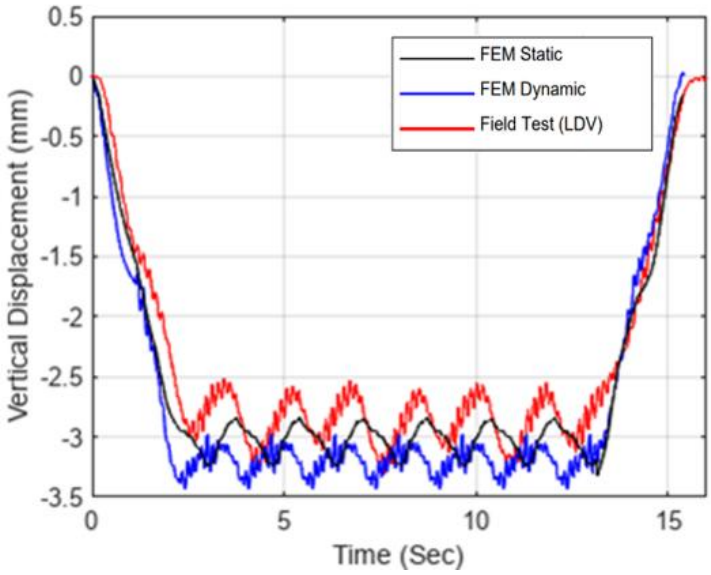

Figure 50 – Cos Cob Bridge Vertical Displacement @ Vib 2 under Metro-North M8 Train Load, Train speed: 37 mph

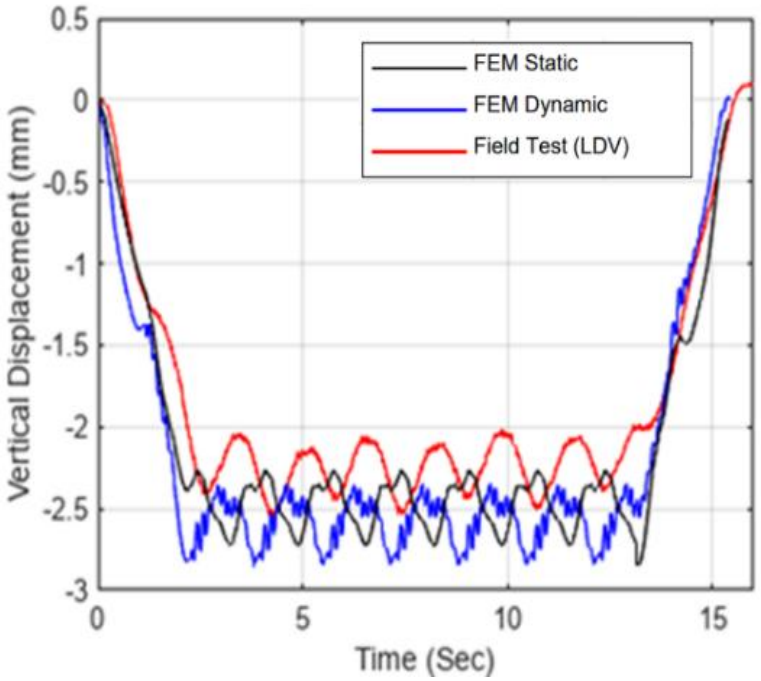

Figure 51 – Cos Cob Bridge Vertical Displacement @ Vib 3 under Metro-North M8 Train Load, Train speed: 40 mph

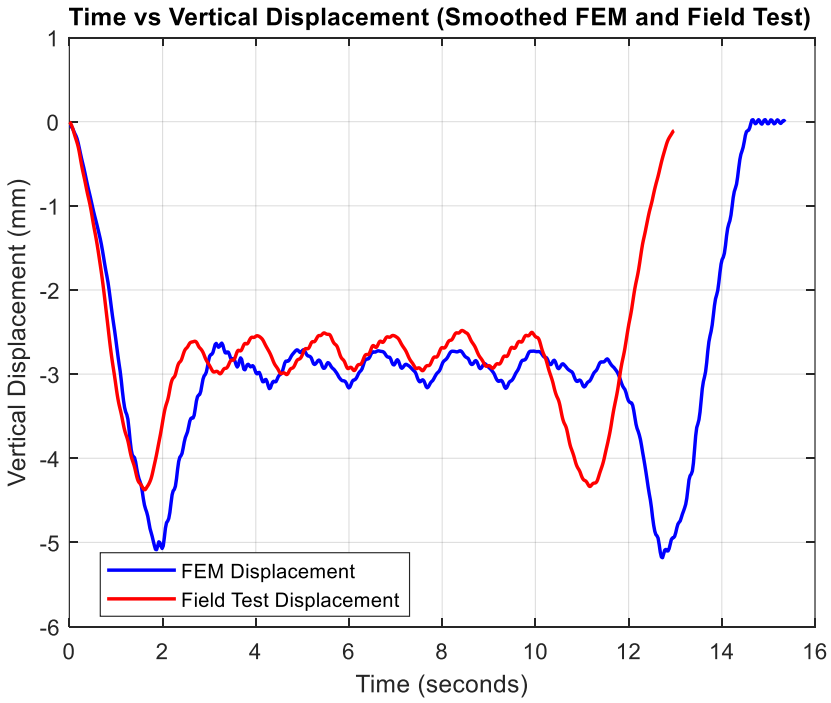

Figure 52 – Cos Cob Bridge Vertical Displacement @ Vib 2 under Amtrak Acela Train Load, Train speed: 35 mph

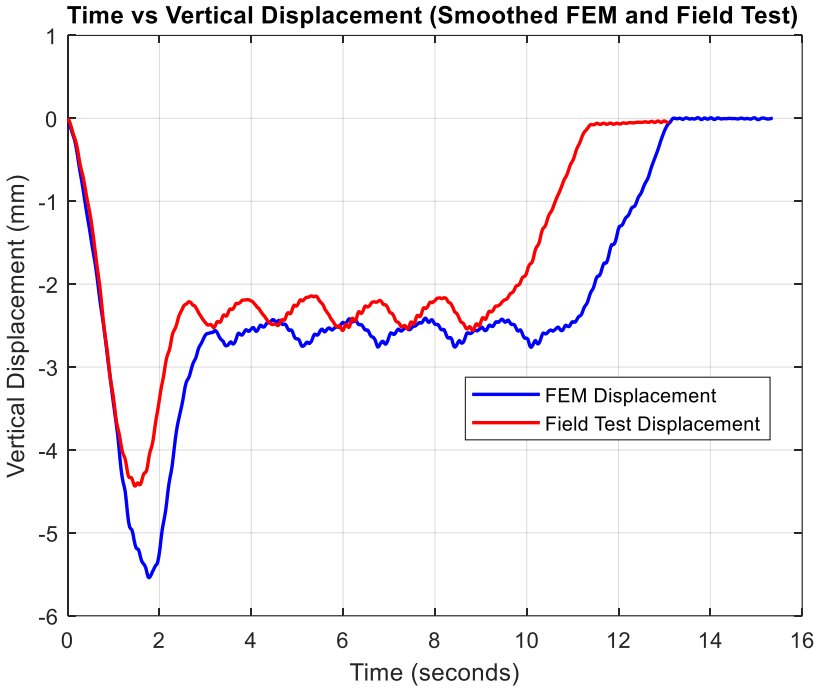

Figure 53 – Cos Cob Bridge Vertical Displacement @ Vib 2 under Amtrak Regional Train Load, Train speed: 35 mph

3.2.2 Sensitivity Study for Model Calibration

In this study, a comprehensive sensitivity analysis was conducted to assess how key structural parameters influence the performance of a finite element (FE) model of a steel railroad bridge, with the objective of calibrating the model to minimize discrepancies between FE model predictions and field test data. This calibration focused on vertical displacements and natural frequencies, which are crucial to understanding the dynamic behavior of the structure. The sensitivity analysis employed a hybrid approach that combines both log-normal random sampling and a Genetic Algorithm (GA) leveraging the roulette wheel selection method to effectively explore and refine the parameter space, allowing for a robust evaluation of complex, non-linear structural behavior.

The analysis was performed by generating a diverse initial population of parameters through log-normal distribution sampling. This approach was chosen for its capability to handle skewed distributions and the natural variability often present in material properties, making it well-suited for initializing parameters over a wide, realistic range while preventing extreme outliers. The parameters considered in this study were selected due to their significant influence on the bridge's dynamic response, with ranges grounded in engineering understanding and field observations:

- **Young's modulus (E)**: 1.9×10^{11} to 2.1×10^{11} Pa. This range covers the potential variability in stiffness of steel members, accounting for both material inconsistencies and structural conditions over time.
- **Density (ρ)**: 7000 to 8100 kg/m³. The range was chosen to reflect potential deviations in material density due to construction variations, aging, and corrosion, as well as to ensure an accurate representation of the structure's mass and inertial properties.

- **Cross-sectional area change (A%)**: 0% to -20%. This range simulates potential reductions in member cross-sectional area due to damage, corrosion, or retrofitting, and aims to capture how deterioration might affect the structural stiffness and load distribution.
- **Longitudinal stiffness (k)**: 50,000 to 250,000 N/mm. This range accounts for variability in structural end connections, particularly stiffness changes in the connections at the bridge's east side, which can significantly influence the boundary conditions and overall structural response.

The initial sets of parameters were generated using log-normal distribution to ensure realistic variability around a mean value and to allow for a balanced exploration of the parameter space while adhering to engineering constraints. This distribution type was specifically chosen because it is better suited for parameters that are strictly positive and where variations can be naturally skewed, such as material properties.

After generating the initial sets using log-normal sampling, the study shifted to a Genetic Algorithm (GA)-based approach to refine the parameters from the third iteration onward. The GA was used because of its powerful ability to search large, complex, and non-convex spaces, which are characteristic of structural calibration problems. It operates by simulating natural selection, evolving a population of potential solutions over successive generations through selection, crossover, and mutation. The roulette wheel selection method was employed to simulate reproduction. This method assigns a higher selection probability to parameter sets with a lower error (higher fitness), while maintaining some diversity by allowing less fit individuals to be chosen occasionally. This method prevents premature convergence and ensures thorough exploration of the parameter space.

Once the best candidates were selected, the GA applied a crossover operation to generate new offspring. The offspring were produced by taking the average of the parameter values from two randomly selected parent sets, allowing for the inheritance of characteristics from both parents and promoting gradual improvement in the population's overall fitness. A mutation step followed, where each parameter in the offspring was slightly perturbed (up to 5%) to introduce variability and prevent the algorithm from becoming trapped in local optima. This mutation maintained genetic diversity within the population, a crucial factor for exploring the parameter space effectively and reaching a global optimum.

The optimization process was iterative. At each step, the top 12 sets of parameters from the previous generations were used to create the next generation. This iterative refinement required manually inputting the optimized parameter sets into **ANSYS** to obtain FE simulation results (displacements and frequencies), which were then fed back into **MATLAB** to recalculate the fitness function. This interactive feedback loop ensured that the GA was accurately guided by the most recent FE simulation results, leading to reliable and progressively better calibration.

The iterative process continued until the stopping criteria were met, either when the maximum number of iterations was reached or when the fitness improvements became negligible. By integrating the initial broad exploration through log-normal sampling with the focused optimization of the GA, the study effectively calibrated the model to reflect the real-world behavior of the bridge. This comprehensive sensitivity study allowed for a calibrated model that accurately predicts structural responses under dynamic loading conditions, enhancing the fidelity of the FE model in simulating the bridge's behavior.

3.2.3 Updated Model and Parametric Study

Following the sensitivity analysis and optimization through the Genetic Algorithm (GA), the finite element (FE) model of the Cos Cob railroad bridge was updated to incorporate the optimized parameter values. The optimization process utilized loading conditions from the **Metro-North M8 train**, as it was the most frequent train operating on the bridge, ensuring that the model was calibrated for the most representative loading scenario. These parameters, obtained through the GA process, were manually incorporated into ANSYS for recalculating the vertical displacements and natural frequencies. The comparison of these new FE simulation results with the field test data demonstrates a marked improvement in model accuracy, indicating the success of the optimization process.

The optimized parameters included a **Young's modulus (E)** of 1.918×10^{11} Pa, a **density (ρ)** of 8100.00 kg/m³, a **cross-sectional area reduction** of -6.23%, and a **longitudinal stiffness (k)** of 164927.053 N/mm. These values were strategically chosen by the GA to minimize the error between the FE model predictions and the observed field test results.

Upon applying these optimized parameters in ANSYS, the vertical displacements at three critical locations—**Vib1**, **Vib2**, and **Vib3**—were computed. The maximum displacements obtained were -3.243 mm, -3.131 mm, and -2.559 mm, respectively. These results show a strong alignment with the field test values of -3.089 mm, -3.044 mm, and -2.587 mm, respectively. The comparison of the peak vertical displacement results at the three different locations is presented in **Table 9**. **Figure 54**, **Figure 55**, and **Figure 56** represent the comparison of the vertical deflection results of the Cos Cob bridge at Vib 1, Vib 2, and Vib 3 during the Metro-North M8 passage. The improvements in accuracy, particularly in displacements, demonstrate that the optimized model has significantly reduced the discrepancy between the model's predictions and the real-world behavior of the bridge span.

Table 9 - Comparison of Vertical Displacement Results of the Cos Cob bridge with Field Test, initial FE model, and Optimized FE model

Location	Field Test max deflection (mm)	Initial FE max. Deflection (mm) and discrepancy (%)	Updated FE max deflection (mm) and discrepancy (%)
Vib 1	-3.089	-3.475 (12.49%)	-3.243 (4.99%)
Vib 2	-3.044	-3.350 (9.13%)	-3.131 (2.85%)
Vib 3	-2.587	-2.776 (7.306%)	-2.559 (0.464%)

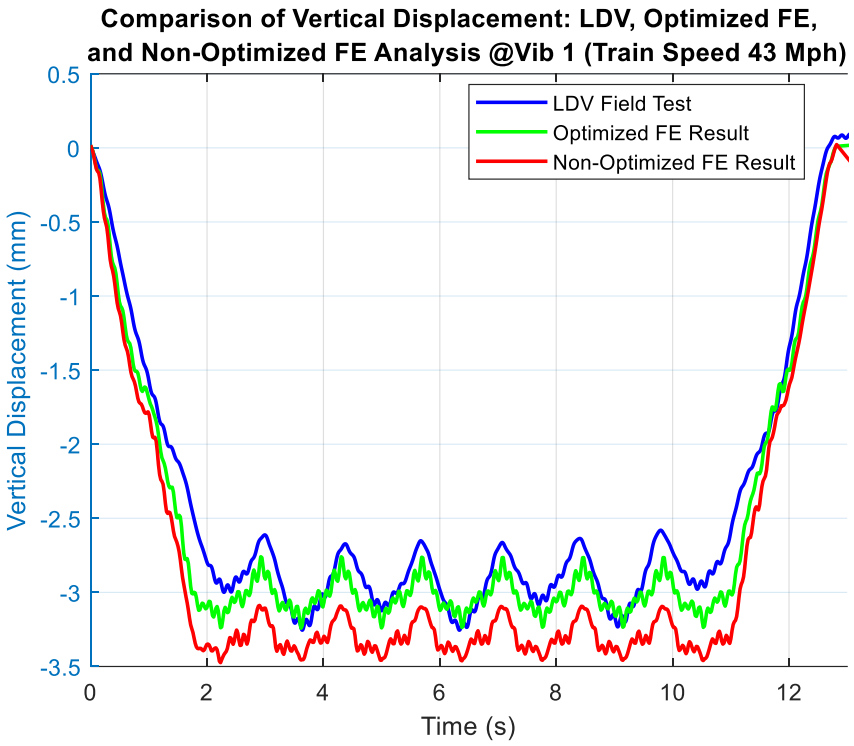

Figure 54 - Comparison of Cos Cob Bridge Vertical Displacement: LDV, Optimized FE Analysis, and Non-Optimized FE Analysis @Vib 1 During Metro-North M8 Passage

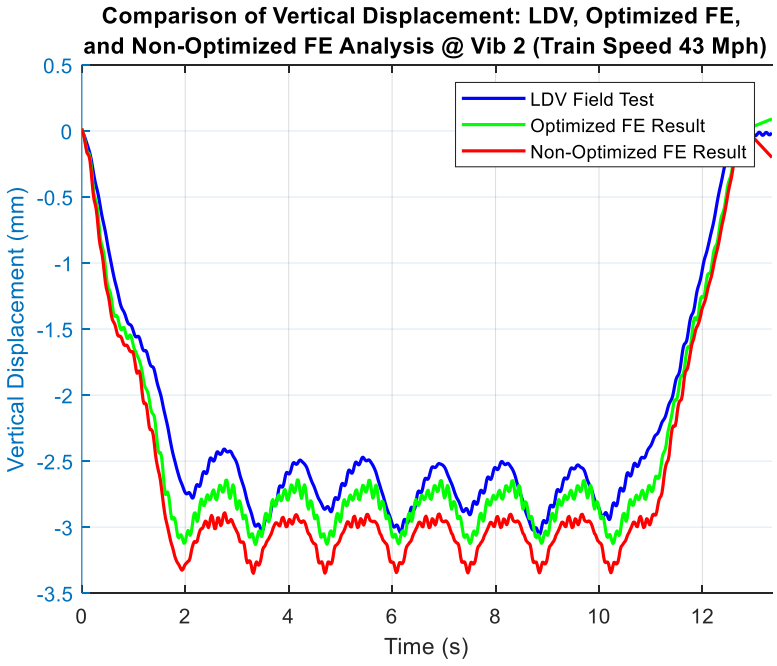

Figure 55 - Comparison of Cos Cob Bridge Vertical Displacement: LDV, Optimized FE Analysis, and Non-Optimized FE Analysis @Vib 2 During Metro-North M8 Passage

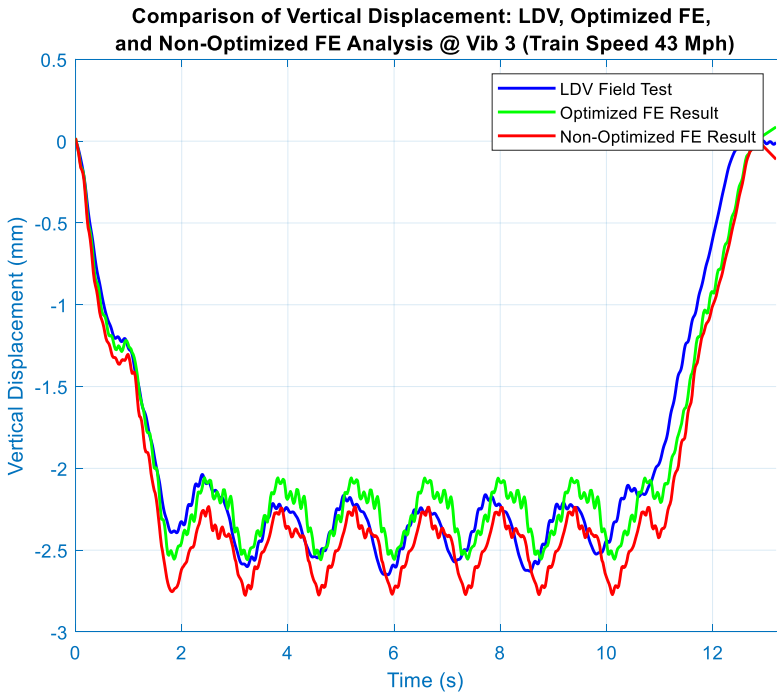

Figure 56 - Comparison of Cos Cob Bridge Vertical Displacement: LDV, Optimized FE Analysis, and Non-Optimized FE Analysis @Vib 3 During Metro-North M8 Passage

Similarly, the natural frequencies were recalculated for the first three modes, yielding values of 3.87 Hz, 8.63 Hz, and 8.86 Hz from the FE model. These values closely match the corresponding field test frequencies of 3.22 Hz, 7.66 Hz, and 8.52 Hz, further affirming the effectiveness of the optimization process. The differences between the FE simulation-based predictions and field data for both displacements and frequencies now fall within a small margin of error. The comparison of the natural frequencies of the field test with the non-optimized FE and optimized FE model are presented in **Table 10**. This is a significant improvement compared to the pre-optimization model, where deviations were notably larger.

Table 10 - Comparison of Natural Frequencies of Field Test Results with FE models

Mode	Natural Frequencies (Hz) and Discrepancies (%)		
	Field Test	Non-Optimized FE Model	Optimized FE Model
1st Lateral	3.22	3.60 (11.80%)	3.87 (16.7%)
1st Vertical	7.56	7.19 (4.89%)	7.63 (0.91%)
2nd Lateral	8.51	8.14 (4.54%)	8.86 (4.11%)

The close alignment of the FE model's outputs with the field data is indicative of the model's enhanced predictive capability following the GA optimization. The adjustments in **Young's modulus**, **density**, **cross-sectional area**, and **longitudinal stiffness** have improved both the static and dynamic accuracy of the model. The reduction in vertical displacement errors suggests that the structural stiffness is now better captured, while the improved frequency predictions indicate that the model's dynamic response characteristics have been refined.

3.2.3 Identification of Critical Members and Connections

The structural integrity of a steel truss bridge, such as the Cos Cob Bridge, is inherently dependent on the performance of its members and connections under various loading conditions. As truss systems distribute loads through multiple paths, connections become critical points where forces are transferred between members. Failure at any of these connections can lead to localized damage, which could propagate and severely compromise the overall stability of the structure. Therefore, identifying the critical connections—those most susceptible to failure or excessive load—becomes paramount in assessing the bridge's resilience, especially under high dynamic loads, such as those from the Metro-North M8 train.

The Cos Cob Bridge, being a riveted steel truss bridge, presents a unique set of challenges regarding load redistribution, member interaction, and connection behavior under stress. Connections, particularly those involving gusset plates, experience a complex combination of axial forces, shear forces, and bending moments. The structural complexity of these connections makes them potential weak points, especially when subjected to repeated and high-magnitude loading, which can lead to fatigue and fracture over time.

Current Practices and Advancements in Critical Connection Identification

In current engineering practice, identifying critical connections in truss bridges frequently relies on the **Demand-to-Capacity (D/C) ratio** method. This approach compares the forces acting on members and connections to their allowable capacity, thus providing a snapshot of the structural performance under load. However, while widely used, the D/C ratio method has certain limitations—it primarily focuses on global load distribution and may overlook localized effects such as stress concentrations at critical connections, particularly where geometric discontinuities like rivet holes or gusset plates exist. This limitation becomes critical when assessing the long-term performance and safety of connections under complex loading conditions, such as those experienced by the Cos Cob Bridge.

To address these limitations and provide a more comprehensive analysis, this study adopts two advanced methods: the **Stress Concentration Method** and the **Interaction Ratio Method**. These techniques enable a more nuanced understanding of how combined forces (axial loads, shear forces, and moments) affect specific connection points, offering a more detailed identification of critical connections within the bridge structure.

1. Stress Concentration Method

The **Stress Concentration Method** was used to analyze local stress distributions in key connections. This method is particularly effective for identifying areas of the bridge where stress amplifications occur due to geometric irregularities, such as rivet holes or complex gusset plate configurations. It is also particularly effective for highlighting regions where rivet holes and intricate gusset plate configurations may lead to elevated stress levels. Understanding these localized stress concentrations is crucial for predicting potential sites of fatigue and failure under varying loading conditions.

In this study, the von-Mises stress on the gusset plates was obtained through a detailed FE analysis. The FE analysis combined both shell and beam elements where gusset plates were modeled as shell elements and other structural members as beam elements. The details of the gusset

plates are presented in **Appendix D. Figure 57** illustrates the FE model of the Cos Cob Bridge, highlighting the locations of the gusset plates. As part of this study, it was determined that the forces exerted by the Metro-North M8 train are not significantly high. Consequently, to obtain a more conservative and accurate assessment of stress impacts on the bridge's gusset plates, the Cooper E80 load specified by AREMA standards was applied. **Figure 58** shows the axle loading of Cooper E80 applied in the FE model. This allows for a robust analysis of the bridge's stress behavior, even under higher-than-expected loads. The analysis identified several critical locations. L0, L6, and L16 on the lower chords and U0 and U2 on the upper chords experienced higher stress levels. These connections exhibited the highest stress levels among all analyzed, indicating their vulnerability to stress concentration and subsequent fatigue damage over time. The stress at the gusset plates is presented in **Table 11**.

By identifying these stress concentrations, we can predict which connections are likely to degrade faster under long-term loading conditions, particularly under long-term service loads. (Dowswell 2011).

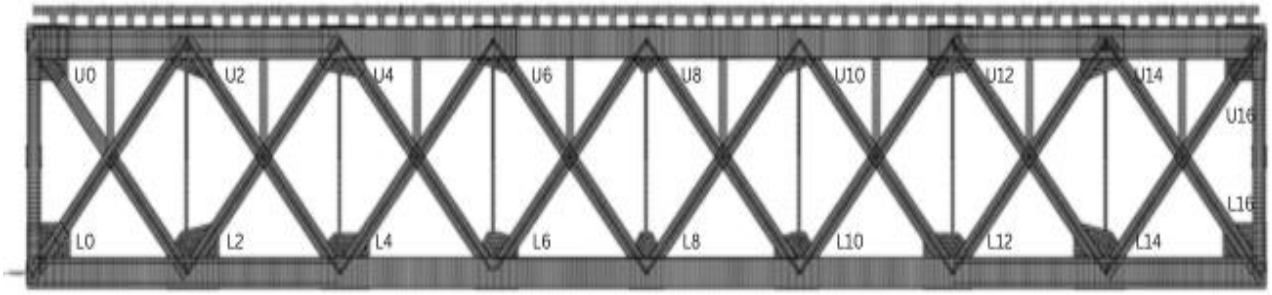

Figure 57 - FE Model of Cos Cob Bridge with Gusset Plates

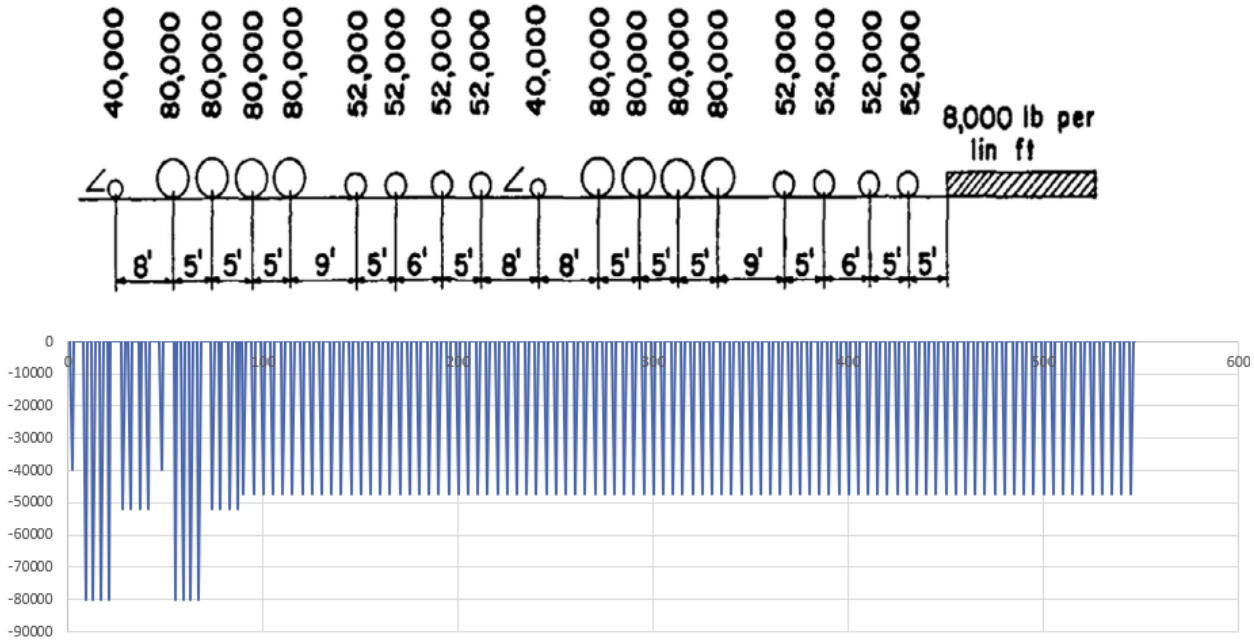

Figure 58 - Axle Loads of Cooper E80 Train, Applied as Triangular Pulse Loads in the FE Model of the Cos Cob Bridge

Table 11 - Stress Distribution at Gusset Plates of Cos Cob Bridge

Connection	Stress (psi)
U0	19,397
U2	20,995
U4	7,267
U6	7,791
U8	13,041
U10	6,760
U12	8,561
U14	13,794
U16	9,950
L0	15,465
L2	8,966
L4	7,006
L6	12,632
L8	5,469
L10	5,934
L12	6,553
L14	8,113
L16	10,762

2. Interaction Ratio Method

To complement the insights gained from the Stress Concentration Method, the **Interaction Ratio Method** was employed. This approach evaluates the combined effect of axial forces and bending moments at each connection and compares these against the allowable capacity for combined loading conditions. This method is beneficial when analyzing truss systems, where connections are typically subjected to both axial tension/compression and bending moments (Cao 2015). To ensure that the analysis reflects conservative and realistic conditions, the Cooper E80 load was used on the optimized FE model, providing a comprehensive stress evaluation in line with AREMA standards. The Interaction Ratio (IR) is given by the following expression:

$$IR = \frac{M}{M_{allow}} + \left(\frac{P}{P_y}\right)^2 + \left(\frac{V}{V_y}\right)^4 \qquad \textbf{Equation 7}$$

In Equation 7:

- P is the applied axial force
- P_y is the axial yield capacity

$$P_y = F_y A; \quad F_y = 50\ ksi$$

- M is the applied bending moment
- M_y is the plastic moment capacity

$$M_y = F_y z; z = \frac{tb^2}{4}\ (t = thickness, b = width)$$

- V is the applied shear force, and
- V_y is the plastic shear capacity

$$V_y = 0.6AF_y; A = Cross\ sectional\ area\ of\ Gusset\ Plate$$

Table 12 presents the interaction ratio (IR) for each connection of the Cos Cob Bridge, calculated with respect to the capacity of that connection. The IRs at U0, U2, and U8 are greater than 1, further indicating that these locations are overstressed and critical.

Table 12 - Interaction Ratio of the Gusset Plates

Connection	IR	Connection	IR
U0	1.23	L0	0.14
U2	1.24	L2	0.65
U4	0.92	L4	0.17
U6	0.87	L6	0.46
U8	1.20	L8	0.05
U10	0.96	L10	0.36
U12	0.78	L12	0.16
U14	0.35	L14	0.13
U16	0.16	L16	0.03

3.3 Tilton-Belmont Bridge

After the FE model of the Tilton-Belmont bridge was developed, several static analyses were carried out to evaluate the bridge's response under different railroad loading conditions. These analyses were followed by modal analysis FE simulations to assess the bridge's dynamic properties.

3.3.1 Static Analysis

The static analyses were performed to determine the vertical displacements at various points along the bridge. These analyses provide critical insight into the bridge's behavior under different loading conditions. Four distinct scenarios were analyzed, each representing varying degrees of bridge coverage by a freight train with cars weighing 263,000 lbs each. These scenarios included 25% (1/4 of the bridge length), 50% (1/2 of the bridge length), 75% (3/4 of the bridge length), and 100% (full bridge length) coverage. By analyzing these conditions, the bridge's response to different load distributions was evaluated, with the resulting vertical displacements illustrated in **Figure 59**.

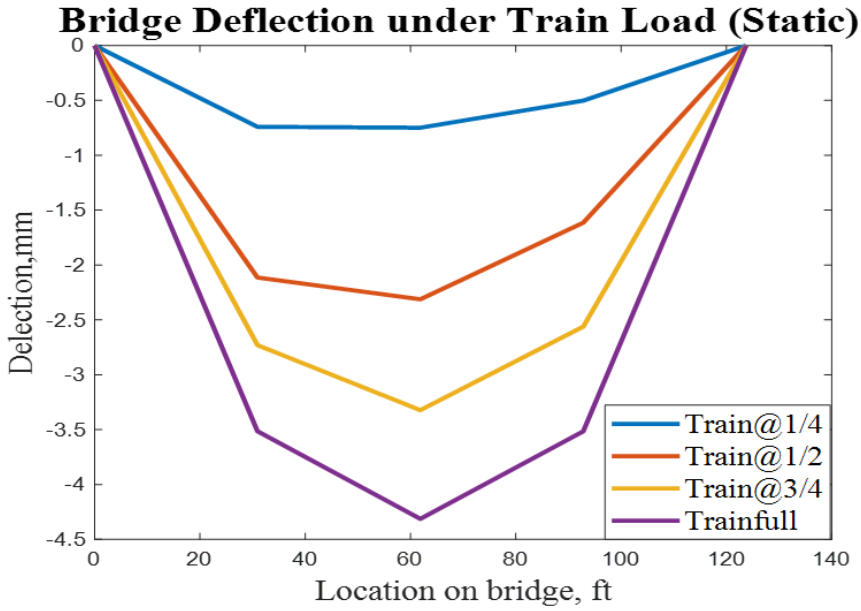

Figure 59 - Vertical displacement on the Tilton-Belmont bridge when train is covering ¼ , ½, ¾, and the full length of the bridge (Max Deflection: 4.32 mm)

As shown in **Figure 59**, the maximum vertical displacement of 4.32 mm occurred at the center of the bridge.

3.3.2 Modal Analysis

The modal analysis of the Tilton-Belmont [New Hampshire (NH)] railroad bridge was conducted in ABAQUS to identify its natural frequencies and corresponding mode shapes. The modal analysis was carried out using the subspace method to determine the first 50 mode shapes and corresponding natural frequencies. **Table 13** presents the summary of the first seven natural frequencies of the bridge.

Table 13 - Tilton-Belmont Bridge: Natural Frequencies from FE model

Vibration Mode	FE Natural Frequency (Hz)
1st Lateral	**1**
1st Vertical	**1.2**
2nd Lateral	**1.9**
1st Twisting	**2**
3rd lateral	**2.4**
4th Lateral	**2.6**
2nd Vertical	**3**

Figure 60 illustrates the first lateral, second lateral, first vertical, and first twisting mode shapes. The first lateral mode occurs at 1.0 Hz, followed by the first vertical mode at 1.2 Hz and the second lateral mode at 1.9 Hz. These lower-frequency modes primarily represent the global dynamic behavior of the bridge, characterized by predominant lateral and vertical displacements. The first twisting mode, occurring at 2.0 Hz, captures the torsional response of the structure, while the third and fourth lateral modes, at 2.4 Hz and 2.6 Hz respectively, exhibit more complex lateral deformation patterns.

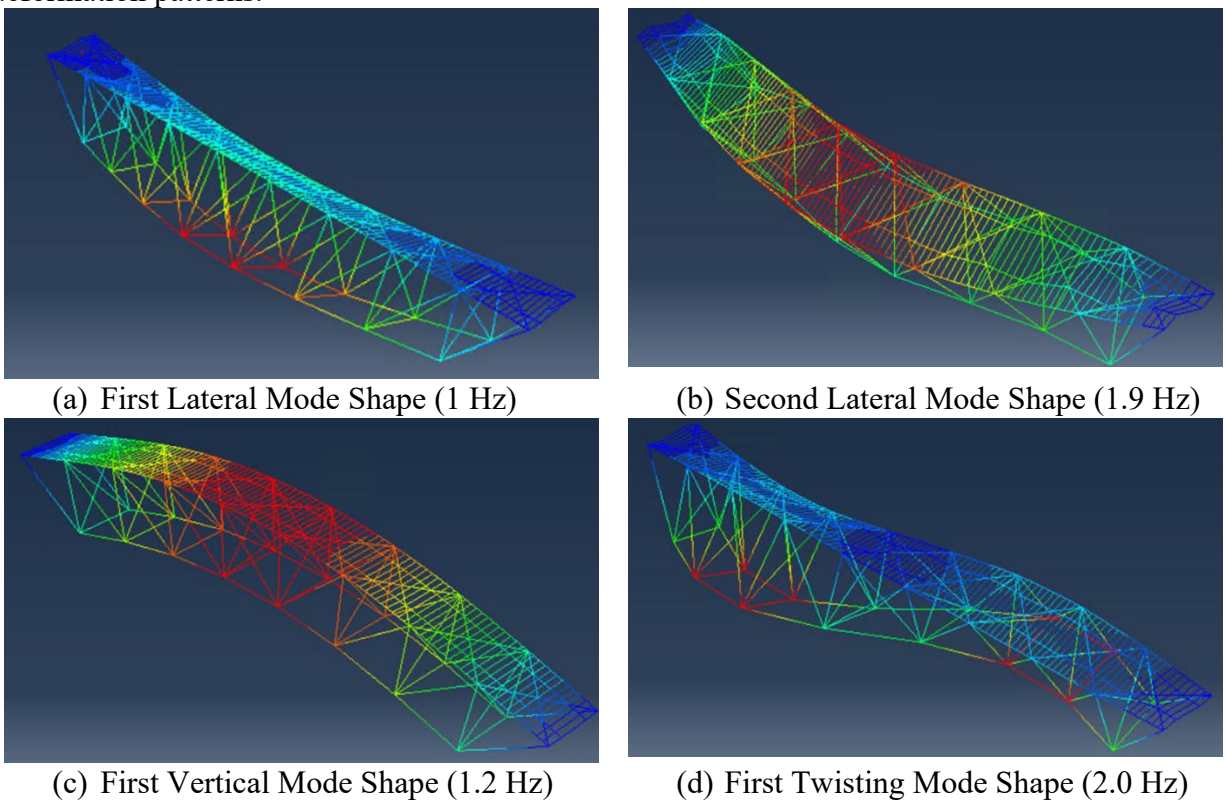

(a) First Lateral Mode Shape (1 Hz) (b) Second Lateral Mode Shape (1.9 Hz)

(c) First Vertical Mode Shape (1.2 Hz) (d) First Twisting Mode Shape (2.0 Hz)

Figure 60 - FE Mode Shapes of the Tilton-Belmont (NH) railroad bridge

The highest frequency mode, at 3.0 Hz, represents the second vertical mode, which captures vertical displacements, potentially impacting localized regions of the bridge. The visualization of these mode shapes illustrates the distinct deformation patterns at each frequency, with global movements dominating the lower modes and more localized effects emerging in the

higher modes. These insights are critical for understanding how the bridge may respond to dynamic loading scenarios, such as vibrations induced by passing trains.

3.3.3 Modeling of Train Loads

In the analysis of railway structures, accurate modeling of train loads is essential to ensure the proper assessment of the structural response under dynamic conditions. Traditional methods of simulating moving train loads involve the determination of axle loads based on the train configuration and then applying these loads as a function of time and speed. While effective, this method becomes cumbersome when varying speeds are considered, as it requires the generation of new load tables for each combination of speed and time step. To overcome the complexity and inefficiency of this traditional approach, a more efficient strategy using the DLOAD user subroutine in ABAQUS has been explored. This subroutine enables the direct application of moving train loads without the need to generate and modify large tabular data for different train speeds.

3.3.3.1 Traditional Method for Modeling Train Loads

The following steps are taken while implementing the traditional method of modeling train loads:

Axle Load Determination

The traditional method starts by determining the axle loads of the train. Given a specific train configuration (i.e., the number and arrangement of axles, and the load distribution across the axles), the total load is divided among the individual axles. This load is typically calculated as:

$$P_{axle} = \frac{P_{total}}{n_{axles}}$$

Here, P_{total} is the total train load, and n_{axles} is the number of axles.

Speed and Load Application

Once the axle load is known, it is applied to the structure as a moving load. The speed of the train defines how these loads are distributed over time. For each time step, the location of each axle must be recalculated based on the train's speed. A table of load positions for each time step is generated, which mimics the motion of the train across the structure. For different train speeds, a new table must be created to account for the different load positions over time. This makes the process very tedious and time-consuming when multiple speed scenarios are required.

3.3.3.2 ABAQUS DLOAD Subroutine Method

To simplify this process and eliminate the need for manual table generation, the DLOAD user subroutine in ABAQUS can be utilized, which allows for the direct application of a moving load based on input parameters such as axle load and train speed. This method offers several advantages:

- The movement of the load is calculated dynamically based on the train's speed, avoiding the need for pre-defined load tables.
- It allows for easy modifications in train speed without the need to regenerate load data.
- The subroutine automatically adjusts the load application based on time, ensuring accuracy in simulating both the static and dynamic response of the structure.

The DLOAD subroutine defines the loading condition applied at each element in the model. In this case, the subroutine was written to compute the position of the train axles as a function of time and apply the corresponding axle loads to the structure. The subroutine has been coded in FORTRAN.
The general form of the subroutine used is given in Appendix F.

In the DLOAD subroutine coded in FORTRAN, the position of each axle changes dynamically based on the velocity of the train, and the load is applied only if the axle is within a certain proximity of the element's position. This simulates the moving train as it passes over the structure. The key parameters used in this sample FORTRAN code are as follows (see Appendix F for the actual code):

- Velocity: The speed of the moving train (15 mph).
- Axle_dis1, Axle_dis2, Axle_dis3: Distances between axles and bogies.
- Fmax: The maximum force exerted by each axle (-100,000 N in this case).
- dis_intpoint: The interaction distance (0.619 m) within which the load is applied.
- COORDS(1), COORDS(2), COORDS(3): Element coordinates (X, Y, Z).

In this subroutine, the train speed is set to 15 mph, and the distances between the axles are defined as follows:

- Axle_dis1: 6.0 ft between consecutive axles on the same bogie.
- Axle_dis2: 25.0 ft between the first and second bogies of a railroad car
- Axle_dis3: 7.0 ft between consecutive bogies of adjacent coaches.

The code computes the positions of up to 20 axles (covering five coaches) based on the time, which is incremented as the simulation progresses. For each time step, the position of each axle is calculated relative to the element's coordinates, representing the horizontal position of the element. To determine whether a particular axle is close enough to apply a load to an element, the subroutine calculates the absolute difference between the element's position and each axle's position. If the minimum distance between the element and any axle is less than a specified tolerance distance (dis_intpoint), the load is applied to that element. The load magnitude is interpolated based on the distance from the axle, starting from the maximum force (Fmax) when the axle is directly over the element and gradually decreasing as the axle moves away.

For each time step, the subroutine ensures that the dynamic position of the axles is considered when applying loads, thereby simulating the effect of a train moving across the structure. If no axle is close enough to an element, no load is applied to that element. **Figure 61** illustrates the static displacement response at the middle of the span of the bridge under the load of a moving train. In a static analysis, the displacement is calculated assuming that the loads are applied gradually, without accounting for any dynamic effects such as inertia or damping. As the train moves across the bridge, the load from the axles applies force to different points on the structure. The plot shows how the displacement at the middle of the span evolves as the train approaches, crosses, and moves away from the bridge.

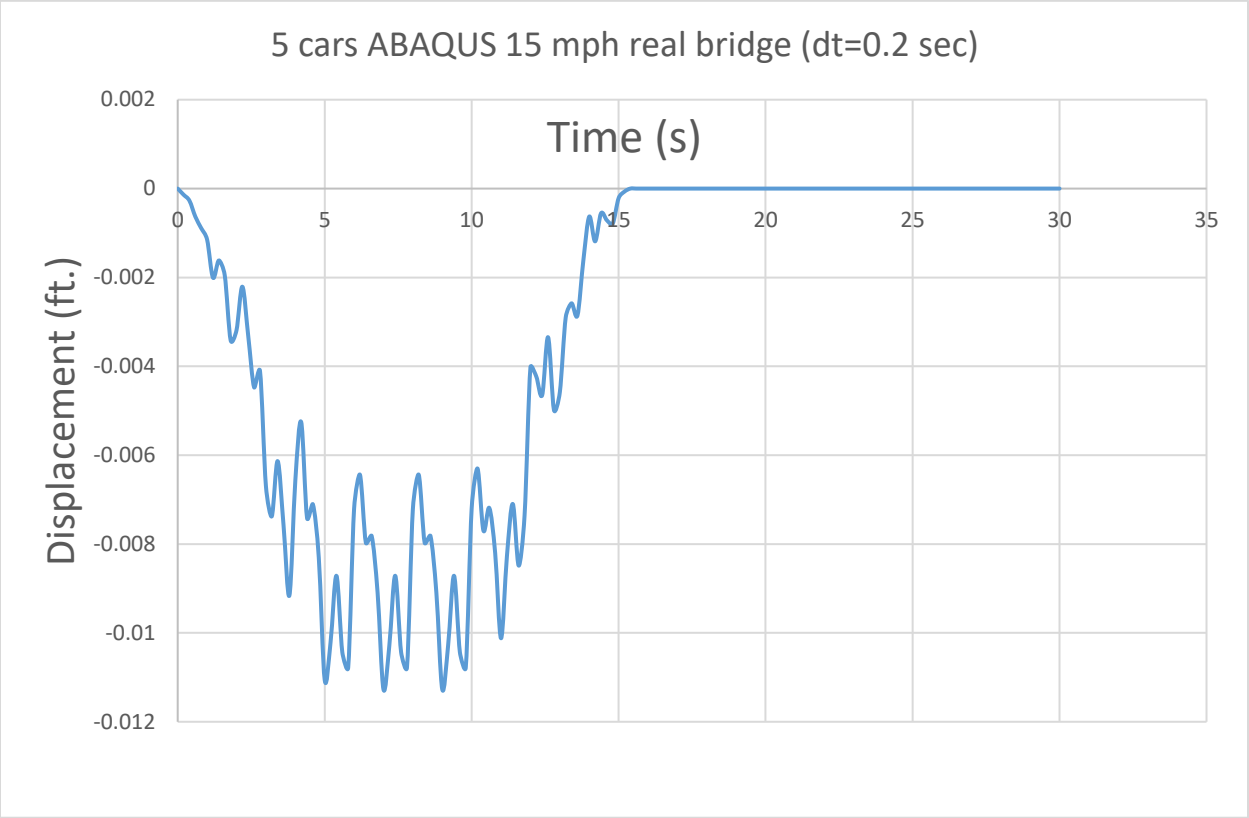

Figure 61 - Vertical Displacement of the center of the Tilton-Belmont NH railroad bridge

Initially, as the train approaches the span, the displacement starts to increase, indicating the bridge's deflection under the applied loads. The displacement becomes more pronounced as the train gets closer to the middle of the span, where the bending moment and deflection are typically greatest. At around 5.5 seconds into the simulation, the displacement reaches its peak, approximately -0.0115 ft (-0.5 cm), reflecting the maximum deflection when the train fully covers the railroad bridge. This negative displacement is due to the downward forces exerted by the train's weight on the bridge. Once the train begins to move past the midspan, the displacement starts to decrease as the loading shifts away from the middle of the bridge. The deflection gradually diminishes, eventually returning to zero after the train has left the span. The smooth return to zero displacement indicates that the bridge recovers its original position without any residual deflection once the train is no longer applying force to that section. This plot helps assess the structural behavior of the bridge under static loading conditions, ensuring that the deflection remains within safe limits. Since this is a static response, the plot does not capture any dynamic oscillations that might occur due to vibrations or dynamic loading, focusing solely on the static (i.e., gradual) response to the moving train's weight.

Chapter 4: Summary, Conclusions and Recommendations

This study examined the dynamic structural performance of three aging steel truss bridges: the Devon Bridge and Cos Cob Bridge in Connecticut and the Tilton-Belmont Bridge in New Hampshire. These bridges, built over a century ago, are still in use despite facing increased loading conditions from modern train operations. The study sought to address the challenges of aging infrastructure and the impact of modern train operations on these historic bridges. The research involved field testing, Finite Element (FE) modeling, and sensitivity analysis to better understand the dynamic behavior of these aging bridges.

4.1 Summary

This study evaluated the dynamic structural performance of three aging steel truss bridges: the Devon Bridge and Cos Cob Bridge from Connecticut, and the Tilton-Belmont Bridge in New Hampshire. These bridges were constructed over a century ago and are critical components of New England's regional rail network and continue to serve under increased loading conditions imposed by modern train operations. The aging infrastructure poses unique challenges, as the original design standards do not fully account for the increased weight and speed of modern-day trains. Thus, a detailed study of their current conditions is necessary.

To address this, the research involved an integrated field-testing approach, Finite Element (FE) modeling, and sensitivity analysis. Field testing utilized Laser Doppler Vibrometers (LDV) and accelerometers to capture real-time dynamic responses of the bridges during train crossings. These tests focused on recording the dynamic responses of the bridges. The field test data were further processed using MATLAB to generate the vertical displacement and the natural frequencies of the bridge to accurately understand the behavior of the bridges under dynamic loading conditions.

Finite element (FE) models were developed for all three bridges using their respective as-built structural details. These models simulated the impact of train-induced loads and enabled in-depth analysis of stress distribution and deflection within the structures. The accuracy of the FE models was validated by comparing the results with the data obtained from the field tests. While the models aligned well with the observed data, some discrepancies in predicted vertical displacements highlighted areas for refinement, particularly in the representation of boundary conditions.

Additionally, a sensitivity analysis was conducted on the Cos Cob Bridge to explore the effect of varying key parameters, such as material properties, cross-sectional dimensions, and longitudinal stiffness. This analysis provided valuable insights into the structural robustness of the bridges, identifying critical parameters that significantly influence their dynamic performance. Overall, the study offers a comprehensive framework for understanding the dynamic behavior of these aging bridges, helping to inform future maintenance and retrofitting strategies.

4.2 Conclusions

Several significant conclusions emerged from this investigation of the Devon and Cos Cob bridges in Connecticut, and the Tilton-Belmont bridge in New Hampshire:

1. The field tests were conducted exclusively for the Devon and Cos Cob bridges to capture their vertical displacement and acceleration. The dynamic responses were recorded from

LDV and accelerometers during train passages. The collected data were processed to obtain critical information on the bridges' vertical displacement and natural frequencies.

2. The FE models developed for the Cos Cob and Devon bridges provided a close approximation of their real-world behavior, particularly concerning natural frequencies. However, discrepancies in vertical displacements suggest that further refinement is needed. The observed uplift at the Devon Bridge abutment, for example, indicates potential issues with the bridge's boundary conditions that the FE models did not fully capture. This highlights the importance of accurate representation of boundary conditions in future assessments.
3. A sensitivity analysis conducted as part of the calibration process identified the critical influence of parameters such as Young's modulus, density, and cross-sectional area on the bridge's dynamic response. For the Cos Cob bridge, the optimized parameters were a Young's modulus of 1.918×10^{11} Pa, a density of 8100 kg/m^3, and a 6.23% reduction in cross-sectional area. These parameters directly impacted the displacement and frequency responses, underscoring the need for accurate material characterization. These refinements successfully minimized discrepancies between the model and field test results, further improving the model's accuracy.
4. The analysis identified several critical components, particularly gusset plates and truss joints, as areas of concern. These components are subjected to complex stress interactions during train passage, making them vulnerable to fatigue and eventual failure. The results suggest that these connections require close monitoring and potential strengthening to ensure long-term structural integrity.
5. The identification of uplift at the Devon Bridge abutment was one of the notable findings. This behavior could indicate foundation-related issues or shifts in boundary conditions. Given the critical role of the abutments in load transfer, further investigation is needed to determine the underlying cause of this uplift and to assess its long-term impact on the bridge's stability.
6. The comprehensive FE model developed for the Tilton-Belmont Bridge provided insights into the natural frequencies and mode shapes. A peak vertical displacement of 4.32 mm was observed under the freight train loading considered in this study, and the first vertical frequency was recorded at 1.2 Hz, offering critical insights into the dynamic behavior of this structure. These findings highlight the necessity for individual assessments of structurally similar bridges to account for variations in their dynamic response.

4.3 Recommendations

Based on the findings from this comprehensive analysis, several recommendations are made to enhance the safety, performance, and longevity of the Devon, Cos Cob, and Tilton-Belmont (New Hampshire) bridges:

1. **Refinement of Finite Element Models**: The current FE models provided valuable insights into the dynamic behavior of the bridges, but further refinement is necessary. In particular, the models should better account for vertical displacements and boundary conditions, such as those observed at the Devon Bridge abutment. Incorporating more detailed representations of the connections and non-linear behavior under dynamic loads would improve the accuracy of the models and better reflect the real-world performance of the bridges.
2. **Investigation of Uplift at Devon Bridge**: The uplift observed at the Devon Bridge abutment is a significant finding that requires further attention. Additional field monitoring

should be conducted to determine whether this is a localized issue or indicative of a broader problem with load transfer through the foundation. Addressing this issue is crucial to ensuring the long-term stability of the bridge, particularly as train speeds and loads continue to increase.

3. **Regular Monitoring and Strengthening of Critical Connections**: The gusset plates, truss joints, and other connections identified as vulnerable during the analysis should be prioritized for regular inspections. Given the high levels of stress these components experience, strengthening measures — such as retrofitting with advanced materials – should be explored to enhance their load-carrying capacity and extend their service life.
4. **Structural Health Monitoring Systems (SHMS)**: Installing a structural health monitoring system on all three bridges would provide continuous, real-time data on their performance. Sensors placed at critical locations would allow for early detection of issues such as stress accumulation, displacement, or abnormal vibrations. Such a system would enable proactive maintenance and reduce the risk of sudden structural failures.
5. **Further Sensitivity Analysis and Material Testing**: The sensitivity analysis highlighted the importance of accurately characterizing material properties, particularly Young's modulus and density. Future studies should include detailed material testing to ensure these properties are accurately represented in the models. Additionally, fatigue testing of key structural components would provide further insights into their remaining service life, helping to inform targeted retrofitting efforts.
6. **Broader Implications for Aging Infrastructure**: The methodologies developed in this study can be applied to similar aging bridges across the country. Many railroad bridges are nearing or exceeding their design lifespans, and dynamic assessments like those conducted in this study can provide critical insights into their structural health. Implementing regular monitoring and proactive maintenance strategies will be essential to ensuring the continued safety and functionality of these vital infrastructure components.

By implementing these recommendations, transportation authorities can ensure the continued safe operation of the Devon, Cos Cob, and Tilton-Belmont (NH) bridges. These actions will not only preserve these critical assets but also enhance their resilience against the increasing demands of modern rail traffic, ensuring they remain functional for many years to come.

References

AAR, Association of American Railroads. *Field Investigation of a Truss Span on the Great Northern Railway.* Chicago, IL: AAR Research Center, 1968.

Adams, R., and D. Lin. "Determination of damping characteristics of structures by transient testing using Zoom-FFT." *Journal de Physique Colloques*, 1983: 363-369.

ANSYS Inc. *Theory reference for the mechanical APDL and mechanical applications.* Practice Periodical on Structural, PA, 2009.

AREMA. *Manual for railway engineering.* Vols. Chapter 15 - Steel Structures. Lanham, MD: American Railway Engineering and Maintenance-of-Way Association, 2022.

AREMA. *Special consideration for structures and HSR operations.* Final Draft, High speed rail structures task force, Lanham: American Railway Engineering and Maintenance-of-Way Association: High speed rail structures task force, 2017, 1-24.

ASTM, American Society of Testing & Materials. "ASTM Standard A7." In *Standard Specifications for Steel for Bridges and Buildings*, 6. West Conshohocken, PA: ASTM International, 1939.

ASTM, American Society of Testing & Materials. "ASTM Standard E111-17-16a." In *Standard Test Method for Young's Modulus, Tangent Modulus, and Chord Modulus*, 7. West Conshohocken: ASTM International, 2017.

ASTM, American Society of Testing & Materials. "ASTM Standard E8/E8M-16a." In *Standard Test Method for Tension Testing of Metallic Materials*, 30. West Conshohocken, PA: ASTM International, 2016.

Bajer, Czestaw I., and Bartomiej Djniewicz. *Numerical analysis of vibration of structures under moving inertial load.* New York, NY: Springer, 2012.

Baniya, Surrendra. *Modeling and Analysis of a Steel Truss Railroad Bridge Traversed by Trains at Various Speeds.* Storrs, CT: M.S. Thesis, Department of Civil & Environmental Engineering, University of Connecticut, 2015.

Biggs, M. Biggs. *Introduction to Structural Dynamics.* New York, NY: McGraw-Hill Inc, 1964.

Bolotin, V. V. *The dynamic stability of elastic systems.* San Francisco, CA: Holden-Day, 1964.

Bro, Rasmus, and K. Smilde Age. "Centering and scaling in componet analysis." *Journal of Chemometrics*, 2003: 16-33.

Burns, Adam. "Amtrak's Acela Express." *https://www.american-rails.com/.* March 2022, 2022. https://www.american-rails.com/acela.html.

Cao, Youyou. "System Redundancy Evaluation for Steel Truss Bridges." Blacksburg, VI: Ph.D. Thesis, Department of Civil Engineering, Virginia Polytechnic Institute and State University, 2015.

Casiano, M. J. *Extracting damping ratio from dynamic data and numerical solutions.* NASA Langley Research Center, Hampton: NASA STI Information Desk, 2016.

Chopra, K. Anil. *Dynamic of structures.* New York, NY: Pearson, 2017.

de Oliveira, Celso C., Santosh Dhakal, and Ramesh B. Malla. "Deflections and Frequencies of Long-Span Steel Railroad Truss Bridges Under Passenger Train Excitation Using Laser Doppler Vibrometer." *Journal of Structural Integrity and Maintenance* (STR-Journal of Structural Integrity and Maintenance), no. http://dx.doi.org/10.1080/24705314.2024.2411864 (2024): 9 (4).

Dowswell, Bo. *Connection Design for Steel Structures* . 2011.

FRA, Federal Railroad Administration;. *Bridge safety Standards compliance manual.* Washington, DC, 2018.

Frýba, L. "A rough assessment of railway bridges for high speed trains." *Engineering Structures*, 2000: 548-556.

Giltner, Brian, and Aslam Kassimali. "Equivalent Beam Method for Trusses." *Practice Periodical on Structural Design and Construction* 5 (2000): 70-77.
Halliday, David, Robert Resnick, and Jearl Walker. *Fundamentals of Physics.* Vol. 10th Edition. Hoboken, NJ: John Wiley & Sons, 2014.
Hatch, Michael R. *Vibration simulation using MATLAB and ANSYS.* Boca Raton, FL: CRC Press LLC, 2000.
Hilal, M. Abu, and H. S. Zibdeh. "Vibration analysis of beams with general boudary conditions traversed by moving load." *Jornal of sound and vibration*, 1999: 377-388.
Jacobs, David W., Suvash Dhakal, and Malla B. Ramesh. "Live-load response of eyebars on a 110-year-old steel truss railroad bridge." *Practice Periodical on Structural*, 2021: 1-16.
Lochner & TranSystem. *Railroad Bridge Inspection - Devon Railroad Bridge.* Newington, CT: Connecticut Department of Trasportation, 2021.
Lochner. *Connecticut Rairoad Equipment - Equivalent Cooper Load Charts.* Office of Rail, Connecticut Department of Transportation, Newington: Conn DOT, 2011.
Löwenborg, Per B., Oscar Gustafsson, and Lars Wanhammar. "Filter design using MATLAB." *ReserchGate*, 1999: 1-5.
Malla, Ramesh B., Celso de Oliveira, and Santosh Dhakal. *Condition/Health Monitoring of Railroad Bridges for Structural Safety, Integrity, and Durability.* Storrs, CT: Transportation Infrastructure Durability Center (TIDC), 2022.
Malla, Ramesh B., David W. Jacobs, Suvach Dhakal, and Surendra Baniya. *Dynamic Impact Factors on Existing Long-span Railroad Bridges," IDEA Rail Safety Project – 25 Final Report.* TRB, 2017.
Malla, Ramesh B., Surendra Baniya, and David W. Jaccobs. "Study of Dynamic and Static Response of an Old Truss Railroad Bridge." *ASCE ASD Earth & Space 2016 Conference.* Reston: ASCE, 2016. 1052-1062.
Mazurek, David F. "Vibration-based estimation of tension stress in steel eyebars." *Journal of Structural Engineering*, 2016: 1-8.
Mottershead, J. E., and M. I. Friswell. "Model updating in structural dynamics: A survey." *Journal of sound and vibration*, 1993: 347-375.
Nakamura, Naohiro. "Extended Rayleigh damping model." Edited by The University of New Zealand. *Frontiers in Built Environment* 2 (July 2016).
Nassif, Hani H., Mayrai Gindy, and Joe Davis. "Comparison of laser Doppler vibrometer with contact sensors for monitoring bridge deflection and vibration." *NDT&E International*, 2005: 213-218.
Norén-Cosgriff, Karin, and Amir M. Kaynia. "Estimation of natural frequencies and damping using dynamic field data from an offshore wind turbine." *Marine Structures 76*, 2021.
Nutakor, Charles, R. Scott Semken, and Janne E. Heikkinen. "Layed sheet-steel damping estimation using optical vibrometer." *International Design Engineering Technical Conferences & Computers and Information in Engineering Conference.* Boston: ASME, 2015. 10.
Petrescu, Florian Ion. *A new doppler effect.* Germany: Books on Demand GmbH, Norderstedt, 2012.
Polytec Inc. *Polytec scanning vibrometer - PSV theory.* As of software 9.1. Hudson, MA, 2015.
Reiterer, Michael, Stefan Lachinger, Josef Fink, and Sebastian-Zoran Bruschetini-Ambro. "In-Situ Experimental Modal Testing of Railway Bridges." *18th International Conference on Experimental Mechanics.* Brussels, Belgium: MDPI, 2018. 1-7.
Rossi, G., V. Gussella, and M. Gioffré. "Comparison between accelerometer and laser vibrometer to measure traffic excited vibrations on bridges." *Shock and Vibration*, 2002: 11-18.

Salcher, Patrick, and Christoph Adam. "Modeling of dynamic train–bridge interaction in high-speed." *Springer-Verlag Wien*, 2015: 2473-2495.
Schiefer, Mark I., and Jeffrey Dosch. *ICP® BASED REFERENCE ACCELEROMETERS.* Depew: PCB Piezotronics Inc, 2012, 1-4.
Siekierski, Wojciech. "ANALYSIS OF GUSSET PLATE OF CONTEMPORARY BRIDGE TRUSS GIRDER." *THE BALTIC JOURNAL OF ROAD AND BRIDGE ENGINEERING*, 2016: 188-196.
Siemens. *Amtrak Cities Sprinter ACS-64 - Electric Locomotive.* Munich: Siemens Mobility, 2019.
Song, Zhiqiang, and Chenhui Su. ""Computation of Rayleigh damping coefficients for the seismic analysis of a hydro-powerhouse"." *Hindawi - Shock and Vibration*, 2017: 10.
Tedesco, Joseph W., William G. McDougal, and C. Allen Ross. *Structural Dynamics: Theory and application.* Menlo Park, CA: Addison Wesley Longman, Inc, 1999.
The MathWorks, Inc. *Signal Processing Toolbox - User's Guide.* Natick, MA, 2022.
Wenzel, Helmut. *Health monitoring of bridges.* Chichester, UK: John Wiley & Sons Ltd, 2009.
Yang, Y. B., Bin Zhang, Tianyi Wang, Hao Xu, and Yuntian Wu. "Two-axle test vehicle for bridges: Theory and applications." *International Journal of Mechanical Sciences*, 2019: 51-62.
Yang, Y. B., J D. Yau, and Y. S. Wu. *Vehicle-bridge interaction dynamics - with appilcation to high-speed railways.* Hackensack, NJ: World Scientific Publishing Co., 2004.
Yoon, Hyejin, Won Jong Chin, Jae Yoon Kang, Jongwon Kwark, and Eui-Seung Hwang. "Computation of impact factor of high-speed railway bridge by KTX train riding Test." *Scientific research*, 2013: 751-755.

UCONN SCHOOL OF ENGINEERING

Project 1.2: Condition/Health Monitoring of Railroad Bridges for Structural Safety, Integrity, and Durability

PI: Ramesh B. Malla, Ph.D., F. ASCE, F. EMI, Professor

Sponsor: US DOT Region 1 UTC-TIDC Program

Devon Bridge Field Test - LDVT LDV ACCEL

TIDC Transportation Infrastructure Durability Center AT THE UNIVERSITY OF MAINE

DATE: 2/11/2023 WEATHER CONDITION: Cloudy

TEMPERATURE: 32-58 °F

Test No	Recording Time	Location (Node)	Travelling Conditions			Type of Train		General Notes
			Direction	Velocity*	Track no	Train Type	No of Cars	
1		LDV 1	W-E		4	M8		Test Run (LVD)
2		LDV 1	W-E		4	ACELA	8	(LDV + ~~LVDT~~) - LDVT don't show consistency
3	13:52	LDV 1	W-E		4	M8	6	(LDV)
4	14:04	LDV 1	W-E		4	REGIONAL	8	(LDV + LVDT)
5	14:12	LDV 1	W-E		4	M8	6 to 7	(LDV + LVDT)
6	14:52	LDV 2	W-E	42 MPH	4	M8		(LDV + LVDT)
7	14:56	LDV 2	W-E		4	ACELA	8	(LVDT)
8		LDV 2	W-E		4	M8	8	(LDV + LVDT)
9		LDV 2	W-E		4	M8		(LDV, LVDT + VIDEO)

* Using Radar Gun.

(a)

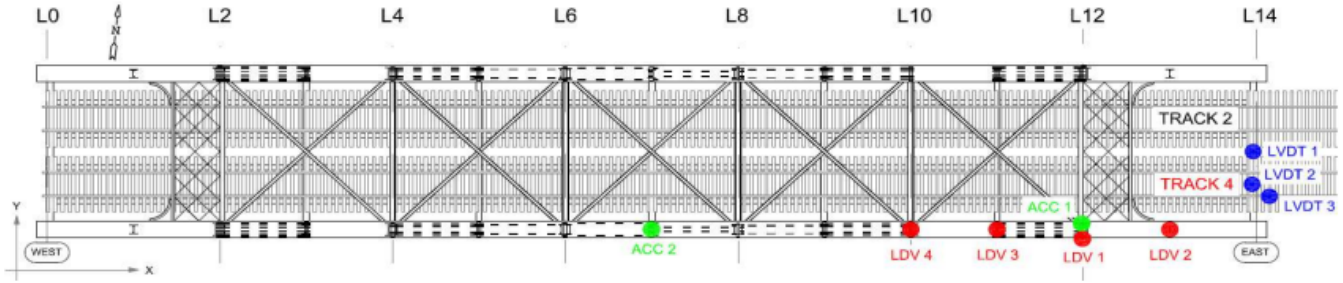

(b)

Appendix A 1 – (a) Devon Bridge Field Test Records of Nov 2, 2023: train types, speeds, direction, and sensor location, and (b) Devon bridge Southbridge Span 7 - Plan View

UCONN SCHOOL OF ENGINEERING

Project 1.2: Condition/Health Monitoring of Railroad Bridges for Structural Safety, Integrity, and Durability

PI: Ramesh B. Malla, Ph.D., F. ASCE, F. EMI, Professor

Sponsor: US DOT Region 1 UTC-TIDC Program

Devon Bridge Field Test - LDVT LDV ACCEL

TIDC Transportation Infrastructure Durability Center AT THE UNIVERSITY OF MAINE

DATE: 3/11/2023 WEATHER CONDITION: Sunny

TEMPERATURE: 35-62 °F

Test No	Recording Time	Location (Node)	Travelling Conditions			Type of Train		General Notes
			Direction	Velocity*	Track no	Train Type	No of Cars	
10	9:09	LDV 3	W-E		4	M8		(LDV, LVDT + VIDEO)
11	9:29	LDV 3	W-E	32 MPH	4	REGIONAL		(LDV, LVDT + VIDEO)
12	9:52	LDV 3	W-E	30 MPH	4	M8		(LDV, LVDT + VIDEO)
13	10:11	LDV 3	W-E	35 MPH	4	M8		(LDV, LVDT + VIDEO)
14	10:28	LDV 3	W-E	42 MPH	4	REGIONAL		(LDV, LVDT + VIDEO)
15	10:37	LDV 3	W-E	43 MPH	4	ACELA		(LDV, LVDT + VIDEO)
16	10:52	LDV 4	W-E	38 MPH	4	M8		(LDV, LVDT + VIDEO) - Late Recording
17	11:13	LDV 4	W-E	34 MPH	4	M8		(LDV, LVDT + VIDEO)
18	11:25	LDV 4	W-E	39 MPH	4	ACELA		(LDV, LVDT + VIDEO)
19	11:55	LDV 4	W-E	42 MPH	4	M8		(LDV, LVDT + VIDEO)
20	12:14	LDV 4	W-E	40 MPH	4	M8		(LDV, LVDT + VIDEO)
21	12:40	LDV 4	W-E	42 MPH	4	REGIONAL		(LDV, LVDT + VIDEO)
22	13:03	LDV 1	W-E	42 MPH	4	REGIONAL	2 Power Engine	(LDV, LVDT + VIDEO)
23	13:11	LDV 1	W-E	37 MPH	4	M8	6 (From video)	(LDV, LVDT + VIDEO)
24	13:26	LDV 1	W-E	43 MPH	4	ACELA		(LDV, LVDT + VIDEO)

* Using Radar Gun.

(a)

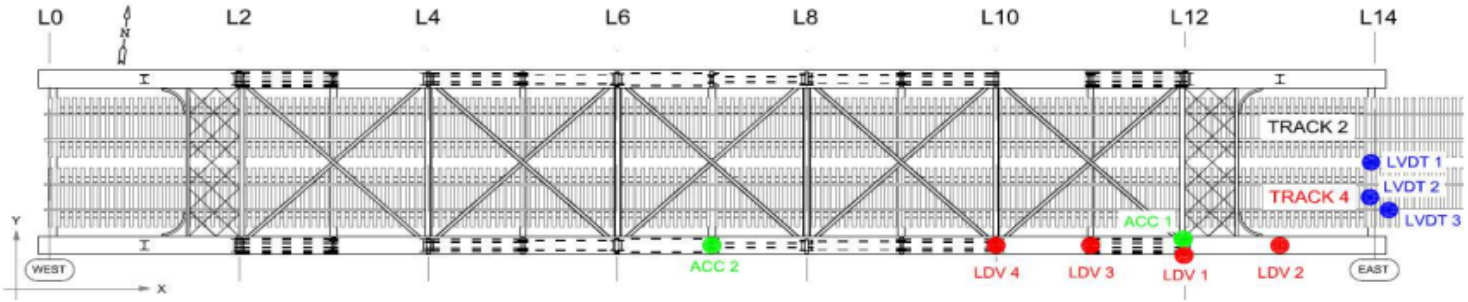

(b)

Appendix A 2 – (a) Devon Bridge Field Test Records Nov 3, 2023: train types, speeds, direction, and sensor location, and (b) Devon bridge Southbridge Span 7 - Plan View

UCONN SCHOOL OF ENGINEERING

Project 1.13: Condition/Health Monitoring of Railroad Bridges for Structural Safety, Integrity, and Durability

PI: Ramesh B. Malla, Ph.D., F. ASCE, F. EMI, Professor

Sponsor: US DOT Region 1 UTC-TIDC Program

TIDC Transportation Infrastructure Durability Center AT THE UNIVERSITY OF MAINE

Cos Cob Bridge Field Test - LDVT LDV ACCEL

DATE: 11/12/2023 WEATHER CONDITION: Sunny

TEMPERATURE: 30-65 °F

Test No	Location (Node)	Travelling Conditions			Type of Train		General Notes
		Direction	Velocity*	Track no	Train Type	No of Cars	
1	Vib 1	W-E		4	M8	8	(LDV + LVDT)
2	Vib 1	W-E		4	M8	6	(LDV + LVDT)
3	Vib 1	W-E		4	M8	9	(LDV + LVDT)
4	Vib 1	W-E		4	M8	8	(LDV + LVDT)
5	Vib 1	W-E		4	M8	5	(LDV + LVDT)
6	Vib 1	W-E		4	Acela	8	(LDV + LVDT)
7	Vib 1	W-E		4	M8	8	(LDV + LVDT)
8	Vib 1	W-E		4	M8	8	(LDV + LVDT)
9	Vib 1	W-E		4	N/A	N/A	N/A
10	Vib 1	W-E		4	M8	6	(LDV + LVDT)

* Using Radar Gun.

(a)

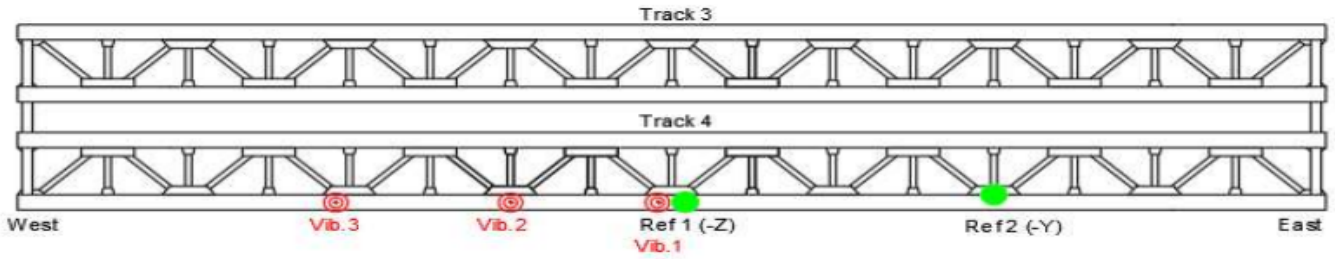

(b)

Appendix A 3 – (a) Cos Cob Bridge Field Test Records on Nov 12, 2023: train types, speeds, directions, and sensor location, and (b) Cos Cob Bridge Span 3 - Plan View

UCONN SCHOOL OF ENGINEERING

Project 1.13: Condition/Health Monitoring of Railroad Bridges for Structural Safety, Integrity, and Durability

PI: Ramesh B. Malla, Ph.D., F. ASCE, F. EMI, Professor

Sponsor: US DOT Region 1 UTC-TIDC Program

Cos Cob Bridge Field Test - LDVT LDV ACCEL

TIDC Transportation Infrastructure Durability Center AT THE UNIVERSITY OF MAINE

DATE: 11/13/2023 WEATHER CONDITION: Sunny

TEMPERATURE: 35-65 °F

Test No	Location (Node)	*Travelling Conditions*			*Type of Train*		*General Notes*
		Direction	Velocity*	Track no	Train Type	No of Cars	
10	VIB 2	W-E	40 MPH	4	M8		(LDV, LVDT)
11	VIB 2	W-E	35 MPH	4	M8		(LDV, LVDT)
12	VIB 2	W-E	40 MPH	4	M8		(LDV, LVDT)
13	VIB 2	W-E	35 MPH	4	M8		(LDV, LVDT)
14	VIB 2	W-E	25 MPH	4	M8		(LDV, LVDT)
15	VIB 2	W-E	-	4	M8		(LDV, LVDT)
16	VIB 2	W-E	37 MPH	4	REGIONAL		(LDV, LVDT)
17	VIB 2	W-E	40 MPH	4	M8		(LDV, LVDT)
18	VIB 2	W-E	40 MPH	4	M8		(LDV, LVDT)
19	VIB 2	W-E	38 MPH	4	ACELA		(LDV, LVDT)
20	VIB 3	W-E	40 MPH	4	M8		(LDV, LVDT)
21	VIB 3	W-E	40 MPH	4	M8		(LDV, LVDT)
22	VIB 3	W-E	25 MPH	4	M8		(LDV, LVDT)
23	VIB 3	W-E	43 MPH	4	M8		(LDV, LVDT)
24	VIB 3	W-E	36 MPH	4	M8		(LDV, LVDT)
25	VIB 3	W-E	41 MPH	4	M8		(LDV, LVDT)

* Using Radar Gun.

(a)

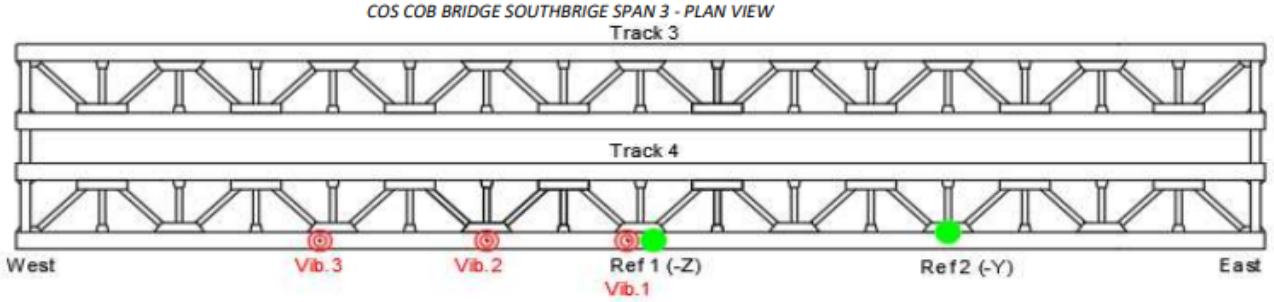

(b)

Appendix A 4 - Cos Cob Bridge Field Test Records on Nov 13, 2023: train types, speeds, directions, and sensor locations, and (b) Cos Cob Bridge Span 3 – Plan View with

Appendix B: Devon Bridge: Cross Sections Assigned to Truss Members in FE Model

U2-L2, U4-L4, U6-L6, U8-L8, U10-L10, U12-L12	L0-U6, L14-L8	U6-U8	M1-L1, M3-L3, M5-L5, M7-L7, M9-L9, M11-L11
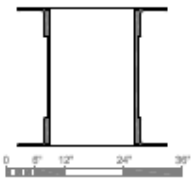	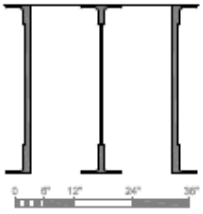	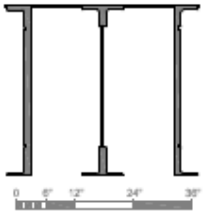	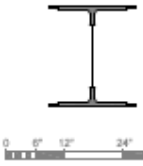
A_g= 55.43 in²	A_g= 124.56 in²	A_g=152.19 in²	A_g= 27.14 in²
I_{strong}= 6264 in^4	I_{strong}= 21524 in^4	I_{strong}= 28962 in^4	I_{strong}= 2330 in^4
BEAM188	BEAM188	BEAM188	BEAM188

M1-L2, M13-L12	L2-M3, L12-M13	M3-L4, M11-L10	U4-M5, U10-M9
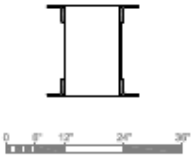	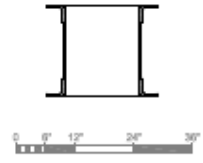	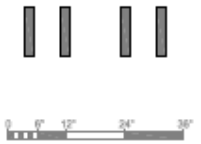	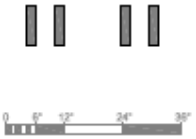
A_g= 17.72 in²	A_g= 24.58 in²	A_g= 36,00 in²	A_g= 28,00 in²
I_{strong}= 947 in^4	I_{strong}= 1653 in^4	LINK10	LINK10
LINK8	LINK8		

L0-L2, L14-L12 (U2-M3, U12-M11)	L2-L4, L12-L10	L6-L8	M5-L6, M9-L8
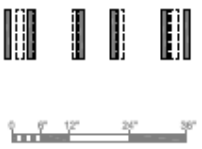	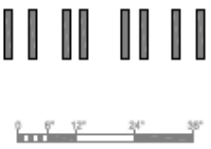	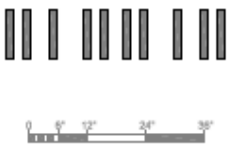	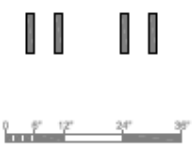
A_g= 47.12 in²	A_g= 62.82 in²	A_g= 78.52 in²	A_g= 21.00 in²
LINK10	LINK10	LINK10	LINK10

L4-M5, L10-M9	U6-M5, L8-M9	U6-M7 (U8-M7)	L6-M7 (L8-M7)
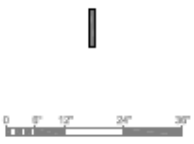	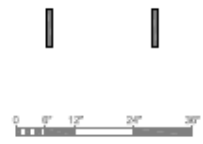	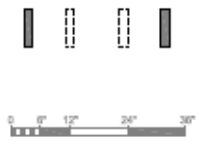	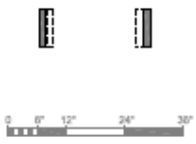
A_g= 7.50 in²	A_g= 7.00 in²	A_g= 14.00 in²	A_g= 10.50 in²
LINK10	LINK10	LINK10	LINK10

Appendix C: Devon Bridge: Cross Sections Assigned to Truss Members in FE Model (Continued)

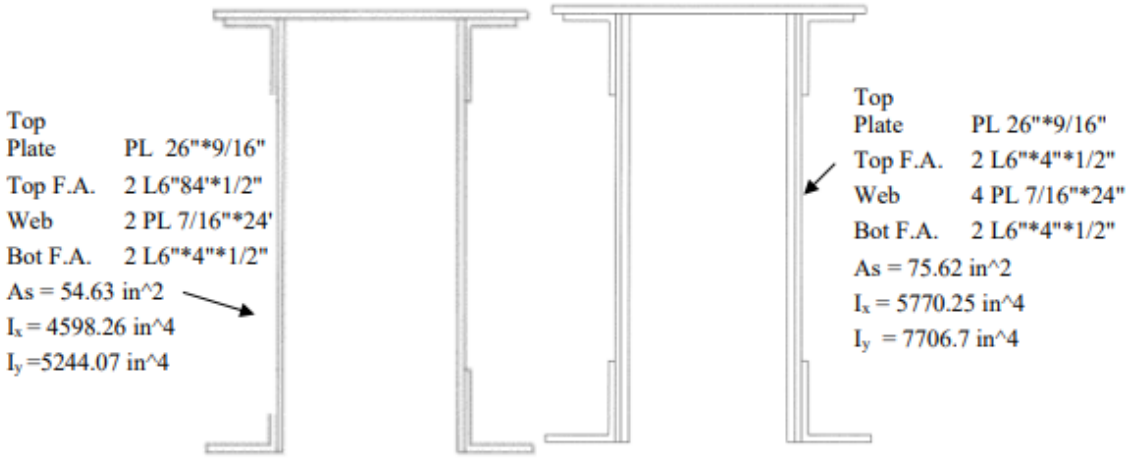

(a). Typical section; Node U0-U1, U7-U8 (Top Chord)

(b). Typical section; Node U1-U2, U6-U7 (Top Chord)

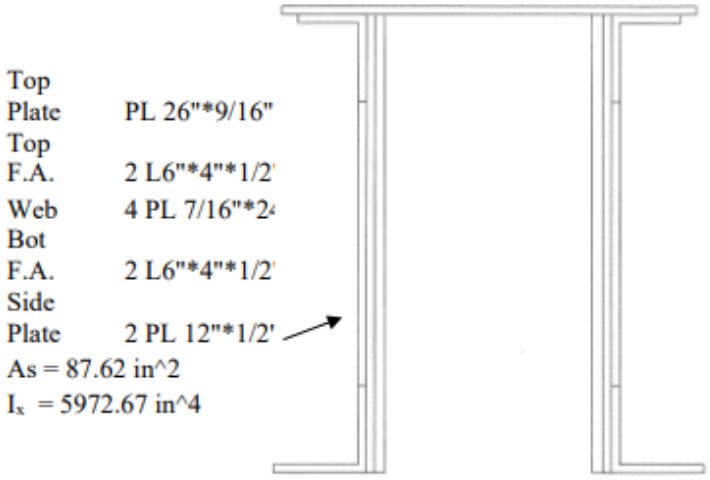

(c). Typical section; Node U2-U3, U5-U6 (Top Chord)

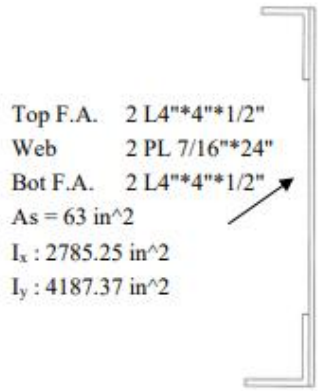

(d). Typical section; Node L0-L1, L7-L8 (Bottom Chord)

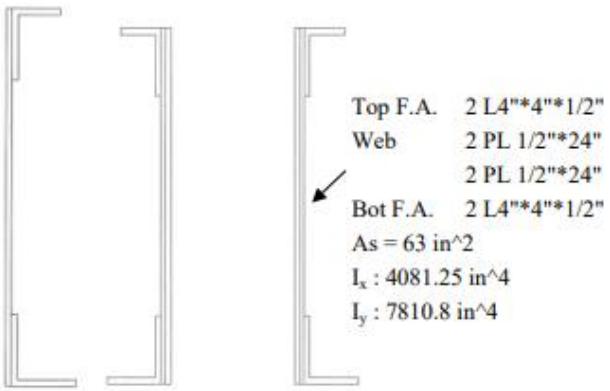

(e). Typical section; Node L1-L2, L6-L7 (Bottom Chord)

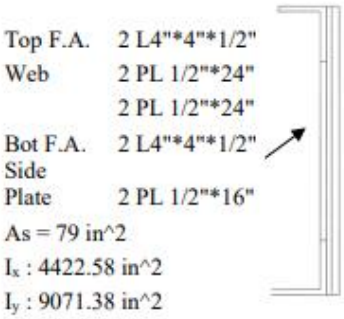

(f). Typical section; Node L2-L3 L5-L6 (Bottom Chord)

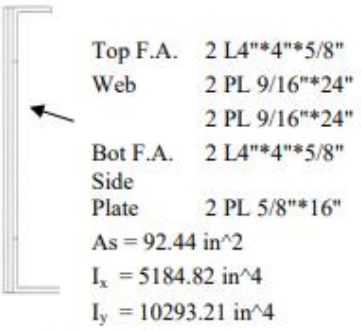

(g). Typical section; Node L3-L4, L4-L5 (Bottom Chord)

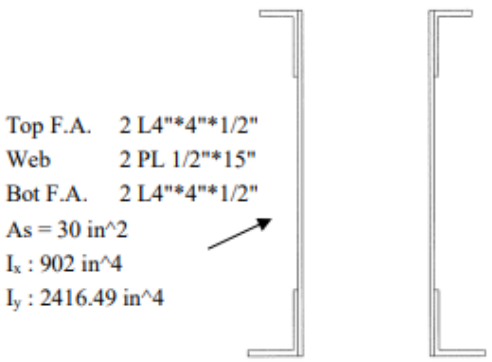

(h). Typical section; Node U0-L0, U8-L8 (End Post)

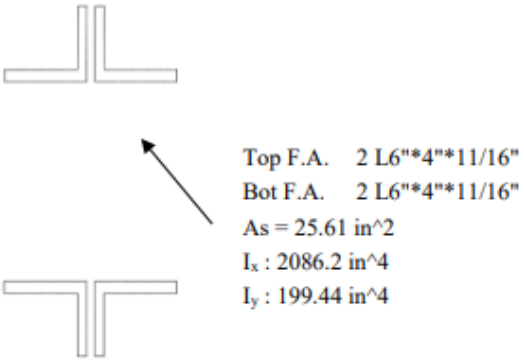

(i). Typical section; Node U2-L1 (Counters)

Appendix D: Cos Cob Bridge Bottom Chords Gusset Plate Details

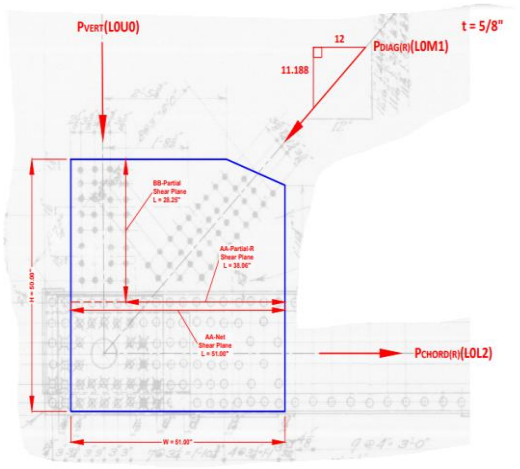

Gusset Plate L0/L16

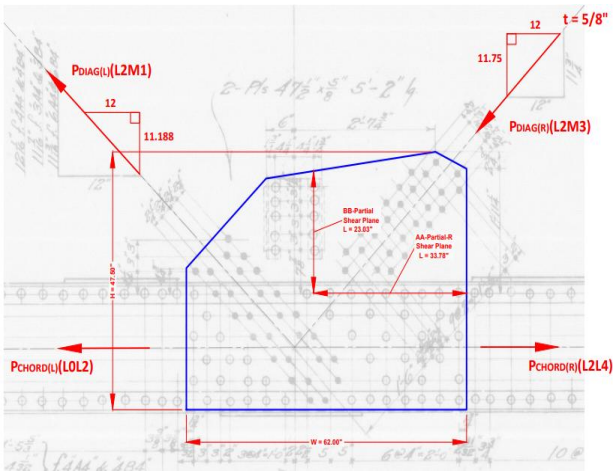

Gusset Plate L2/L14

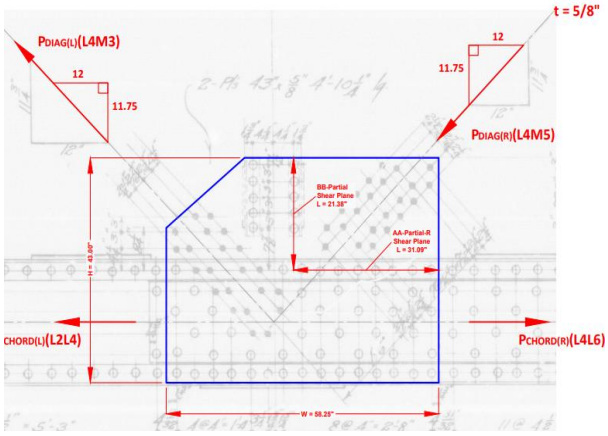

Gusset Plate L4/L12

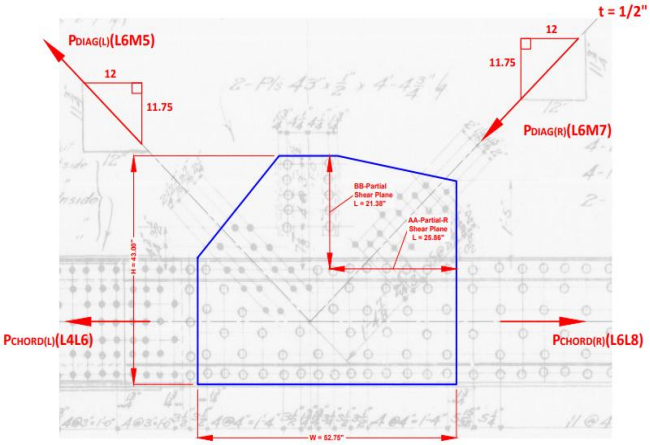

Gusset Plate L6/L

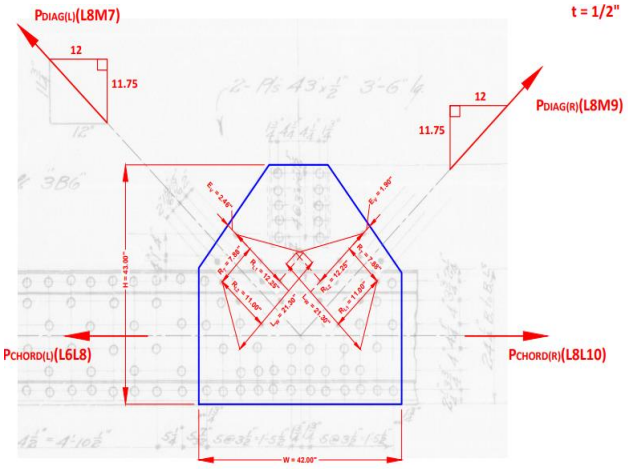

Gusset Plate L8

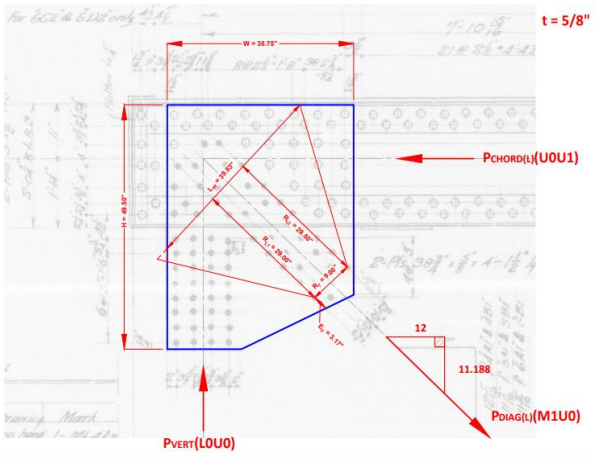

Gusset Plate U0/U16

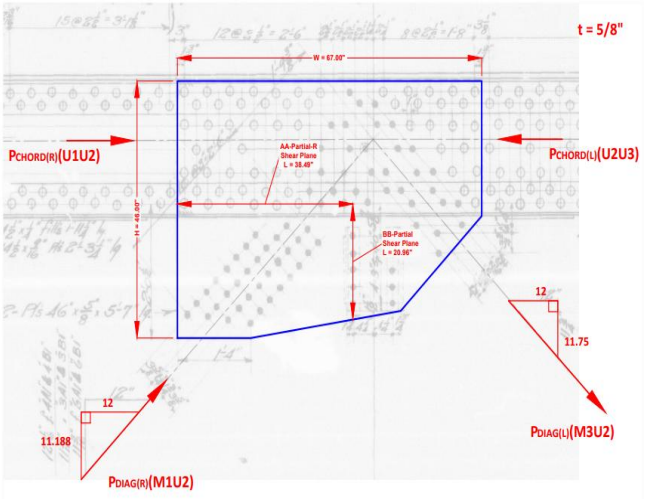

Gusset Plate U2/U14

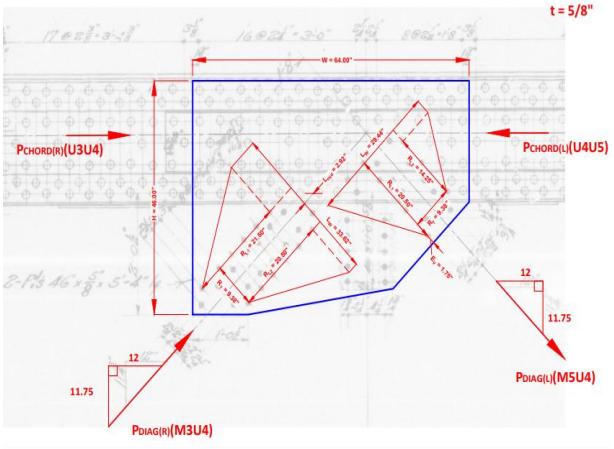

Gusset Plate U4/U12

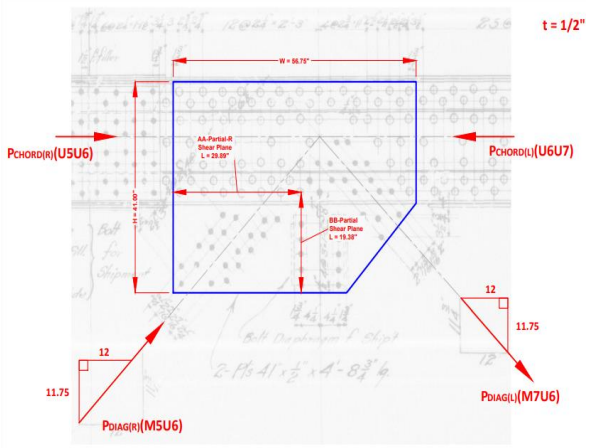

Gusset Plate U6/U10

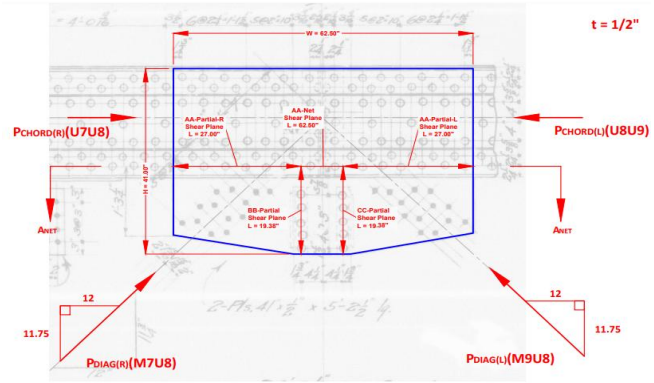

Gusset Plate U8

Appendix E: Cos Cob Bridge: Additional Vertical Deflection Results

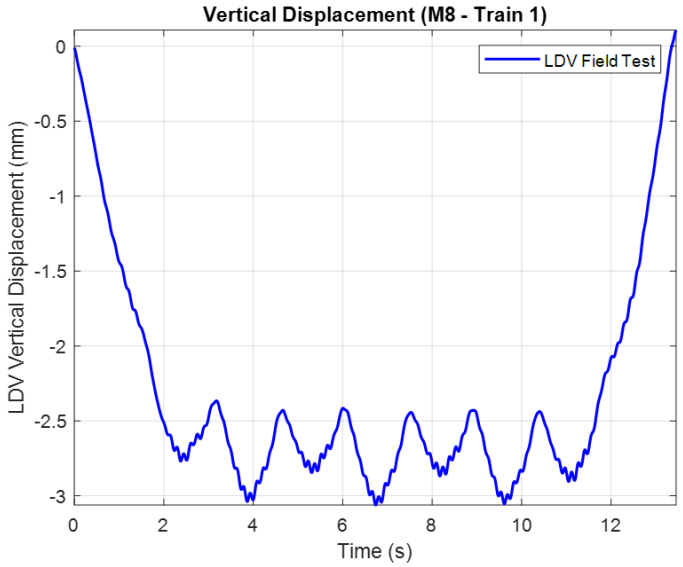

Figure E1 - Vertical Displacement of the Cos Cob Bridge @ Vib1 during Metro-North M8 Traversal (Train 1)

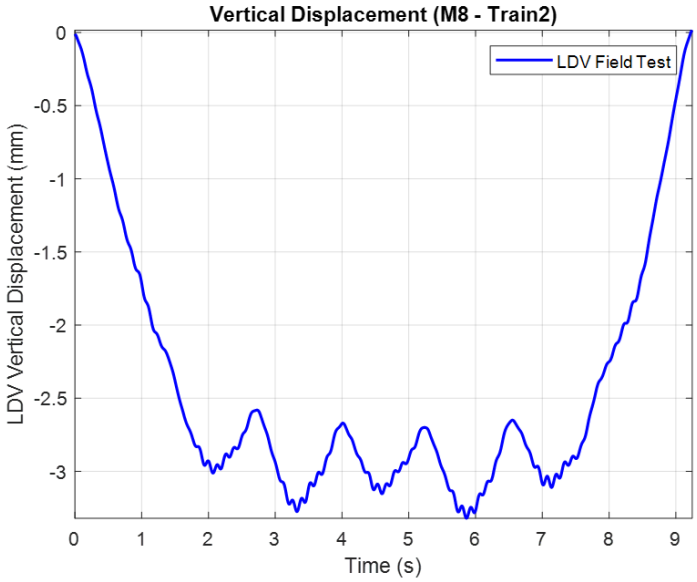

Figure E2 - Vertical Displacement of the Cos Cob Bridge @Vib 1 during Metro-North M8 Traversal (Train 2)

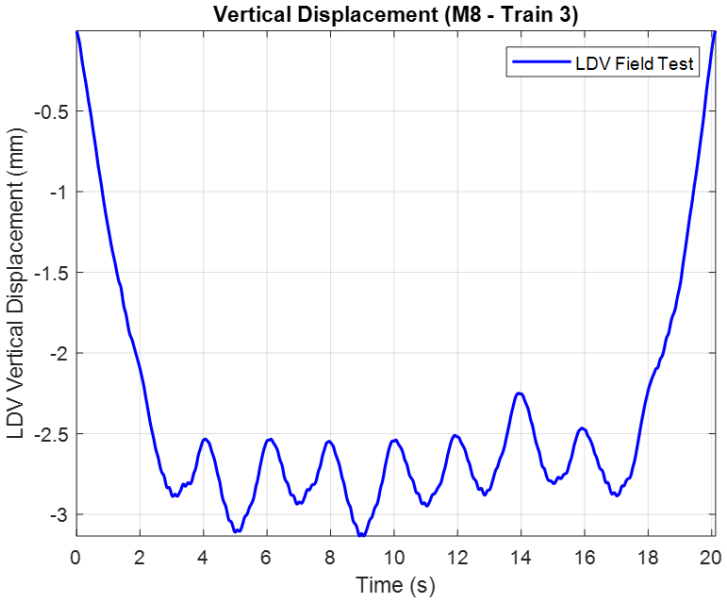

Figure E3 - Vertical Displacement of the Cos Cob Bridge @Vib 1 during Metro-North M8 Traversal (Train 3)

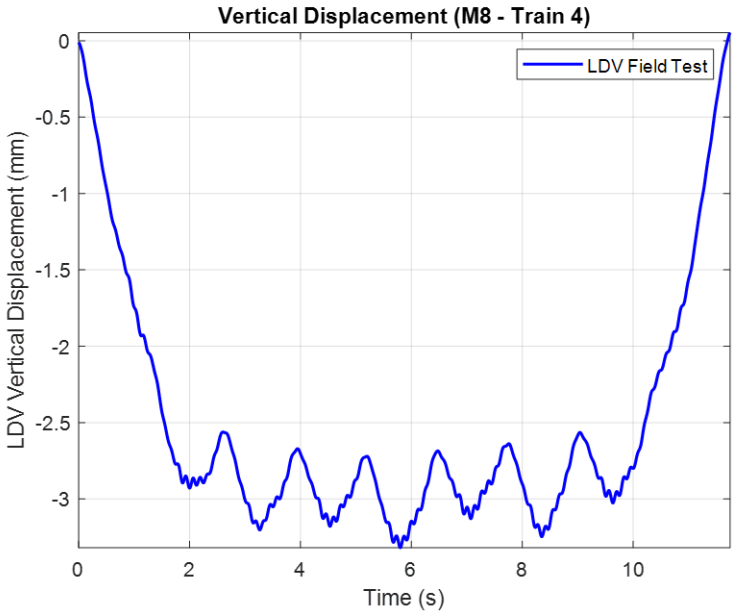

Figure E4 - Vertical Displacement of the Cos Cob Bridge @Vib 1 during Metro-North M8 Traversal (Train 4)

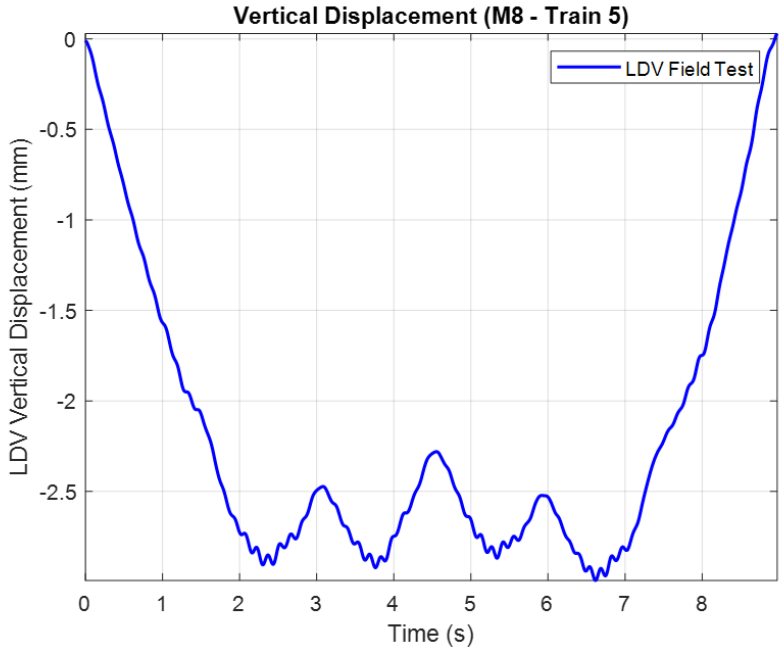

Figure E5 - Vertical Displacement of the Cos Cob Bridge @Vib 1 during Metro-North M8 Traversal (Train 5)

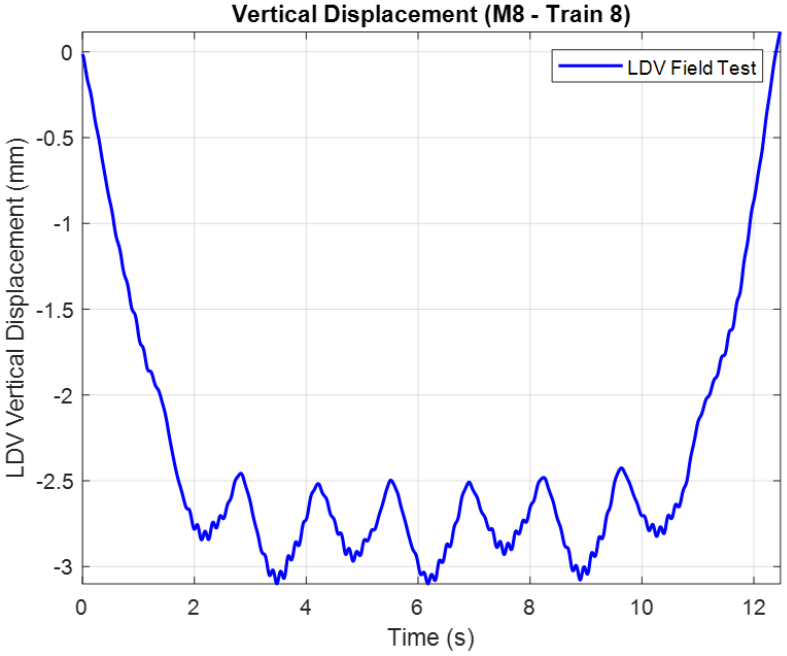

Figure E6 - Vertical Displacement of the Cos Cob Bridge @Vib 1 during Metro-North M8 Traversal (Train 8)

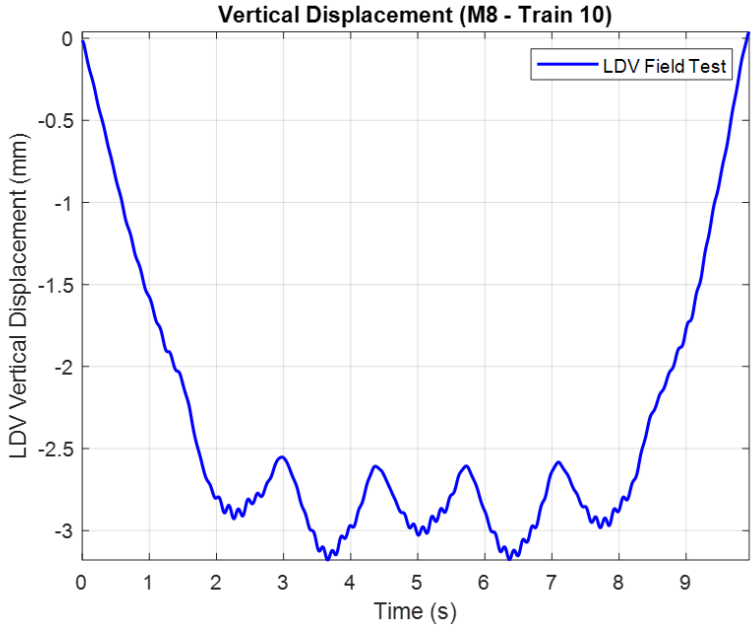

Figure E7 - Vertical Displacement of the Cos Cob Bridge @Vib 1 during Metro-North M8 Traversal (Train 10)

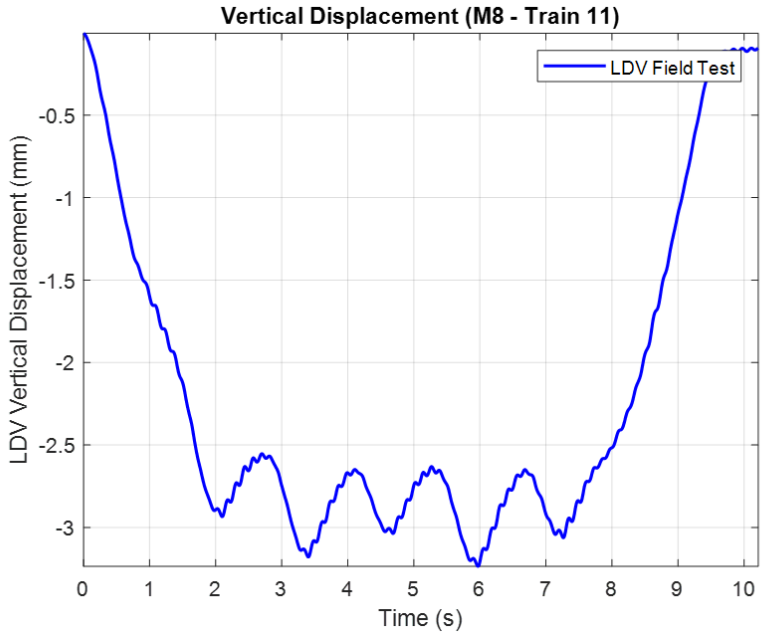

Figure E8 - Vertical Displacement of the Cos Cob Bridge @Vib 2 during Metro-North M8 Traversal (Train 11)

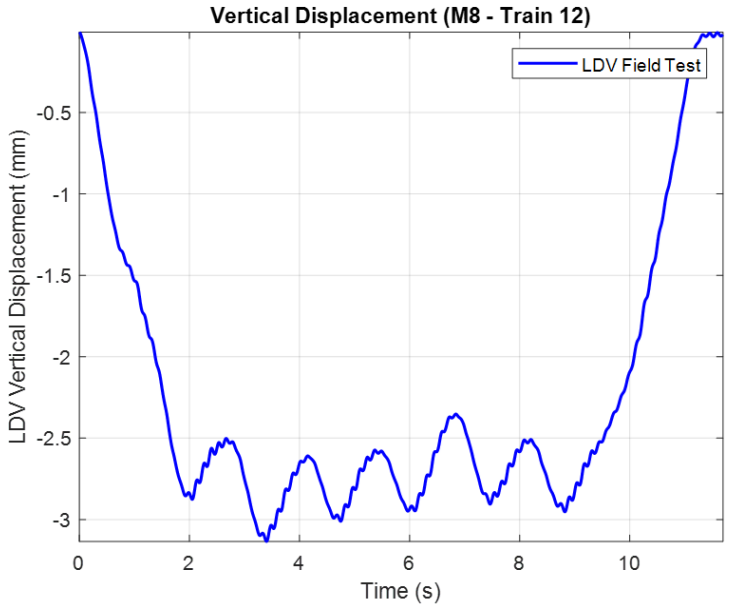

Figure E9 - Vertical Displacement of the Cos Cob Bridge @Vib 2 during Metro-North M8 Traversal (Train 12)

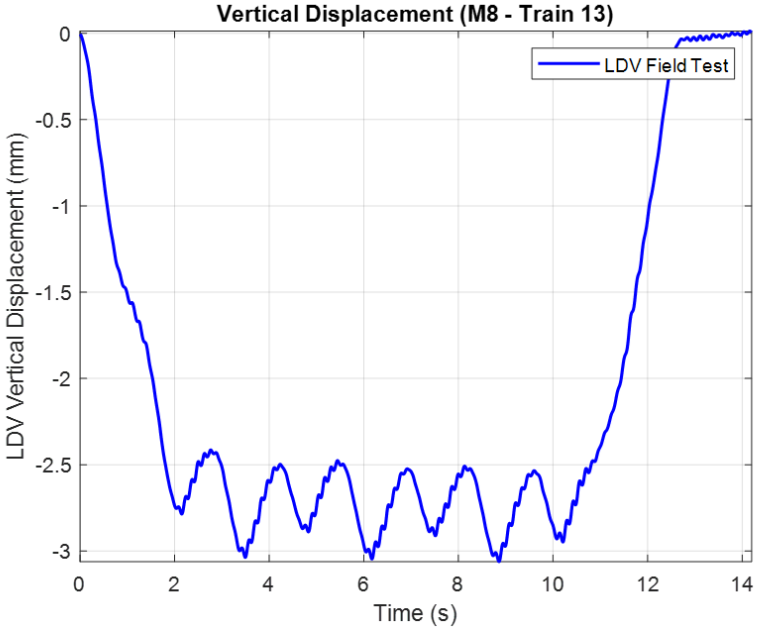

Figure E10 - Vertical Displacement of the Cos Cob Bridge @Vib 2 during Metro-North M8 Traversal (Train 13)

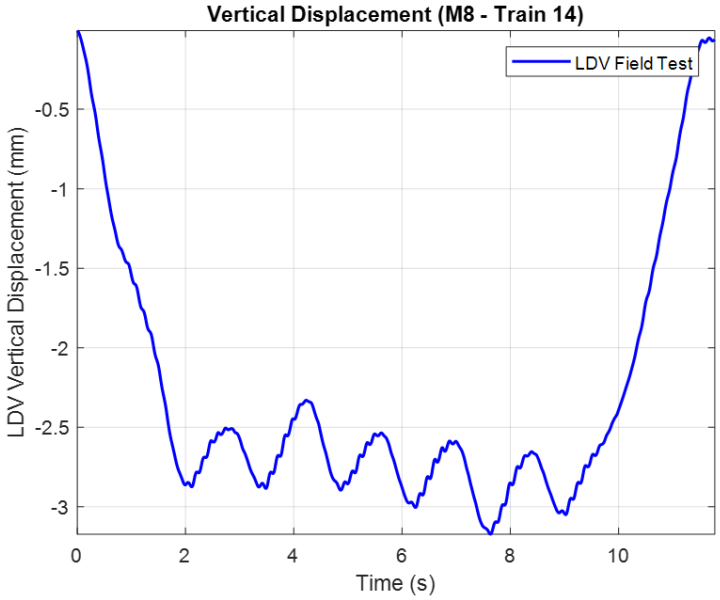

Figure E11 - Vertical Displacement of the Cos Cob Bridge @Vib 2 during Metro-North M8 Traversal (Train 14)

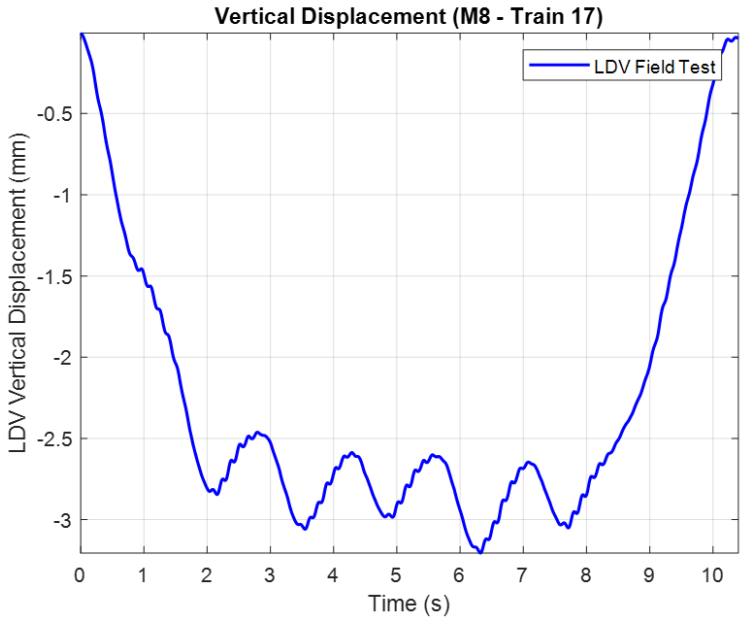

Figure E12 - Vertical Displacement of the Cos Cob Bridge @Vib 2 during Metro-North M8 Traversal (Train 17)

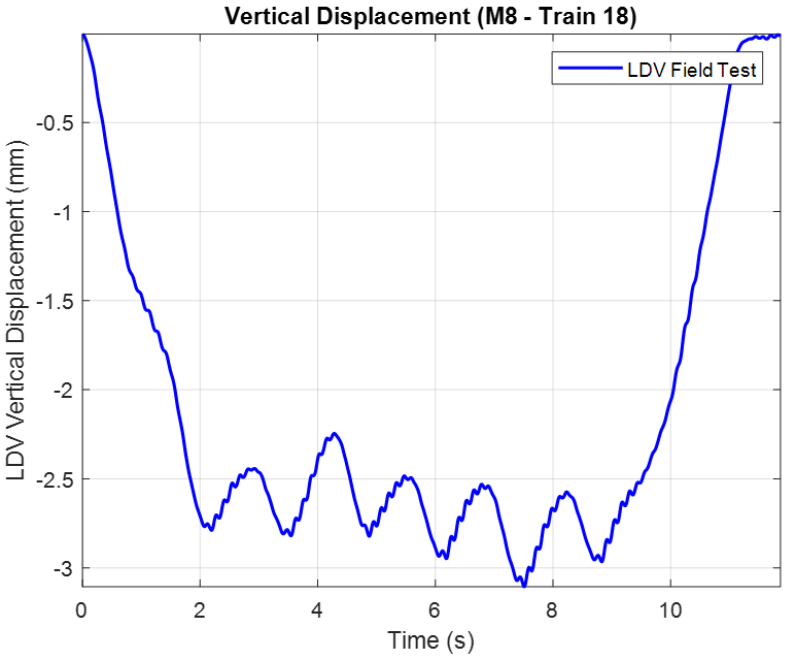

Figure E13 - Vertical Displacement of the Cos Cob Bridge @Vib 2 during Metro-North M8 Traversal (Train 18)

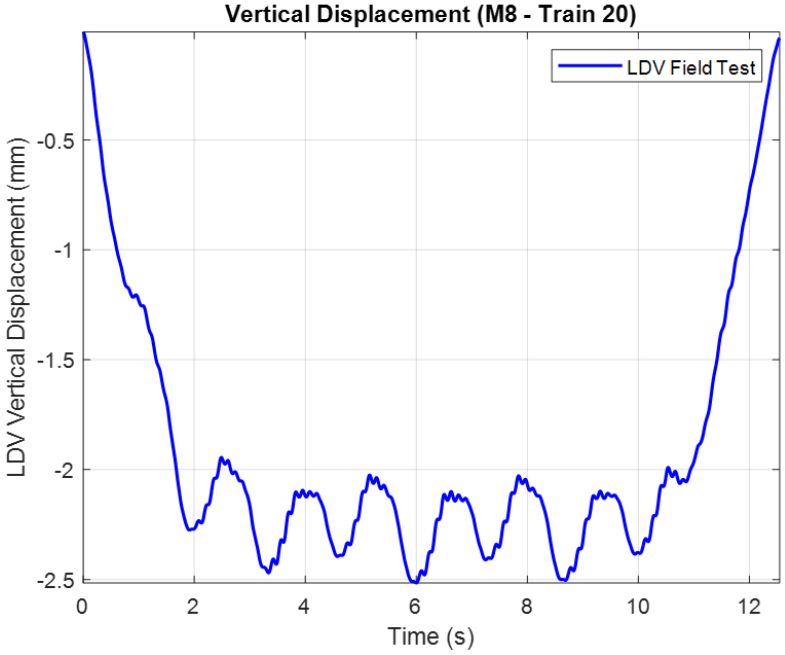

Figure E14 - Vertical Displacement of the Cos Cob Bridge @Vib 2 during Metro-North M8 Traversal (Train 20)

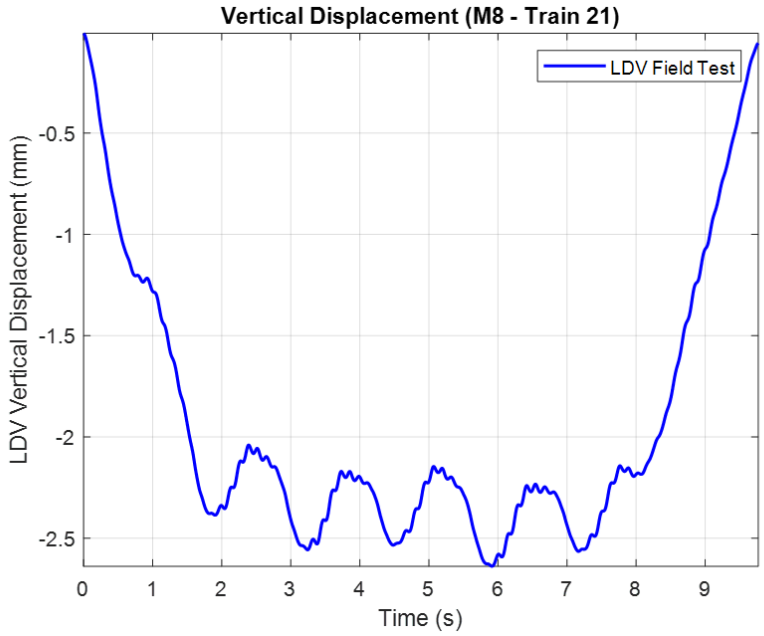

Figure E15 - Vertical Displacement of the Cos Cob Bridge @Vib 3 during Metro-North M8 Traversal (Train 21)

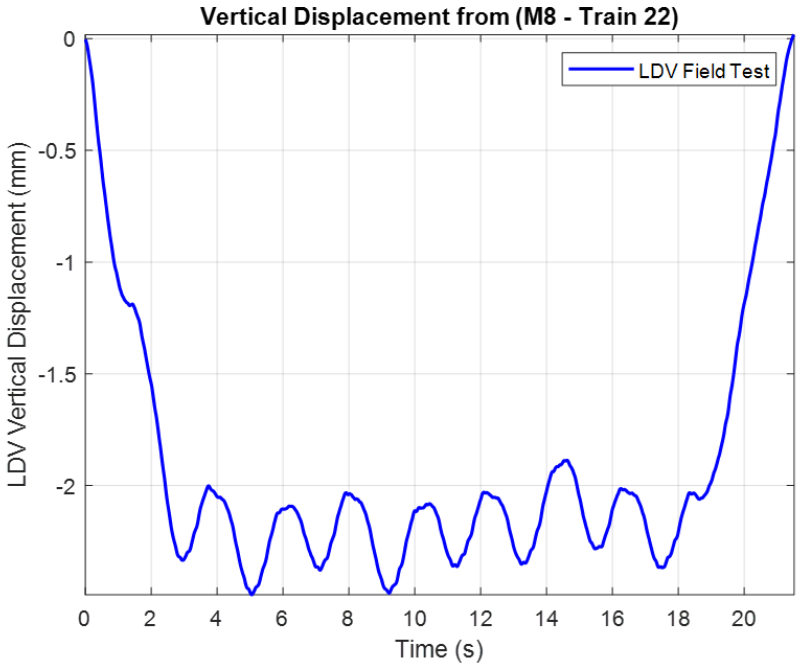

Figure E16 - Vertical Displacement of the Cos Cob Bridge @Vib 3 during Metro-North M8 Traversal (Train 22)

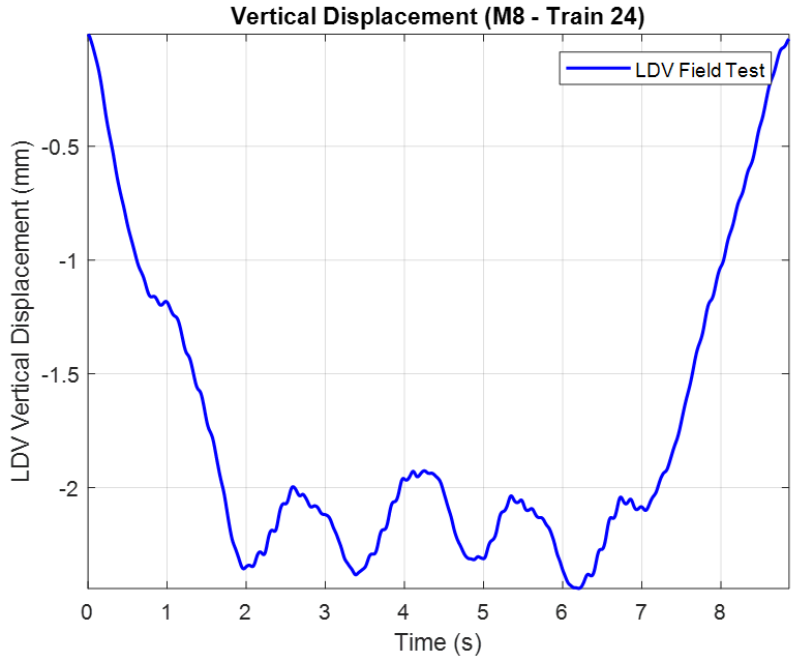

Figure E17 - Vertical Displacement of the Cos Cob Bridge @Vib 3 during Metro-North M8 Traversal (Train 24)

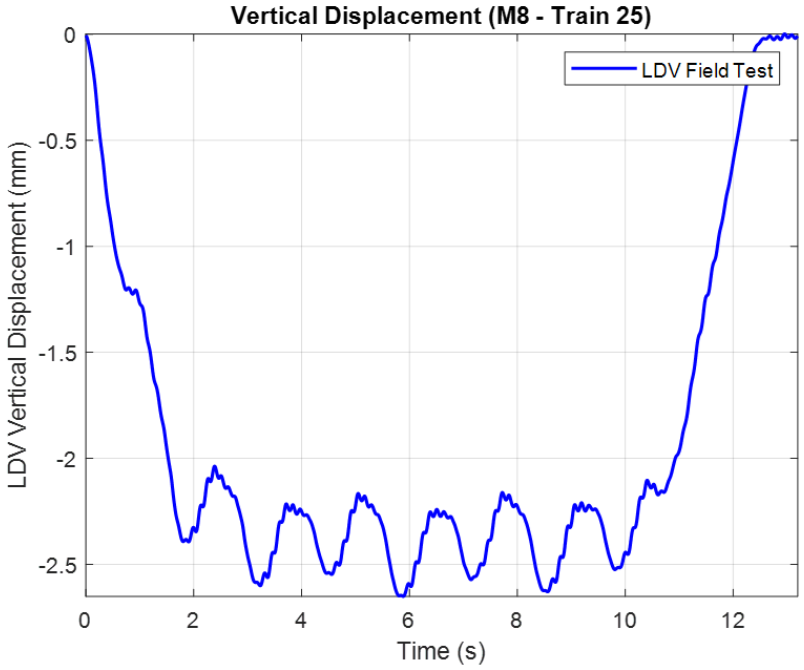

Figure E18 - Vertical Displacement of the Cos Cob Bridge @Vib 3 during Metro-North M8 Traversal (Train 25)

```
subroutine DLOAD(F,KSTEP,KINC,TIME,NOEL,NPT,LAYER,KSPT,
    &                 COORDS,JLTYP,SNAME)
C
      include 'ABA_PARAM.INC'
C
      dimension TIME(2), COORDS(3)
      CHARACTER*80 SNAME

      X=COORDS(1)
      Y=COORDS(2)
        Z=COORDS(3)

      Velocity = 22.0
      Axle_dis1=6.0
      Axle_dis2=25.0
      Axle_dis3=7.0
      dis_intpoint = 0.619
      Fmax = -100000.0

        X_pos1 = Velocity*TIME(2)
      X_pos2 = X_pos1-Axle_dis1
      X_pos3 = X_pos1-Axle_dis1-Axle_dis2
      X_pos4 = X_pos1-2.0*Axle_dis1-Axle_dis2

c   Second coach
      X_pos5 = X_pos1-2.0*Axle_dis1-Axle_dis2-Axle_dis3
      X_pos6 = X_pos1-3.0*Axle_dis1-Axle_dis2-Axle_dis3
      X_pos7 = X_pos1-3.0*Axle_dis1-2.0*Axle_dis2-Axle_dis3
      X_pos8 = X_pos1-4.0*Axle_dis1-2.0*Axle_dis2-Axle_dis3

C   Third coach
      X_pos9 = X_pos1-4.0*Axle_dis1-2.0*Axle_dis2-2.0*Axle_dis3
      X_pos10 = X_pos1-5.0*Axle_dis1-2.0*Axle_dis2-2.0*Axle_dis3
      X_pos11 = X_pos1-5.0*Axle_dis1-3.0*Axle_dis2-2.0*Axle_dis3
      X_pos12 = X_pos1-6.0*Axle_dis1-3.0*Axle_dis2-2.0*Axle_dis3

C   Fourth coach
      X_pos13 = X_pos1-6.0*Axle_dis1-3.0*Axle_dis2-3.0*Axle_dis3
      X_pos14 = X_pos1-7.0*Axle_dis1-3.0*Axle_dis2-3.0*Axle_dis3
      X_pos15 = X_pos1-7.0*Axle_dis1-4.0*Axle_dis2-3.0*Axle_dis3
      X_pos16 = X_pos1-8.0*Axle_dis1-4.0*Axle_dis2-3.0*Axle_dis3

C   Fifth coach
      X_pos17 = X_pos1-8.0*Axle_dis1-4.0*Axle_dis2-4.0*Axle_dis3
      X_pos18 = X_pos1-9.0*Axle_dis1-4.0*Axle_dis2-4.0*Axle_dis3
      X_pos19 = X_pos1-9.0*Axle_dis1-5.0*Axle_dis2-4.0*Axle_dis3
```

```
      X_pos20 = X_pos1-10.0*Axle_dis1-5.0*Axle_dis2-4.0*Axle_dis3


C   Check if the point is within the 0.15 units of either axle position

      abs1=abs(X-X_pos1)
      abs2=abs(X-X_pos2)
      abs3=abs(X-X_pos3)
      abs4=abs(X-X_pos4)
      abs5=abs(X-X_pos5)
      abs6=abs(X-X_pos6)
      abs7=abs(X-X_pos7)
      abs8=abs(X-X_pos8)
      abs9=abs(X-X_pos9)
      abs10=abs(X-X_pos10)
      abs11=abs(X-X_pos11)
      abs12=abs(X-X_pos12)
      abs13=abs(X-X_pos13)
      abs14=abs(X-X_pos14)
      abs15=abs(X-X_pos15)
      abs16=abs(X-X_pos16)
      abs17=abs(X-X_pos17)
      abs18=abs(X-X_pos18)
      abs19=abs(X-X_pos19)
      abs20=abs(X-X_pos20)

min_abs=min(abs1,abs2,abs3,abs4,abs5,abs6,abs7,abs8,abs9,abs10,abs11,abs12,abs13,abs14,abs
15,abs16,abs17,abs18,abs19,abs20)
      if (min_abs <= dis_intpoint)then
        F = Fmax+min_abs/dis_intpoint*abs(Fmax)
      else
           F = 0.0
        endif


      RETURN
      END
```

35 Flagstaff Road
Orono, Maine 04469
tidc@maine.edu
207.581.4376

www.tidc-utc.org